Flow Behavior and Emplacement of the Northwest Dike Swarm in the Jagged Rocks Complex, Hopi Buttes Volcanic Field, Arizona

By Michaela Kim

A Thesis

Submitted in Partial Fulfillment

Of the Requirements of the Degree of

Master of Science

In Geology

Northern Arizona University

August 2017

Approved:

Michael Ort, Ph.D., Chair

Nancy Riggs, Ph.D.

Ryan Porter, Ph.D.

ABSTRACT

The Jagged Rocks Complex in the Hopi Buttes Volcanic Field provides excellent exposure of shallow dikes and sills as well as massifs and buds that fed three to five maar-diatreme volcanoes. The northwest dike swarm consists of a series of six en-echelon dikes as well as five massifs and many smaller buds. The excellent exposure of these shallow plumbing structures provides a unique opportunity to study the role of shallow dikes in supporting maar-diatreme eruptions.

Anisotropy of magnetic susceptibility (AMS) and other rock magnetic methods were used to investigate the timing of the intrusions, the characteristics of their magnetic mineralogy, and the flow history preserved within the dikes. Curie point analysis shows the magnetic minerals have a low Curie point indicative of high-titanium titanomagnetite. The isothermal remanent magnetization (IRM) measurements indicate that the grains are dominantly pseudo-single domain (PSD) edging on single domain (SD). This is supported by anisotropy of anhysteretic remanent magnetization (AARM) measurements, which also indicate the influence of SD grains on some sites' anomalous AMS fabrics. AMS shows dominantly horizontal flow in the majority of the sites. Only half of the margin pairs provide reliable imbricated K_1 lineations for flow direction interpretation. The use of the K_3 method to define the main foliation plane does not reveal any imbricated fabrics beyond those seen with the K_1 method.

The interpretable margin pairs all show flow to the northwest, providing flow directions for five out of the six dikes analyzed. This direction is generally away from the other main series of intrusions to the southeast, indicating a lateral diversion of magma away from a magma-supply system located somewhere to the southeast. The lateral intrusion of the northwest dike swarm

could have been a response to overpressure in the shallow subsurface due to the formation of a volcanic edifice or due to overpressure in the magma supply system. Coherent dikes formed first, with limited water/magma interactions, and later reduction in flux or withdrawal of magma initiated the phreatomagmatism that formed the massifs.

Acknowledgements

Firstly, I would like to thank my advisor, Michael Ort, for his continued guidance and support through this project. He helped guide me through the difficult parts of my research, ensuring that as I found more questions, the appropriate steps were taken to answer them fully. This included adding additional analyses rather late in the game, but ultimately these helped strengthen my results. He also guided me through the process of understanding and interpreting my data, and to some degrees helped me gain confidence in the quality of my results (even if they were not exactly as perfect as I would have wished them to be). His endless support and guidance was very much appreciated at all points while working on my thesis. I would also like to thank Nancy Riggs and Ryan Porter for their valued feedback at various stages throughout this process.

Secondly, I would like to thank Mike Petronis for allowing me to essentially take over his lab for an entire weekend, so that I could get additional analyses done in the short amount of time I had off from work. Also, thank you for taking the time to finish the Curie Point Analyses that I could not get done while I was there in person. You proved to be an immensely valuable resource for understanding the purpose of the analyses I was doing and what they meant in regard to the magnetic properties of my specimens. Your help was very important to the completion of my thesis and immensely appreciated.

I would like to thank my parents for their love and support; without them I would not be where I am today. I am also immensely thankful for the continual support of Garrett Erickson through the last year and a half. Without his love and support, I likely would not have made it through the final year of writing my thesis. He always believed in me, even when I had trouble

believing in myself, and for that I am eternally grateful. I would also like to thank my good friends Liana, Eileen, and Twitch (Elizabeth…?) for their support and endless conversations even from the other side of the country. You all kept me sane through the ups and downs of the last three years.

Also a big thank you to Karl, Davis, and Garrett, all of whom helped with my field work. Drilling cores is a two-person job and often involved working in inclement weather, carrying awkwardly shaped jugs of water great distances to drilling locations, and frequently forcing stuck cores out of drill bits with an array of screwdrivers. Your assistance and company was greatly appreciated. Thank you to Sue and Buddy the dog for always chatting with me and letting me drill and camp on your property.

I would also like to thank the Arizona Conservation Corps and AmeriCorps for providing me with really interesting summer work in Flagstaff. Balancing school with outdoor-focused trail work and survey jobs was essential to keeping me sane. I got to meet some really great people and learn some awesome outdoor skills along the way. I would have never known the depth of my own physical and interpersonal capabilities without these experiences. Additionally, I am grateful for the Segal Education Awards I earned after the completion of each service term. They ended up being immensely valuable in helping fund the final year of completing my thesis.

This project was funded by the Geological Society of America Graduate Research Grants.

Table of Contents

Chapter 1: Introduction 1
1.1 Maar-Diatreme Volcanic Systems and Existing Models 2
1.2 Background on the Hopi Buttes Volcanic Field and Regional Stratigraphy 5
1.3 The Jagged Rocks Complex 10
1.4 Previous AMS and AARM work on dikes 13
1.5 Purpose and Objective of This Study 16
Chapter 2: Project Methods 16
2.1 Field Methods 17
2.2 Rock Magnetic Methods 19
2.2.1 Anisotropy of Magnetic Susceptibility (AMS) 20
2.2.2 Anisotropy of Anhysteretic Remanent Magnetization (AARM) 24
2.2.3 Isothermal Remanent Magnetization (IRM) 25
2.2.4 Curie Point Analysis 26
2.2.5 Characteristic Remanent Magnetization (ChRM) 27
2.3 Magnetic Survey Methods 28
Chapter 3: Results from Magnetic Analyses 29
3.1 AMS Results 30
3.1.1 Dike 1 31
3.1.2 Dikes 2 and 3 37
3.1.3 Dike 4 40
3.1.4 Dikes 5 and 6 42
3.2 AARM Results 44
3.3 Curie Point and IRM Results 46
3.4 ChRM Results 50
3.5 Magnetic Survey Results 52
Chapter 4: Discussion 55
4.1 Determination of Dike Flow Directions 57
4.1.1 K_1 vs K_3 Method for Determination of Imbrication 59
4.1.2 Dike Flow Directions, Azimuth, and Plunge 61
4.2 Implications for Injection of Northwest Dike Swarm 71
4.2.1 Implications of sub-horizontal flow for dike injection 72
4.2.2 Model for emplacement of NW dike swarm and SE intrusions in JRC 75
4.2.3 Emplacement History of the Northwest Dike Swarm and Associated Massifs 76

4.3 Problems with AMS Analyses on Dikes 83
Chapter 5: Conclusions 85

List of Figures

Figure 1.1 6
Figure 1.2 7
Figure 1.3 11
Figure 2.1 18
Figure 3.1 32
Figure 3.2 35
Figure 3.3 39
Figure 3.4. 41
Figure 3.5. 43
Figure 3.6 45
Figure 3.7 49
Figure 3.8 52
Figure 3.9 54
Figure 4.1 59
Figure 4.2 62
Figure 4.3 65
Figure 4.4 66
Figure 4.5 70
Figure 4.6 71
Figure 4.7 78
Figure 4.8 81

List of Tables

Table 3.1 33-34
Table 3.2 47
Table 3.3 50
Table 3.4 51
Table 4.1 63
Table 4.2 64

Chapter 1: Introduction

Shallow volcanic plumbing structures in monogenetic volcanic fields are typically not well exposed in close proximity to the surface deposits, often hindering a full understanding of their role in magma storage and feeding of eruptions at the main conduits. In the Hopi Buttes Volcanic Field, the differential erosion throughout the field allows for the study of maar-diatreme volcanic structures at various depths as well as the study of shallow feeder structures such as dikes and sills over lateral distances of kilometers. The excellent exposure of shallow volcanic feeder structures in the Jagged Rocks Complex in the southernmost part of Hopi Buttes Volcanic Field provides an ideal area to study the role of shallow intrusions in the storing of magma and feeding of eruptions at the surface. Understanding the role of the shallow intrusions, particularly the dikes, in the Jagged Rocks Complex can provide a greater understanding of the role that shallow intrusions play in monogenetic volcanic systems and possibly aid in the interpretation of shallow plumbing systems of other monogenetic volcanic complexes.

Anisotropy of magnetic susceptibility (AMS) and anisotropy of anhysteretic remanent magnetism are commonly used techniques for evaluating rock fabric and interpreting the flow history through dikes (e.g. Knight and Walker 1988; Rochette et al. 1992; Raposo and Ernesto 1995; Borradaile and Henry 1997; Borradaile and Gauthier 2001; Herrero-Bervera et al. 2001; Callot and Guichet 2003; Callot et al. 2004; Poland et al. 2004; Krasa and Herrero-Bervera 2005; Philpotts and Philpotts 2007; Soriano et al. 2008; Delcamp et al. 2014). Based on alignment of K_1 axes and imbrication of AMS ellipsoids relative to the dike plans, flow fabrics allow for the interpretation of how magma moved through the dikes during different stages of the eruptions (Knight and Walker 1988). Overall flow patterns in the dikes can provide insight into the relation between the dikes, massifs, sills, and possible conduits as well as how magma moves in the

subsurface in the time between different pulses of magma (e.g. Raposo and Ernesto 1995; Borradaile and Gauthier 2001; Herrero-Bervera et al. 2001; Callot et al. 2004; Soriano et al. 2008). Additional analyses, such as isothermal remanent magnetization (IRM) and Curie point analyses, can provide information about the magnetic mineralogy and domain state of the magnetic grains that is useful when interpreting the AMS and AARM results (e.g. Hillhouse and Wells 1991; Soriano et al. 2016). All of these techniques are well suited for looking at the magma-flow history through dikes and can provide critical information about the movement of magma. Understanding the flow history recorded in the dikes in Jagged Rocks Complex can aid in understanding the role they played in eruptions and their relation to other structures exposed in the complex and in other monogenetic systems. This provides crucial information about the role of shallow intrusions as storage and feeder systems for conduits in maar-diatreme systems and can further understanding of the role of dikes and shallow intrusions in other monogenetic systems.

1.1 Maar-Diatreme Volcanic Systems and Existing Models

In maar-diatreme volcanoes and other phreatomagmatic systems, magma-fuel-coolant-interaction (MFCI) is the main mechanism for magma fragmentation. MFCIs occur when hot magma comes in contact with ground or surface water during its ascent to the surface. The heat from the magma causes super-heating of the surrounding liquid water into vapor and, as the magma and water mix, the expansion of the vapor causes fragmentation (Zimanowski et al. 1997). Explosive MFCIs have four main phases: 1) magma and water premixing while the vapor film between them is stable; 2) vapor film collapse leading to direct contact between melt and water; 3) rapid increase in heat transfer and fine fragmentation; 4) generation of superheated steam leading to system expansion (Zimanowski et al. 1997). The critical pressure is an

important aspect of the fragmentation process, because it is the pressure below which water can react more explosively with a hot liquid, magma in this case, and consequently has a large control on the depth at which MFCIs can occur in a maar-diatreme system (Zimanowski et al. 1997).

Two main models exist regarding the processes that contribute to the formation of maar-diatreme volcanoes. Lorenz (1986) proposed that, after an initial fragmentation event near the surface excavates the maar crater and diatreme, the explosive eruptions migrate downward and excavate the diatreme deeper into the country rock, typically creating a cone of depression in the groundwater around the site of the eruption. More recent studies have amended this model in an attempt to better reflect the complexity of the processes that drive the formation of maar-diatreme volcanoes (White and Ross 2011; Valentine and White 2012). The Valentine and White (2012) model proposes that as magma ascends, MFCI-driven explosions can occur at any level along the diatreme as long as the pressure is below the critical pressure for water. Because fragmentation can only occur below the critical pressure, depth has a large control on where MFCIs can occur in a maar-diatreme system.

Both of these models and other detailed studies of maar-diatreme volcanoes allow for better understanding of the anatomy and evolution of maar-diatreme volcanoes. In the early stages of the eruption, initial explosions near the surface excavate the maar crater and form the surrounding tephra ring. The tephra ring is composed of layered lapilli and blocks of underlying country rock that have been ejected during the eruptions. As the eruption progresses, MFCI-driven explosions can occur anywhere along the diatreme, but only shallow or particularly strong explosions erupt at the surface (Valentine and White 2012). The eruptions at all depths continue to excavate and widen the diatreme. The explosions at different levels effectively mix the

country-rock breccia throughout the diatreme, moving country-rock fragments from deeper in the subsurface upward, allowing them to eventually be erupted at the surface. The diatreme develops a cone shape, wider at the top and narrower at the bottom, for three main reasons: 1) the explosive eruptions are more effective at lower pressures, 2) the explosions damage the surrounding country rock more at shallower depths because of the lower lithostatic pressure, and 3) the diatreme and crater walls collapse more near the surface (Valentine and White 2012). After the eruption ends, the maar crater may be filled in with post-eruptive sediments. Because of the variability in the effectiveness of the explosions throughout the diatreme, it develops different characteristics at different levels (Figure 1.1).

Generally, a diatreme is split into the upper diatreme, lower diatreme, and the root zone facies (Figure 1.1). The upper diatreme facies consists of bedded pyroclastic deposits, which can dip slightly and be crosscut by zones of non-bedded volcaniclastic material (White and Ross 2011). The lower diatreme facies contains a mix of pyroclastic debris with some cross-cutting dikes and debris jets that are subsurface sites of fragmentation (White and Ross 2011; Valentine and White 2012). The root zone facies, which marks the transition between the diatreme and the feeder dike, is composed of a mixture of coherent rock as well as brecciated material and broken country rock (Lorenz 1986, White and Ross 2011). This mix of brecciated material and broken country rock is produced by fragmentation in the transition zone. Below the root zone, the system connects to coherent dikes that transport magma to the diatreme system. These dikes are the subject of this thesis. Together with the models for the evolution of maar-diatreme volcanic systems, detailed descriptions of maar-diatreme deposits provide an outline for understanding maar-diatreme eruptions and their associated deposits.

1.2 Background on the Hopi Buttes Volcanic Field and Regional Stratigraphy

The Hopi Buttes Volcanic Field is a maar-diatreme volcanic field located on the Colorado Plateau in northeastern Arizona (Figure 1.2). The field consists of volcanic deposits and structures associated with approximately 300 maar-diatreme volcanoes that formed during the late Miocene epoch (Hack 1942; Shoemaker et al. 1962; White 1989). The country rock strata consist of Paleozoic, Mesozoic, and Cenozoic carbonate and clastic sedimentary rocks. The main Formations of concern in ascending order are the Moenkopi Formation, Chinle Formation (Shinarump, Petrified Forest, and Owl Rock Members), Moenave Formation, and Bidahochi Formation. The Early and Middle(?) Triassic Moenkopi Formation and in north-central and east-central Arizona it consists of reddish-brown siltstone, silty sandstone, and sandstone (Reppening et al. 1969, Stewart et al. 1972b). The Late Triassic Chinle Formation consists of three main members in northeastern Arizona: the Shinarump, Petrified Forest, and Owl Rock Members (Billingsley et al. 2013). The Shinarump Member consists primarily of thin, cross-stratified sandstone and conglomerate (Reppening et al. 1969, Stewart et al. 1972a). The Petrified Forest Member lies on top of the Shinarump Member and is the thickest member. It consists primarily of brightly colored, horizontally-stratified claystone and clayey siltstone and cross-stratified clayey sandstone (Reppening et al. 1969, Stewart et al. 1972a). The Owl Rock Member lies on top of the Petrified Forest Member and consists of calcareous siltstone layers that alternate with thin beds of limestone and cherty limestone (Reppening et al. 1969, Stewart et al. 1972a). Evidence for altered volcanic debris exists in all three members (Reppening et al. 1969, Stewart et al. 1972a). The Jurassic Moenave Formation unconformably overlies the Owl Rock Member of the Chinle Formation and consists of red siltstone and sandstone strata (Billingsley et al. 2013). The Miocene and Pliocene Bidahochi Formation unconformably

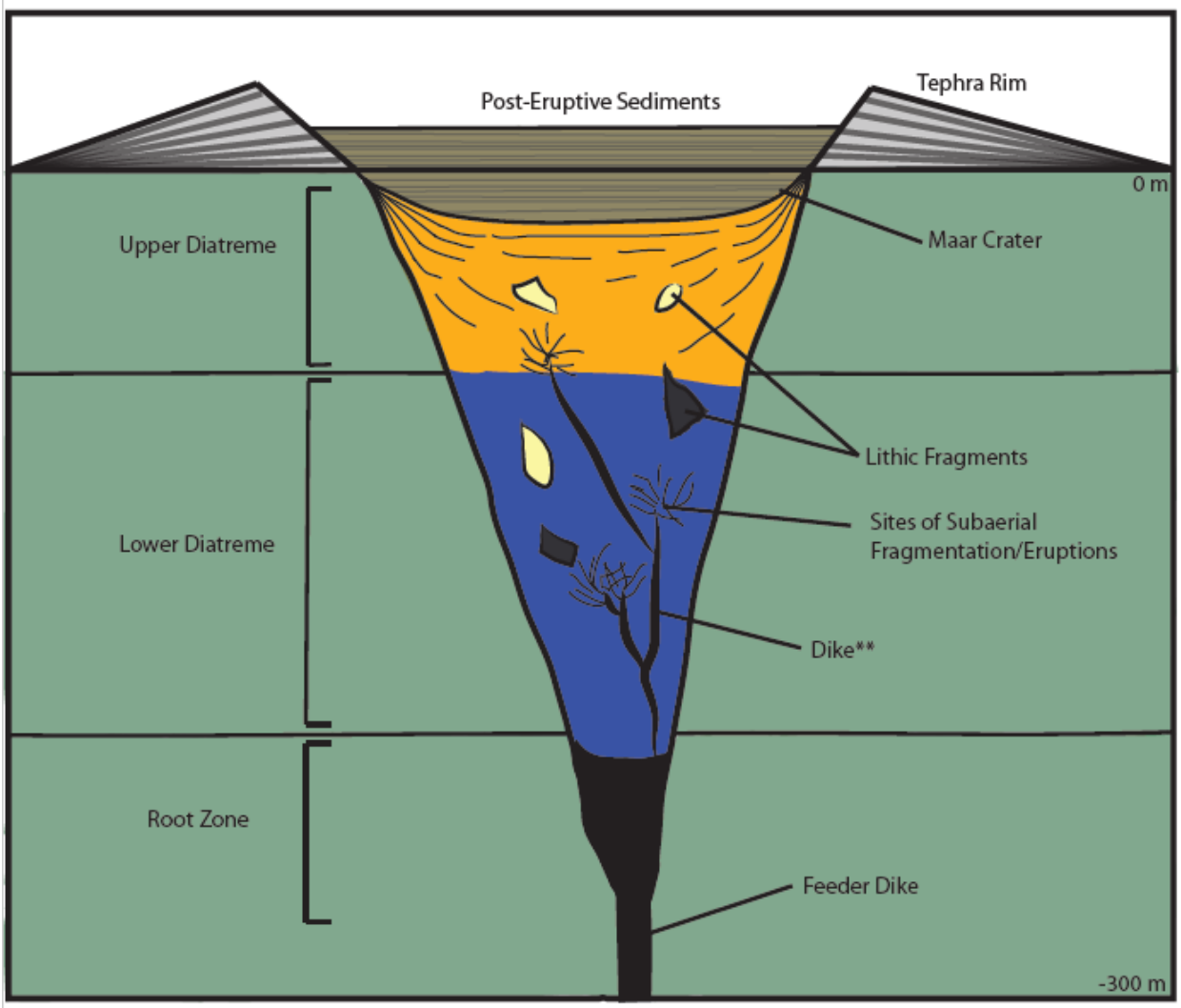

Figure 1.1 An illustration of the general anatomy of a maar-diatreme volcano compiled from descriptions in White and Ross (2011), Valentine and White (2012), and Lorenz (1986). The maar crater is excavated below the pre-eruptive surface and later filled with post-eruptive sediments. The crater is surrounded by a tephra ring that is composed of bedded lapilli tuff with some lithic fragments. The diatreme forms a cone shape and can be divided into three zones: the upper diatreme, lower diatreme, and the root zone. The upper diatreme is composed of bedded pyroclastic deposits that may be cross cut by nonbedded volcaniclastic material. The lower diatreme is composed of mixed pyroclastic debris with some cross-cutting dikes and debris jet deposits. The root zone marks the transition between the diatreme and the feeder dike and is composed of a mix of coherent igneous material and fragments of country rock. Scale on the right shows approximate depth of the maar-diatreme volcano in meters.

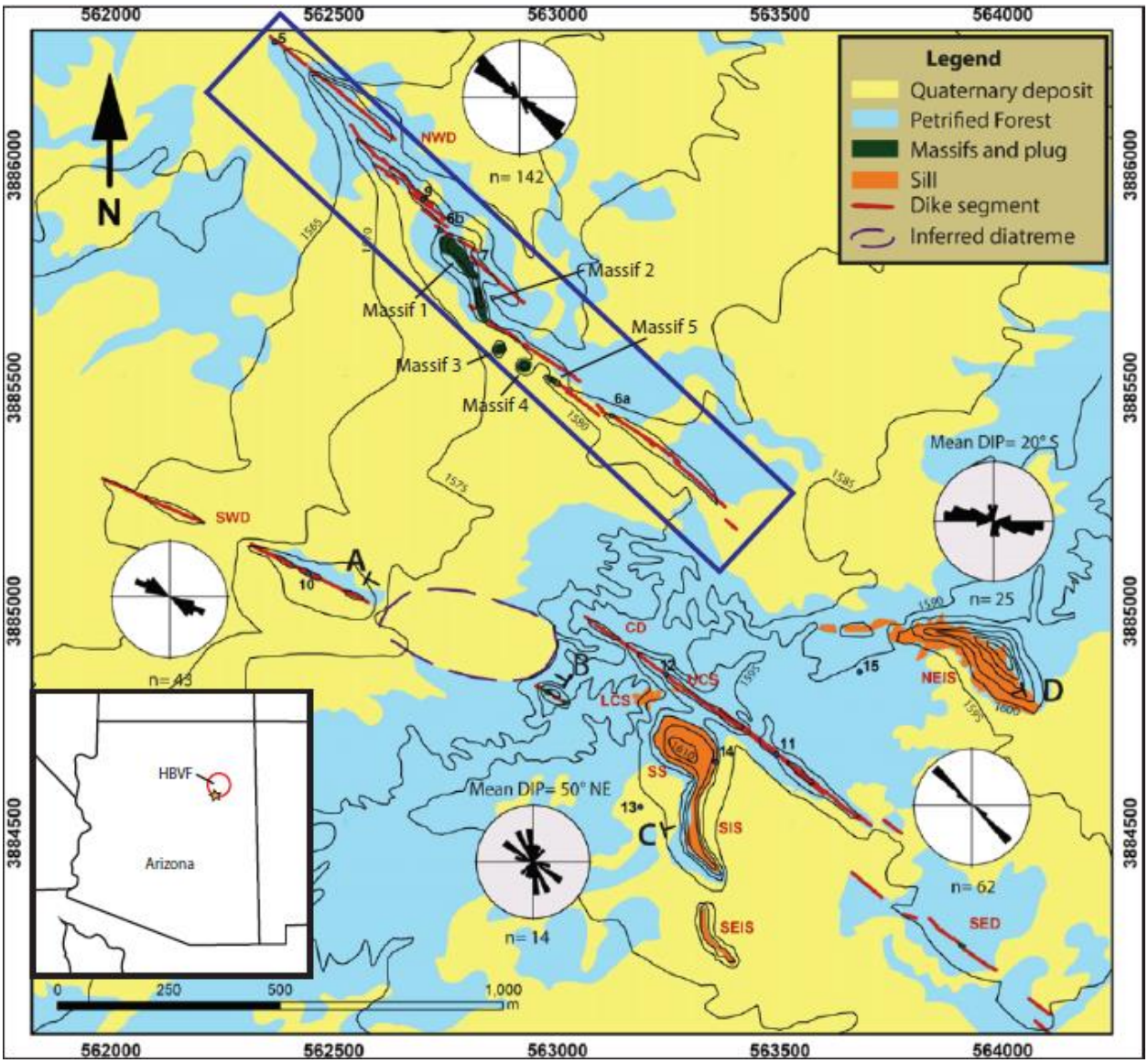

Figure 1.2 Map of the Jagged Rocks Complex in the Hopi Buttes Volcanic Field, including the general location and orientation of the different dike swarms, sills, and massifs present within the field. Strike data from Re et al. (2015) in the form of rose diagrams with 'n' indicating the number of measurements. A blue box surrounds the dike swarm on which this study focuses and massifs in that area are labeled 1 through 5. 'Petrified Forest' refers to the Petrified Forest Member of the Chinle Formation. Inset map shows location of Hopi Buttes Volcanic Field in Arizona. The star indicates the location of the Jagged Rocks Complex. Modified from Re et al. (2015).

overlies the Moenave Formation and consists of fluvial and lacustrine mudstone and sandstone as well as basaltic volcanic deposits (Reppening and Irwin 1954, Billingsley et al. 2013). The groundwater table at the time of the formation of the Hopi Buttes Volcanic Field was near-surface, meaning that the Chinle, Moenave, and Bidahochi Formations were all likely-water saturated at the time of the eruptions (White 1989; 1990).

After the volcanic eruptions ended, erosion related to the development of the Little Colorado River drainage created differential exposure of the maar-diatreme volcanoes and feeder structures with the depth of erosion increasing from northeast to southwest (Shafiqullah and Damon 1986; Re et al. 2016). The Jagged Rocks Complex (JRC) is located in the southern-most portion of the volcanic field and is exposed approximately 350 m below the pre-eruptive surface in the Petrified Forest Member of the Chinle Formation (Re et al. 2015). The deep erosion exposed a series of feeder dikes, transgressive sills, massifs, and buds that supported multiple maar-diatreme volcanoes. Thus, exposures range from dike to root zone facies.

The Hopi Buttes Volcanic Field is an ideal area for the study of maar-diatreme volcanic systems and the deposits associated with their eruptions. The differential exposure in the field allows for studies of surface deposits down through deeper diatreme deposits and subsurface feeder structures. Early studies conducted in the Hopi Buttes Volcanic Field focused on describing the exposed structures, the pre-eruptive conditions that contributed to the formation of the volcanic field, the evolution of the field as a whole, and the stratigraphy of the Bidahochi Formation (e.g. Williams 1936; Hack 1942; Repenning and Irwin 1954; Shoemaker et al. 1957, 1962). These studies provide some insight into the processes that drive maar-diatreme eruptions, in order to help explain the formation of the structures exposed throughout the field. The Hopi Buttes Volcanic Field was also later mapped by Billingsley et al. (2013) as part of a USGS map

for the Winslow Quadrangle. This included unit descriptions and supporting material on the geologic features contained within the Hopi Buttes Volcanic Field. Later studies built upon these early works by using the well-exposed maar-diatreme structures to draw conclusions about the processes that drive maar-diatreme eruptions and how they evolve through their eruptive history (e.g. White and Fisher 1989; White 1989, 1991). These studies focus on understanding the environment in which the eruptions at the Hopi Buttes Volcanic Field occurred and how the saturated sediments of the Bidahochi Formation and water in the lower rock units fueled the evolution of the eruptions at the surface. White (1989) also used the post-eruptive crater deposits to understand the sedimentary environment into which the maar-diatreme volcanoes erupted.

Some recent studies have used the deeper-exposed structures to understand the transition between the diatreme and feeder dikes to gain insights into the evolution of the volcanic eruptions as a whole (e.g. Hooten and Ort 2002; Lefebvre et al. 2012, 2013). Hooten and Ort (2002) used exposed widened sections of dikes with peperitic margins in the Hopi Buttes as well as experimental data to further understand the conditions that control the initial interaction between the dike and wet sediment and the conditions of peperite formation. Lefebvre et al. (2012 and 2013) focused on spatter dikes at the Castle Butte Trading Post and diatremes in Standing Rocks West respectively. These studies focused on subsurface structures as keys to understanding diatreme formation at depth and magma supply and diversion between vents during eruptions.

Lefebvre et al. (2012) studied the role of spatter dikes at the Castle Butte Trading Post volcanic complex is important to my work because it focuses on the diversion of magma near the surface during maar-diatreme eruptions and how pulses of magma through the system influence the eruptions occurring in the related maar-diatreme conduits. Their findings concluded that, near

the surface, magma was diverted into fissure segments, non-exposed dikes, or other vents. Pulses of magma through the system and the diversion of magma into these structures caused stops and starts in eruptive activity at aligned vents. Lefebvre et al. (2012) provides broader implications for the flux of magma supply in small, monogenetic volcanic fields and how magma supply to surface eruptions can change during the development of a shallow feeder dike system.

1.3 The Jagged Rocks Complex

The Jagged Rocks Complex (JRC) is composed of feeder dikes, transgressive sills, large columns of volcaniclastic material called massifs, and smaller columns called buds (defined below) that fed approximately three to five maar-diatreme volcanoes at the surface. These dikes, transgressive sills, buds, and massifs provide insight into the shallow subsurface system that supported the maar-diatreme eruptions. The dikes generally strike NW-SE to WNW-ESE and are segmented in an irregular to en-echelon manner (Figure 1.2). The dikes are composed of coherent intrusive monchiquite with phenocrysts and megacrysts of clinopyroxene +/- phlogopite in a fine to medium groundmass (Re et al.2016, in review). Geochemical analyses done by Re et al. (in review) indicate that the northwest dike swarm is distinct from the remainder of the structures present in JRC. The presence of phlogopite and lack of olivine in the northwest dike swarm and the different chemistry of the cores and rims of the clinopyroxene phenocrysts indicate that, while the magma source for the dikes was the same, this distinct batch of magma had a much quicker ascent rate than the remainder of intrusions in the field (Re et al. in review). The dikes' contact with country rock is sharp and each swarm shows a two- or three-zone pattern that is interpreted to be associated with different phases of magma movement through the dikes (Figure 1.3; Re et al. 2015, 2016). The boundaries of each of the layers roughly parallel the walls of the dike and each layer is distinguished by the vesicle shape, size, and abundance as well as

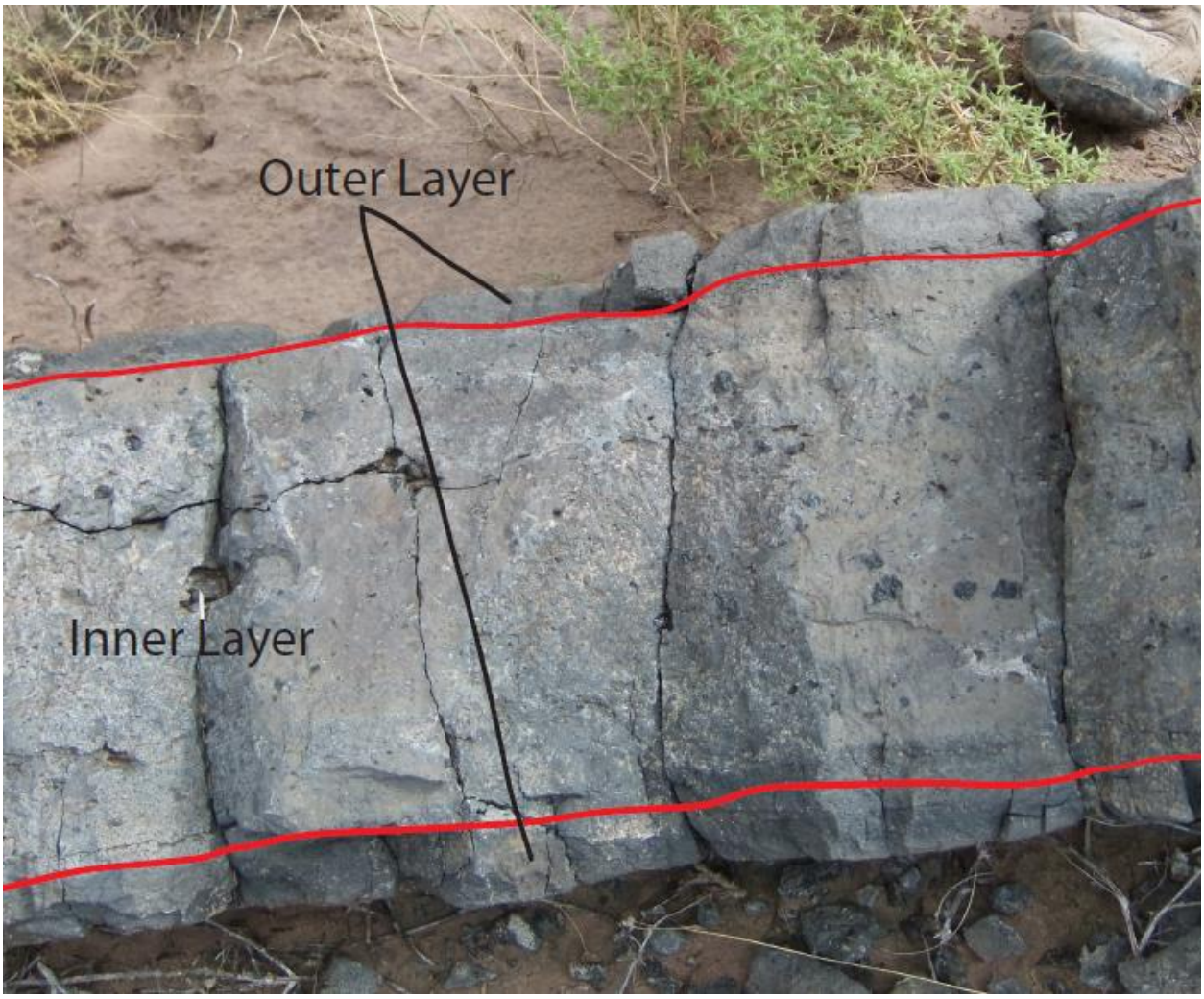

Figure 1.3 Layers in a dike have sharp contact with the country rock. The outer chill margins are darker; contain fewer and smaller vesicles, and few to no phenocrysts. The inner layers generally contain more and larger vesicles as well as more and larger phenocrysts.

variations in phenocryst size and abundance (Re et al. 2015). Dike segments range from tens to hundreds of meters long and their thicknesses do not commonly exceed one meter (Re et al. 2015, 2016; Muirhead et al. 2016). Some of the dike segments contain angular to sub-rounded country-rock fragments that have a spatially variable concentration. Their presence indicates that

during propagation there was local dike-tip bifurcation and country-rock wedging (Re et al. 2016).

The transgressive sills in JRC are concentrated in the southeastern portion of the field. Muirhead et al. (2016) described the combination of sills and inclined sheets found in Hopi Buttes Volcanic Field as one feature, a transgressive sill, which climbs stratigraphy in a step-wise fashion. The transgressive sills have a similar composition to that of the dikes, being composed of coherent intrusive basanite to tephrite, and also have sharp contacts with the surrounding country rock (Re et al. 2015; Muirhead et al. 2016). The sill segments may intrude between layers in bedded sedimentary rocks, but also occur in massive mudstone with no clear bedding (Muirhead et al. 2016). The mean dips and thicknesses of the transgressive sill segments are 21° and 0.85 m respectively (Muirhead et al. 2016).

Buds are anomalously widened sections of dikes (Delaney and Pollard 1981; Hooten and Ort 2002). In JRC, most buds are exposed along the SW dike swarm and occur between dike segments or at dike tips. They are generally two to three meters thick and 15 m long and consist of juvenile and host-rock clasts mixed with coherent intrusive rocks (Re et al. 2016). Massifs are wide (>5 m), elongate to sub-circular, igneous bodies made up of layered and closely packed pyroclastic bomb deposits. They are made up of breccia and lapilli tuff that exhibit varying degrees of welding, but the deposits are generally highly welded. The massifs also contain differing proportions of country-rock fragments (Re et al. 2016). Five massifs are exposed in the northwestern dike swarm, the portion of the JRC studied in this thesis.

The structures exposed in JRC provide insight into how the shallow plumbing below maar-diatreme volcanoes fed eruptions at the surface both in the Hopi Buttes Volcanic Field and

other similar volcanic fields. The Hopi Buttes Volcanic Field has excellent exposures of maar-diatreme structures all the way from the surface maar craters through the diatremes and root zones and down to the feeder systems. This range of exposure is uncommon, allowing for connections between the subsurface feeder systems and the main volcanic vents. The exposures in JRC allow for a detailed study of the diversion of magma below the volcanic vents and how they relate to and influence the eruptions at the surface. By looking quantitatively at the flow fabrics in the dikes as records of magma pulses through the systems, conclusions can be drawn about the magma movement through the system and how it actively supported the eruptions.

1.4 Previous AMS and AARM work on dikes

Anisotropy of magnetic susceptibility (AMS) and anisotropy of anhysteretic remanent magnetism (AARM) have been used to infer magma-flow patterns in dikes in order to understand their relation to main conduits and, in some cases, magma chambers (e.g. Knight and Walker 1988, Herrero-Bervera et al. 2001, Soriano et al. 2008). Knight and Walker (1988) is the oldest study using AMS to interpret flow history and direction within a swarm of dikes. These authors used imbrication of the AMS ellipsoid relative to the dike plane to determine flow directions and azimuth of 59 dikes in the Koolau Complex in Oahu, Hawaii. The physical orientations of magnetite grains have been shown to closely correspond to the principal AMS ellipsoid axes with the long axis of the grain corresponding to the axis of max susceptibility. Therefore, imbrication of AMS ellipsoids can be used as an effective proxy for the orientation of the magnetite grains within the dike (Knight and Walker 1988). Because of this correlation, the orientation of the AMS ellipsoid can be used as a good proxy for grain orientations and therefore is a good tool for understanding the flow fabric of a sample. Following this original study, others have used this principle of imbrication to determine flow history in various different dike

complexes (e.g. Rochette et al. 1992, Raposo and Ernesto 1995, Borradaile and Henry 1997, Borradaile and Gauthier 2001, Herrero-Bervera et al. 2001, Callot and Guichet 2003, Callot et al. 2004, Poland et al. 2004, Krasa and Herrero-Bervera 2005, Philpotts and Philpotts 2007, Soriano et al. 2008, Delcamp et al. 2014).

In their review paper, Rochette et al. (1992) described four main types of fabrics found in AMS studies of dikes of many compositions and viscosities: normal, inverse, intermediate, and other/anomalous fabrics. Normal magnetic fabrics are those directwely associated with magma-flow directions because elongate magnetite grains with K_1 along the long axis are assumed to line up with the flow direction of magma during emplacement. This fabric is defined by K_1 and K_2 axes being parallel to the intrusion plane of the dikes and the K_3 axis being perpendicular to the plane (Rochette et al. 1992; Herrero-Brevera 2001). The magnetic axes parallel to the plane show the direction of magma flow. K_1 axes can be clustered on either side of the dike plane, which may reflect imbrication of the grains against the walls of the dike and can be used to determine the azimuth of the magma flow (Knight and Walker 1988). Inverse magnetic fabrics are controlled by the presence of single domain (SD) magnetite grains in a sample. Magnetite grains can be single domain, pseudo-single domain (PSD) or multidomain (MD). Grain domains form during crystallization of the magnetite particles to lower magnetostatic energy and can influence the magnetic properties of the grains. Grains are inherently assumed to have the axis of maximum susceptibility (K_1) aligned with the long axis of a grain, but in SD grains the axis of maximum susceptibility aligns with the short axis of the grain, causing a switch of the positions of the K_1 and K_3 axes relative to the dike plane. In an inverse fabric the K_3 axis is parallel to the dike plane and the K_1 axis is perpendicular to the dike plane (Rochette et al. 1992; Herrero-Bervera 2001). An intermediate fabric is defined by the K_2 axis being perpendicular to the dike

plane and K_1 and K_3 parallel to the plane (Rochette et al. 1992). The final fabric type is anomalous fabrics. These are fabrics that do not fit into the three main fabric type categories. They are characterized either by a scattered plot of susceptibility axes or a mix of normal, inverse, and intermediate fabrics on one plot (Rochette et al. 1992). These anomalous fabrics have been suggested to be caused by the presence of single domain (SD) and multi-domain (MD) magnetite grains within one dike (Borradaille and Gauthier 2001).

Anisotropy of anhysteretic remanent magnetization (AARM) can be measured to help further define anomalous or inverse fabrics in a sample, allowing for the correct interpretation of magma flow. Measurements of AMS take into account the magnetic contributions of all ferro- and para-magnetic minerals to the susceptibility, but in some cases this can complicate the measurements of rock fabric because the size and orientation of para- and ferromagnetic minerals do not necessarily coincide (Potter 2004). AARM measurements only take into account the contributions of remanence-bearing, ferromagnetic minerals to the magnetization and can thus provide a better representation of the orientation of the ferromagnetic minerals (e.g. magnetite) within the fabric (Soriano et al. 2016). When an AARM plot differs significantly from an AMS plot, it can clarify anomalous or inverse fabrics so that a flow fabric can be determined. The technique for measuring AARM is much slower and generally the data are less precise, thus AMS is the preferred method for analyzing magnetic fabrics in most situations.

Curie Points and Isothermal Remanance Magnetism (IRM) were measured for specimens in addition to AMS and AARM to determine the mineralogy of the remanence-bearing minerals as well as their domains. Both of these properties are important to measure because they help explain how the magnetic minerals contribute to and influence the AMS and AARM as well as provide confidence in the magma-flow-fabric interpretations.

1.5 Purpose and Objective of This Study

Previous AMS studies of dikes have primarily focused on dike swarms associated with complex, long-lived volcanic systems. Studies focused on understanding dikes in short-lived, monogenetic volcanoes are nearly non-existent, likely due to the lack of good-quality exposures of shallow subsurface intrusions associated with these types of volcanoes, especially in close proximity to exposures of volcanic conduits in the same field. The Jagged Rocks Complex is unique in its exposure of shallow intrusions associated with maar-diatreme volcanoes, providing an excellent opportunity to investigate the role of shallow intrusions in the storage of magma and continuation of volcanic activity in monogenetic systems that generally lack the magma chambers of more long-lived volcanic systems.

Previous studies in the Jagged Rocks Complex focused on the physical volcanology and geochemistry of the exposed structures in order to understand how they formed and how they supported maar-diatreme eruptions at the surface. The flow behavior of the northwest dike swarm can provide crucial insights into the role the dikes played in the volcanic plumbing system contained in the complex. Most importantly this study aims to resolve whether the northwest dike swarm formed vertically as a separate system from the other intrusions in the complex or whether the dikes represent a form of shallow magma storage that may have been crucial for continuing eruptions in the complex.

Chapter 2: Project Methods

AMS was measured on specimens in order to obtain a quantitative understanding of the magnetic fabrics recorded within them. AMS measurements allowed for flow interpretation of the fabrics and were the main measurement conducted on the specimens. After AMS

measurements, other rock magnetic properties were measured: AARM, IRM, and Curie Points. AARM was important for understanding the source of anomalous AMS fabrics. AARM measurements aided in the interpretation of AMS flow fabrics. IRM and Curie Points were both important for accessing the domain type of the magnetic grains and the magnetic mineralogy. Together IRM and Curie Point measurements help fully define the magnetic mineralogy within the specimens. The properties of the magnetic minerals were important to understand because they influence the AMS. The ChRM was also measured in order to understanding the timing of the intrusion of the dikes. Understanding the relative timing of the intrusion of the dikes was important for developing and understanding of the formation of the dike swarm as a whole system. Finally, a magnetic survey was conducted to understand the general depth of the intrusions with the goal of understanding the depth of the intrusions below current exposure. Understanding the general depth of the dikes was also critical for the final interpretations of how the dike swarm formed as a whole.

2.1 Field Methods

Sampling in the Jagged Rocks Complex was focused on the northwest dike swarm (Figure 1.2 and 2.1). The locations chosen were thought to represent 'normal' sections of the dikes, meaning that they are nearly straight sections of the dikes with no unusual bends or breaks, which commonly occur near the segment termini. The locations also appeared to be in situ and coherent enough to be drilled. The strike and dip of the contact of the dike with country rock were measured at each location in order to understand the orientation of the dike. Each location was divided into individual sampling sites that correspond to the different near-vertical layers present and assumed to be associated with different phases of magma movement within the dikes. The different sites were divided out based on variations in vesicle size, shape, and

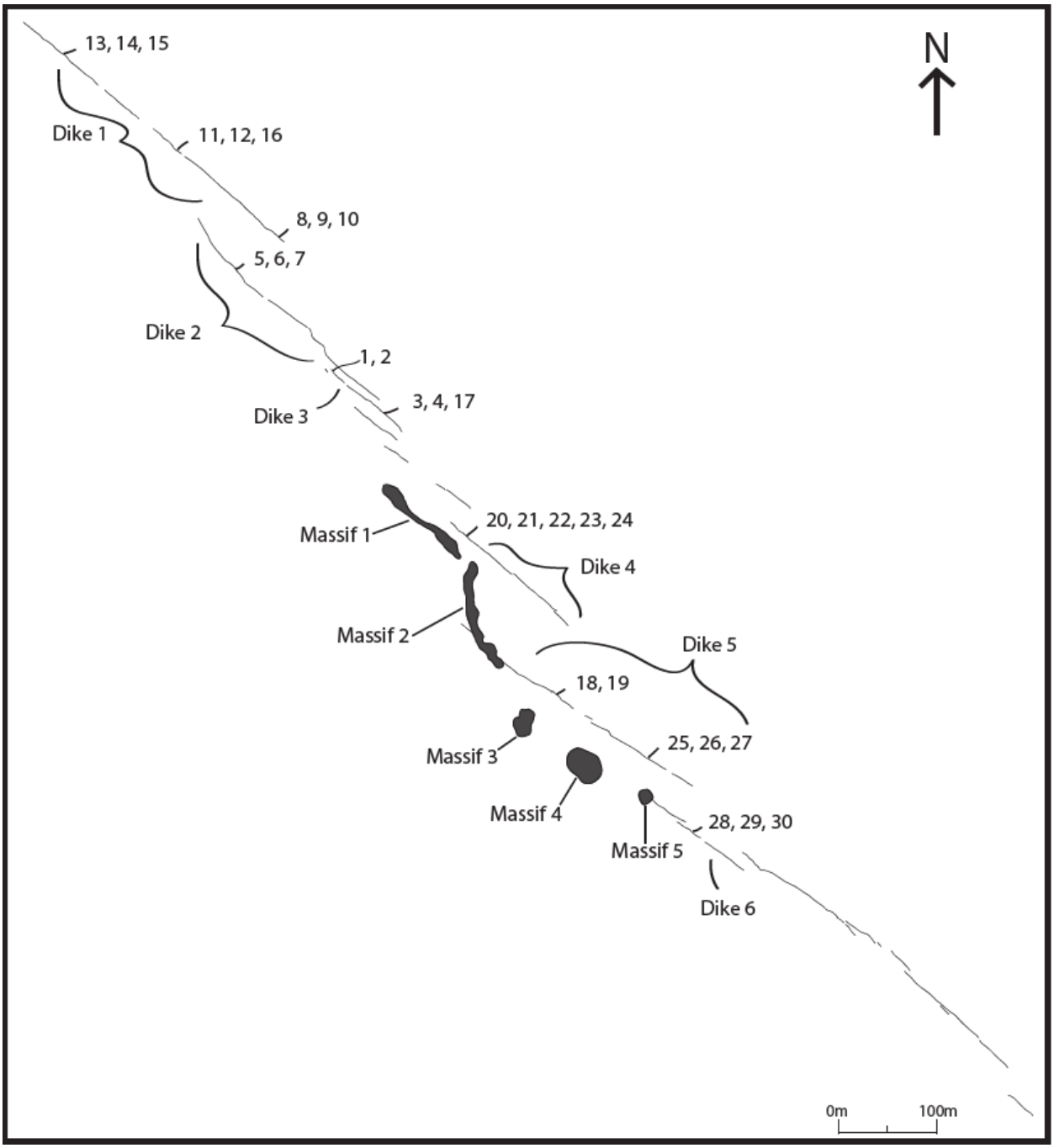

Figure 2.1 Map of the northwest dike swarm showing sampling sites along the different dike segments as well as the location of the five different massifs within the swarm.

abundance as well as phenocryst size and abundance. Each layer was treated as a separate site for a total of 30 sites drilled with an average of 12-15 cores drilled in each site. The cores were

oriented using a Pomeroy orienting fixture that gives the trend and plunge of each core's Z axis while the core is still in place in the dike. Each core was treated as a separate sample and labelled alphabetically along with the site number where the core was extracted. Each sample was then cut into a 22 mm-tall cylindrical core with a 25 mm diameter – a 'specimen'. In some cases, a single sample produced two to three different specimens. Rock magnetic analyses were then carried out on the specimens.

2.2 Rock Magnetic Methods

The rock magnetic methods used to analyze the dikes in JRC were anisotropy of magnetic susceptibility (AMS), anisotropy of anhysteretic remanent magnetization (AARM), isothermal remanent magnetization (IRM), and Curie point analysis. AMS was measured to determine the magnetic fabric in each of the specimens in order to understand the characteristics of the flow fabrics at each site. AARM was then measured on specimens from sites with AMS plots that showed a significant amount of scatter in the orientations of the magnetic axes. AARM allows for the interpretation of anomalous fabrics caused by SD grains. If the scatter is not due to SD grains, the anomalous AMS fabric will be reflected in a scatter of AARM axes as well. IRM was then analyzed on a subset of specimens to determine the domain of the magnetic minerals which was important for understanding the influence of domain on the AMS and AARM results. Curie points were measured for a subset of specimens to determine the mineralogy of the remanence-bearing grains. The mineralogy of the grains was also important to know for accurate interpretation of AMS and AARM. These analyses, used together, define the magnetic properties of the dikes that allowed for accurate interpretation of the flow fabrics preserved within them.

2.2.1 Anisotropy of Magnetic Susceptibility (AMS)

AMS is a fast, non-destructive method for analyzing the magnetic fabrics contained within a specimen. An oriented specimen is measured along six or more dispersed orientations to get a sense of the anisotropy of the minerals within the specimen; these properties define the fabric contained within. With the measurements of multiple specimens from one site, a flow fabric for the dike can be determined.

Magnetic susceptibility, k, is a dimensionless scaling factor between the induced magnetization (J_i) and the external field (H) of a specimen where $J_i = kH$. When the susceptibility, k, exhibits directional dependence, the specimen is considered to have anisotropic magnetic susceptibility (Butler 1992). Anisotropy in a specimen can be derived from two sources: the shape of magnetic mineral grains (called shape anisotropy), and the distribution of magnetic mineral grains contained in a specimen (called distribution anisotropy) (Cañon-Tapía 2001). Where distribution anisotropy is dominant, the magnetic interactions between particles overpower the anisotropy derived from the shape of the grains. Where shape anisotropy is dominant, the situation is reversed. Some studies suggest that the main source of AMS is derived from shape anisotropy, but there is no definitive understanding of the source of AMS within dikes (Cañon-Tapía 2001).

The measurements made during AMS analyses are three principal susceptibility axes measured in SI units (K_1, K_2, and K_3) that define the axes of a triaxial ellipsoid of susceptibility in which $K_1>K_2>K_3$ (Knight and Walker 1988, Rochette et al. 1992). The different AMS fabrics (normal, inverse, etc. see section 1.4 for review) are identified by plotting the three axes (K_1, K_2, and K_3) on a lower-hemisphere equal-area diagram along with the strike and dip of the dike. The mean bulk susceptibility of a specimen is the average of the susceptibilities of the three axes and

is defined as $K_{mean} = (K_1+K_2+K_3)/3$ (Knight and Walker 1988, Rochette et al. 1992). The three axes can also be used to define the lineation (L), foliation (F), and degree of anisotropy (P) of a specimen. The lineation is defined by the ratio of the K_1 and K_2 axes where $L = K_1/K_2$, the foliation is defined by the ratio of the K_2 and K_3 axes where $F = K_2/K_3$, and the degree of anisotropy is defined by the ratio of the K_1 and the K_3 axes where $P = K_1/K_3$ (Jelinek 1981, Knight and Walker 1988, Rochette et al. 1992). The shape factor (T) can also be calculated with the three output axes using the equation $T = \frac{(2\ln(K2))-\ln(K1)-\ln(K3)}{(\ln(K1)-\ln(K3))}$ (Eriksson et al. 2015). If T is between zero and one, the shape is oblate (disc), and if T is between zero and negative one, the shape is prolate (rod). If T is approximately equal to zero, then it is an intermediate configuration and the ellipsoid is described as triaxial. The shape factor, lineation, foliation, and degree of anisotropy can be used to further describe the characteristics of the magnetic fabric present within a site as well as help distinguish between the different sites.

Directional flow is determined through interpretation of imbrication of the AMS ellipsoids relative to the dike plane for each site. Elongate magnetite grains are assumed to be aligned by the laminar flow of the magma within a dike such that the long axis of the grains aligns parallel or nearly parallel to the flow and the short axis aligns perpendicular or near perpendicular to the plane of shear (Knight and Walker 1988). The physical orientation of the magnetite grains (long, short, and intermediate axes) has been shown to correspond closely to the same axes of the AMS ellipsoids with the long axis nearly parallel to flow direction and the short axis near the direction of the velocity gradient (Knight and Walker 1988). The principal axes become tilted in flow imbrication, because imbrication minimizes angular-momentum transfer and makes collisions as minimally impactful as possible (Knight and Walker 1988). Grains subsequently pile up at low angles to the flow plane and dip toward the source of the flow in a

similar manner to imbrication in river channels. Imbrication is reflected in the AMS stereoplots as symmetrically inclined clusters of K_1 axes on either side of the dike plane. Imbrication is discussed in detail in section 4.1. The inclination of K_1 axes for paired dike margins is then used to interpret the absolute flow direction of the magma through that section of the dike. A secondary method can be used if the K_1 axes do not clearly provide a pair of oppositely inclined axes for flow interpretation. This method involves the use of K_3 axis imbrication relative to the pole to the plane of the dike to look at imbrication of the ellipsoid (Alva-Valdivia et al. 2005, Porreca et al. 2015). Using the K_3 axes for interpretation can possibly provide a clearer sense of the imbrication of the AMS ellipsoid relative to the dike plane and can provide interpretable flow fabrics compared to K_1 axes. When comparing chill margins to middles of dikes in the NW dike swarm, the margins reflect the flow behavior during the initial formation of the dikes and can provide information about the swarm's initial formation. The middle sections record later movement within the dikes and can provide information about possible changes in flow behavior.

AMS was measured for 437 specimens from all 30 sites using a Kappabridge KLY-4S spinning specimen magnetic susceptibility bridge in the rock magnetics lab at Northern Arizona University. Each specimen was marked and measured at three separate orientations. The first position spun the specimen about the z axis, which is marked along the in-place core in the field. This position measured the AMS in the x-y plane of the specimen. The second position spun the specimen about the y axis and measured the AMS in the x-z plane of the specimen. The third position spun the specimen about the x axis and measured the AMS in the y-z plane of the specimen. For each position, the susceptibility was measured 64 times during one revolution (with one revolution per 2 seconds). The bridge was zeroed before the specimen was inserted, so

that the susceptibility differences were measured between the direction in which the bridge was zeroed and the susceptibilities in the respective directions. The bulk susceptibilities were also measured for each specimen using the Kappabridge KLY-4S susceptibility meter. This involved the bridge being zeroed followed by insertion and measurement of the specimen. Data from each site were then analyzed using the program Anisoft 4.2, which processed the data from each site using multivariate statistics outlined by Jelinek (1987). Processing in Anisoft 4.2 resulted in an estimate of the mean normalized tensor and the estimates of the principal susceptibilities. From these, the program derived estimates of the mean directions with the respective regions of confidence for each site. The program then can plot these on top of the specimen data for a site resulting in an AMS plot complete with mean directions and error ellipses.

The trend and plunge initially entered when measuring AMS for sites MK1-27 were off by ninety degrees due to a difference in the parameter terms used by the program for converting sun orientations into sun-corrected trends. These were corrected in the Anisoft 4.2 program after the error was found. The correction process involved calculating the correct sun-corrected trend and amending all the orientations of the specimens by switching between the geographic and sample coordinate systems in Anisoft 4.2. Sites MK28-30 were analyzed after the error was discovered and used the correct trend and plunge, thus not needing to undergo the process to fix the specimen parameters.

In the case of MK19, for which both margins of the dike were sampled under the same site name due to poor outcrop quality, the specimens from the margin with worse outcrop quality were divided out from the majority and made into a separate sub-site MK19a. This sub-site of MK19 had too few specimens for good statistical analysis but did allow for the interpretation of a flow direction based on the imbrication of K_1 and K_3 axes for both MK19 and MK19a. In the

case of MK1, for which there was only one specimen from the southern margin, the specimen was not used in the final analysis in Anisoft 4.2 so that the AMS plot represents the main margin sampled. For MK1 and MK19, this was done so that the plots would represent the AMS fabrics from only one margin and the interpretations of the fabrics would not be muddled by specimens from the opposite margin of the dike.

2.2.2 Anisotropy of Anhysteretic Remanent Magnetization (AARM)

AARM was measured to help further define anomalous or inverse fabrics in a specimen, in hopes of acquiring a flow fabric from which a flow direction can be determined. Measurements of AMS take into account the magnetic contributions of all minerals to the susceptibility but sometimes this can complicate the measurements of AMS because the orientation of paramagnetic and ferromagnetic minerals do not necessarily coincide. AARM measurements only take into account the contributions of remanence-bearing ferromagnetic minerals to the magnetization and can thus provide a better test of the actual orientation of the magnetic minerals within the specimen (Soriano et al. 2016). This is done by demagnetizing the specimen and then applying an Anhysteretic Remanent Magnetization (ARM) to it and measuring the remanent magnetization. This process is repeated for nine orientations. The end product of all the measurements is an AARM ellipsoid that is defined by the same three magnetic axes as the AMS ellipsoid.

AARM measurements were conducted at the paleomagnetic lab at New Mexico Highlands University. For these measurements, I chose three sites that showed anomalous fabrics defined by a large amount of scatter in the K_1, K_2, and K_3 AMS axes. I measured five specimens from each of three different sites (MK1, MK11, and MK16). Each specimen was measured in nine distinct orientations (XY, -XY, XZ, -XZ, YZ, -YZ, X, Y, and Z) as well as measured

initially to get a base-line measurement (BLM). The BLM was measured first by demagnetizing the specimen in a peak alternating field of 120 mT in X, Y, and Z orientations using an ASC-Scientific D-2000 AF demagnetizer. The specimen's remanent magnetization was then measured in three different positions using an AGICO JR-6A Dualspeed Spinner Magnetometer. An Anhysteretic Remanent Magnetization (ARM) was then imparted to the specimen along one of the nine specific axes of the specimen by exposing it to a peak alternating field of 100 mT with a coaxial direct current field of 0.1 mT. The remanent magnetization was then measured again and subtracted from the BLM to get the component due to ARM. The specimen was then demagnetized in a peak 120 mT alternating field along its X, Y, and Z axes to remove the previous ARM. The process was then repeated for the remaining orientations. X, Y, Z, and M values and geographic declination and inclination for all nine orientations as well as the BLM were input into an excel spreadsheet prepared by Mike Petronis from New Mexico Highlands University to calculate the AARM K_1, K_2, and K_3 values for each specimen as well as the L, F, P, and K_{mean} values. The measured specimens from a specific site were then compiled into a single AARM plot for the site. The AARM plot can then be compared to its AMS plot.

2.2.3 Isothermal Remanent Magnetization (IRM)

IRM can further help define the magnetic minerals within a specimen by determining whether the magnetite in the specimens is SD, MD, or PSD, which is useful when interpreting the AMS and AARM results. IRM was measured for two specimens from each of the three sites that were analyzed for AARM (MK1, MK11, and MK16). The remanent magnetization was first measured before the specimen was exposed to any magnetic fields. This was done using the same AGICO JR-6A Dual Speed Spinner Magnetometer as was used for the AARM measurements. The specimen was then exposed to a 10 mT field produced by an impulse

magnetizer. The magnetization was then measured again using the spinner magnetometer. This process was repeated for field strengths of: 10, 20, 40, 60, 80, 100, 120, 140, 160, 180, 200, 230, 250, 280, 300, 400, 600, 800, 1000, 1250, and 2500 mT. The shape of the produced curve when magnetization was plotted against field strength indicates which type of magnetite (SD, PSD, MD) is contained within the specimen, based on the field intensity at which half the saturation isothermal remanent magnetization (SIRM) was acquired (Dunlop 1972, Rolph 1997). Background IRM was also measured using a similar process. The specimen was exposed to a magnetization at the same steps as when measuring the IRM, but the specimen is flipped and only exposed to the field until the sign of the measured magnetization changes. This was only a few steps for most magnetite-bearing specimens. From the IRM data, $B_{1/2}$ values can be interpolated. $B_{1/2}$ values are the field strength at which the magnetization of the specimen is half the saturation isothermal remanence. These values provided direct insight into the domain of the titanomagnetite based on the range of values. The domain of the grains is important to know to understand and interpret AMS and AARM fabrics.

2.2.4 Curie Point Analysis

Curie points were determined for one to two sites from each dike to assess the magnetic mineralogy of the dikes. Eleven specimens were analyzed in total. Each specimen was ground down into a fine powder and then a 4-4.5 g portion of the specimen weighed out. This was then placed in a quartz test tube and loaded into an MFK1-A multi-function Kappabridge that was set up to measure Curie points. Heating and cooling curves were then produced through the measurement of susceptibility while gradually heating and then cooling the specimen. The heating and cooling curves were used to determine the Curie point for the measured specimens. The heating curves in particular were of interest for determining the mineralogy of the magnetic

particles contained within my specimens. The heating curves were then analyzed using the Cureval8 program, which plots the heating and cooling curves alongside each other as T (°C) vs the susceptibility (K) plots. Processing in Cureval8 first involved correcting the heating curve for the susceptibility of the empty, clean quartz test tube and then looking for the dominant, high susceptibility peak in the heating curve. This point was then selected within the program as the Curie point for that one specimen. Depending on the value of the acquired temperatures, the mineralogy of the remanence bearing grains can be determined. With multiple Curie points for specimens throughout the sampled dike swarm, a general conclusion can be made about the composition of the magnetic minerals contained within my specimens and dikes.

2.2.5 Characteristic Remanent Magnetization (ChRM)

Characteristic Remanent Magnetization (ChRM) was measured in order to understand whether all six dikes formed at the same time, which would be indicated by similar pole positions for all the measured sites. This was done by Alternating Field Demagnetization in order to calculate an average magnetic pole position for each location along all six dikes. A mean for the entire suite was determined from those averages to compare with the location averages. Two to three specimens were measured from each of the 30 sites along all six dikes. Each specimen was initially measured using the Minispin magnetometer after being calibrated using a standard. The specimen was measured in four positions (+y -z, -x -z, -y +z, +x +z) using the short spin setting in the Spinwin program. The measurements were then averaged to produce a declination, inclination, and magnetization for the specimen. The specimen was then put in a Molspin shielded demagnetizer and exposed to a 25 mT magnetic field while continuously spinning. The field was slowly increased and held at 25 mT for three seconds before slowly coming back down. The specimen was then measured again using the Spinwin program and the Minispin

magnetometer in the same four positions. This process was then repeated for 100, 200, 300, 400, and 600 mT for each specimen. Thirty-two of the specimens were further measured at 800 and 1000 mT to ensure the specimen was demagnetized to ≤10% of the initial value and to get a better idea of the declination and inclination of the specimen. The data were then processed using PuffinPlot (Lurcock and Wilson 2012). The pole positions were determined first by performing a principal component analysis (PCA) for each specimen from the steps where the subtraction curve shows a straight line towards the origin. The Fisher averages were then calculated for each location along each dike to get an average pole position for each location. The suite mean was then calculated from the Fisher averages to find a pole position and confidence ellipse for the entire dike swarm. From the Fisher averages and the suite mean, the differences in pole positions provide crucial information for understanding the general timing of the intrusion of the dikes.

2.3 Magnetic Survey Methods

A magnetic survey was conducted that focused on the northwestern half of the dike swarm with the goal of understanding how the dikes continue at depth and if they continue to the northwest of where their surface exposure terminates. This was done by measuring along a series of transects oriented SW-NE that crossed approximately perpendicular to the strike of the dikes. The survey was conducted on foot using a Geometrics 856 magnetometer. Two people were required to collect the data: one leading with a GPS marking the position and the second following with the magnetometer and GPS data logger taking readings. Individual measurements were taken a few meters apart and transects were spaced approximately 10 to 20 meters apart depending on the topography and exposure of dikes and massifs. A larger loop was also walked around the southeastern part of the dike swarm to see if there were any interesting anomalies that could be associated with unexposed dike segments. The resolution of the southeastern portion of

the dike swarm is much less than that of the northwestern portion due to only one loop being surveyed around the southeastern portion. The magnetic readings were then retrieved from the magnetometer. The base station readings were removed and the data were processed minimally to produce a georeferenced map of magnetic anomalies and transects. The topography was also overlaid as well as a simple map of the dike swarm.

In order to calculate an approximate depth based on the anomalies, the Peter half-slope method was applied to the two strongest anomalies to approximate the depth of the dikes. The calculations involve first plotting the profile of the anomaly using the data collected for the transect line of the anomaly of interest. Then a tangent line is drawn to the point of maximum slope and a second line is drawn with half the slope of the first line. Two additional lines are drawn with the half-slope value where they fit the profile. The horizontal distance between the intersection points of the two additional tangents is a measure for the depth to the magnetized body. For my data, these half-slope calculations were conducted using a script for Matlab prepared by Ryan Porter at Northern Arizona University.

Chapter 3: Results from Magnetic Analyses

The majority of sites' AMS measurements produced normal fabrics, with only three sites showing other fabrics. Their magnetic properties showed variances in prolate or oblate shapes as well as weak lineations and foliations. AARM was used to investigate the sites whose fabrics showed a wide spread of AMS axes or anomalous fabrics. AARM results showed some possible interference of single-domain grains in the AMS fabrics. This finding was reinforced by the IRM results indicating the magnetite domain type was pseudo-single domain edging on single-domain. The Curie Points for the measured specimens showed high-titanium titanomagnetites.

The ChRM was measured to understand the timing of the formation of the dikes relative to one another and showed that the dikes in the northwest dike swarm all formed around the same time. The magnetic survey results indicated that the dikes do not continue deep below their exposed level, building upon the AMS flow directions in the final interpretations of the formation of the northwest dike swarm.

3.1 AMS Results

AMS results were grouped based on which dike they came from along the northwest en-echelon dike sequence. Multiple locations were sampled along half of the dikes, but only one location on dikes 2, 4, and 6 was sampled due to scarcity of drillable outcrop or time limitations (Figure 2.1). The sites were defined and separately sampled at each location based on variations in vesicle shape, size, and abundance, as well as the size and abundance of phenocrysts within the dike. Sites can be defined either as margin or middle sites which is important when interpreting the flow directions and behavior recorded by the AMS. The margin sites record flow within the dikes during their initial formation whereas the middles record later flow within the dikes.

Thirteen sites show an oblate mean AMS ellipsoid shape with a stronger average lineation (L) than foliation (F) and a negative shape factor (T) (Figure 3.1). Shape factor (T) indicates the shape of the AMS ellipse as oblate, prolate, or triaxial. Seventeen of the sites show a stronger average F than L and positive T, making the mean ellipsoid prolate in shape (Figure 3.1). The 21 margin sites show an even split between oblate and prolate ellipsoids whereas the ten middle sites are dominantly prolate with only a few showing oblate ellipsoid shapes. When compared with the middle sites, the paired margins at a location tend to have more similar magnetic properties, such as bulk susceptibilities. The majority of the sites show normal or

dominantly normal fabrics, in which the K_1 and K_2 axes are parallel to the dike plane and the K_3 axis is perpendicular. Dominantly normal fabrics are defined by the majority of the specimens from a site showing a normal fabric with no more than three to five specimens showing deviant axis orientations. Two sites show anomalous fabrics, which are defined by a wide scatter of AMS axes or a mix of different types of fabrics. One site shows a dominantly intermediate fabric, which is defined by the K_1 and K_3 axes being parallel to the dike plane and the K_2 axis perpendicular with a few deviant axis orientations. All three of these sites are middle sites.

3.1.1 Dike 1

Sites MK13-15 are located on the northwest end of dike 1, two to three meters northwest of an offset in the dike (Figure 2.1). MK13 and MK14 are the southern and northern dike margins, respectively, defined by smaller (2-3 mm) vesicles than the center and a lack of phenocrysts. Site MK15 is the center of the dike, which has larger (5-6 mm) vesicles at the zone's margins that become smaller (1-2 mm) toward the center. Clinopyroxene phenocrysts are present in MK15 as well. MK13 and MK15 have oblate ellipsoids, with a stronger foliation (F) than lineation (L) and a positive shape factor (T) (Table 3.1 and Figure 3.1). MK14 has a stronger L than F and a negative T, making the ellipsoid prolate (Table 3.1 and Figure 3.1). MK13 also has a slightly stronger degree of anisotropy than MK14 and MK15 (Table 3.1). The mean susceptibilities of the dike margins MK13 and MK14 are close in value whereas the mean bulk susceptibility of the middle site, MK15, is slightly higher (Table 3.1). MK13 and MK14 show normal magnetic fabrics with the K_1 and K_2 axes roughly parallel and K_3 axes perpendicular to the dike plane. At both these sites, the K_1 axes show some deviation from the exact strike of the dike plane. MK15 shows an anomalous fabric with a general scatter of the

three AMS ellipsoid axes due to a mix of specimens with normal and intermediate fabrics (Figure 3.2).

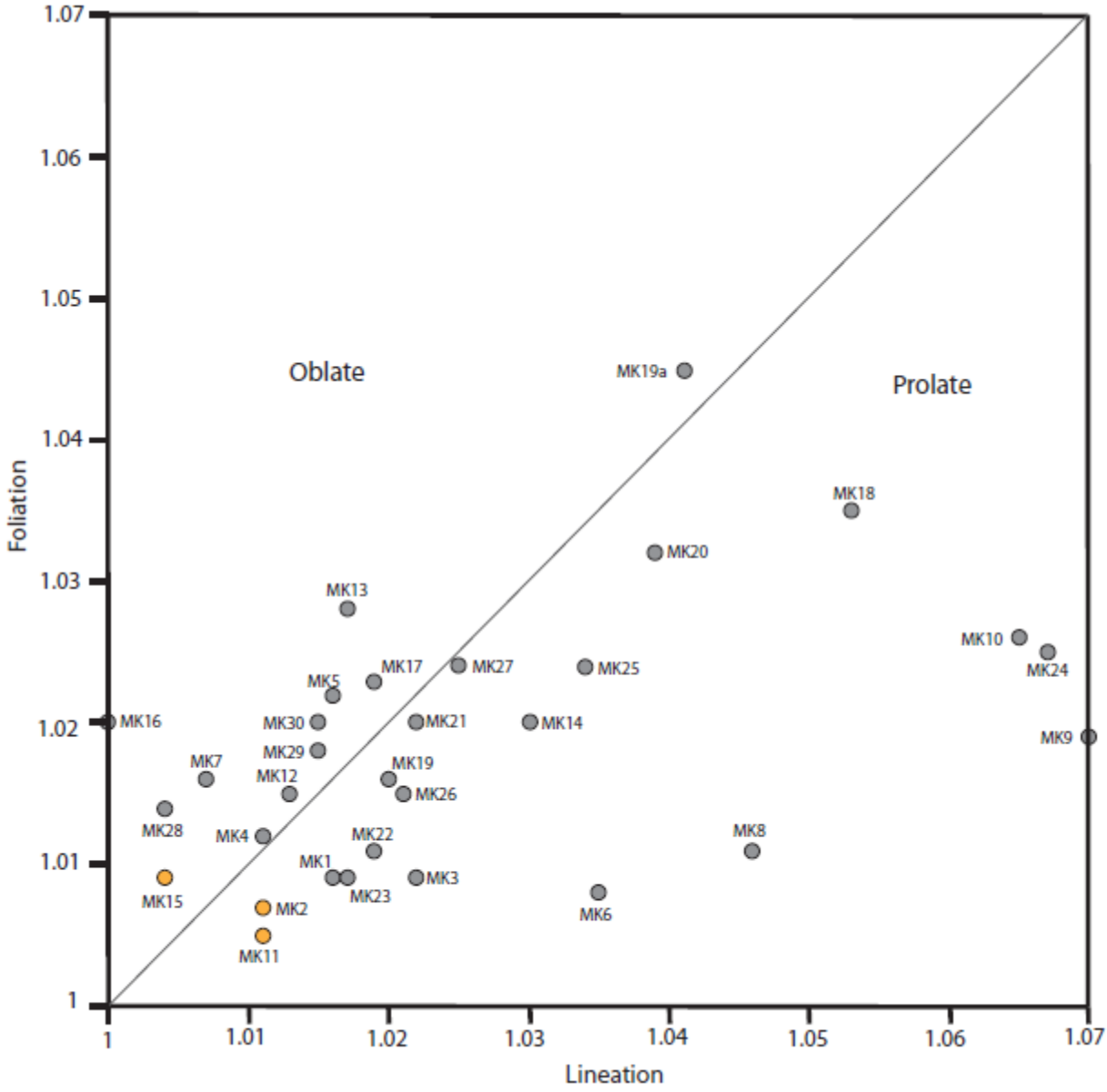

Figure 3.1 Plot of the foliation against the lineation to determine the shape of the AMS ellipsoids for all 31 sites. If the foliation has a higher value than the lineation, then the AMS ellipsoid is oblate. If the lineation has a higher value than the foliation, then the AMS ellipsoid is prolate. Sites with normal fabrics are represented by gray dots and the sites with anomalous or intermediate fabrics are represented by orange dots.

Site	Dike #	N	Kmean (SI)	K_1	K_2	K_3	L_{mean}	F_{mean}	P_{mean}	T_{mean}	K_1D (error)	K_1I (error)	K_2D (error)	K_2I (error)	K_3D (error)	K_3I (error)	E_1-E_2 (D)	E_1-E_2 (I)
MK1	3	11	3.23E-02	1.013	0.998	0.989	1.016	1.009	1.025	-0.256	106.1 (23.2)	25.6 (11.4)	303.7 (38.1)	63.4 (19.8)	199.4 (38.0)	7.0 (16.0)	30.65	15.6
MK2*	3	15	6.20E-02	1.01	0.999	0.992	1.011	1.007	1.018	-0.187	126.4 (27.5)	9.1 (9.0)	249.4 (34.5)	73.7 (25.8)	34.2 (33.4)	13.5 (8.9)	31	17.4
MK3	3	13	5.12E-02	1.017	0.996	0.987	1.022	1.009	1.031	-0.396	124.0 (14.1)	0.4 (7.1)	216.4 (25.0)	79.8 (12.0)	33.9 (24.9)	10.2 (10.1)	19.55	9.55
MK4	3	16	3.04E-02	1.012	1	0.988	1.011	1.012	1.024	0.033	139.6 (33.9)	1.3 (17.6)	233.3 (33.5)	70.2 (16.4)	49.1 (19.0)	19.8 (16.1)	33.7	17
MK5	2	14	3.72E-02	1.018	1.002	0.981	1.016	1.022	1.038	0.163	124.9 (14.6)	3.8 (5.2)	355.1 (14.5)	84.0 (12.2)	215.2 (12.4)	4.6 (5.2)	14.55	8.7
MK6	2	22	4.98E-02	1.026	0.991	0.983	1.035	1.008	1.043	-0.633	134.5 (9.5)	1.0 (6.4)	38.1 (22.7)	81.3 (6.5)	224.7 (22.7)	8.6 (9.2)	16.1	6.45
MK7	2	13	3.45E-02	1.01	1.003	0.987	1.007	1.016	1.023	0.4	311.1 (32.9)	7.8 (17.5)	115.5 (20.1)	81.9 (10.7)	220.8 (32.0)	2.2 (11.5)	26.5	14.1
MK8	1	16	4.82E-02	1.034	0.988	0.978	1.046	1.011	1.057	-0.626	127.7 (10.5)	0.4 (8.5)	218.4 (36.7)	62.1 (9.6)	37.5 (36.7)	27.9 (7.7)	23.6	9.05
MK9	1	12	3.82E-02	1.052	0.983	0.965	1.07	1.019	1.09	-0.569	311.2 (6.8)	1.7 (4.4)	213.9 (11.5)	77.1 (6.2)	41.6 (11.5)	12.8 (5.3)	9.15	5.3
MK10	1	14	3.62E-02	1.051	0.987	0.962	1.065	1.026	1.092	-0.421	301.4 (12.5)	6.2 (4.6)	198.9 (21.8)	63.3 (9.0)	34.4 (21.5)	25.9 (4.9)	17.15	6.8
MK11*	1	14	3.83E-02	1.009	0.998	0.993	1.011	1.005	1.016	-0.369	125.5 (20.6)	12.8 (9.7)	225.2 (38.6)	36.5 (18.5)	19.5 (38.2)	50.6 (11.4)	29.6	14.1
MK12	1	13	3.20E-02	1.013	1.001	0.986	1.013	1.015	1.028	0.077	109.0 (26.1)	27.9 (10.6)	348.3 (28.8)	43.9 (15.8)	219.2 (20.6)	33.2 (10.5)	27.45	13.2
MK13	1	13	3.76E-02	1.021	1.003	0.976	1.017	1.028	1.046	0.229	125.2 (20.1)	10.6 (5.7)	261.1 (20.1)	75.3 (10.1)	33.3 (10.4)	10.0 (5.5)	20.1	7.9
MK14	1	20	3.74E-02	1.026	0.997	0.977	1.03	1.02	1.05	-0.202	120.8 (13.6)	3.8 (7.2)	251.4 (14.6)	84.2 (10.2)	30.5 (15.1)	4.4 (11.0)	14.1	8.7
MK15*	1	20	3.92E-02	1.006	1.001	0.993	1.004	1.009	1.013	0.337	128.1 (42.7)	4.2 (31.3)	244.7 (43.0)	80.8 (23.0)	37.5 (32.8)	8.2 (21.8)	42.85	27.15
MK16	1	17	2.80E-02	1.007	1.006	0.987	1	1.02	1.02	0.97	345.2 (83.4)	66.1 (14.3)	122.4 (83.4)	18.1 (11.4)	217.5 (14.6)	15.2 (12.4)	83.4	12.85
MK17	3	15	3.79E-02	1.02	1.001	0.979	1.019	1.023	1.042	0.11	302.4 (13.1)	8.5 (6.4)	183.9 (12.3)	72.6 (10.9)	34.7 (11.1)	15.1 (7.6)	12.7	8.65
MK18	5	13	4.78E-02	1.047	0.994	0.96	1.053	1.035	1.09	-0.2	112.5	8.8	284.7	81.2	22.3	1.2	8.15	5.8

											(8.3)	(5.6)	(8.0)	(6.0)	(8.7)	(7.2)		
MK19	5	9	2.42E-02	1.019	0.999	0.982	1.02	1.016	1.037	-0.098	114.0 (14.3)	8.5 (8.4)	230.6 (19.9)	71.5 (12.7)	21.5 (19.8)	16.3 (6.8)	17.1	10.55
MK19a	5	6	3.17E-02	1.042	1.001	0.958	1.041	1.045	1.088	0.043	130.2 (26.0)	18.9 (4.7)	293.3 (28.6)	70.3 (3.8)	38.4 (14.4)	5.3 (4.1)	27.3	4.25
MK20	4	12	3.26E-02	1.036	0.998	0.966	1.039	1.032	1.072	-0.089	141.4 (9.7)	7.8 (5.4)	270.7 (13.7)	77.8 (8.1)	50.1 (12.8)	9.3 (5.0)	11.7	6.75
MK21	4	14	4.03E-02	1.021	0.999	0.98	1.022	1.02	1.042	-0.044	139.7 (9.7)	14.1 (8.1)	303.8 (16.0)	75.4 (8.0)	48.7 (16.0)	3.9 (8.0)	12.85	8.05
MK22	4	19	4.51E-02	1.016	0.997	0.987	1.019	1.011	1.03	-0.263	139.4 (11.6)	16.7 (10.6)	289.7 (19.9)	71.0 (10.7)	46.7 (20.0)	8.9 (11.2)	15.75	10.65
MK23	4	15	4.62E-02	1.014	0.997	0.988	1.017	1.009	1.026	-0.334	149.0 (19.1)	15.8 (9.9)	349.9 (41.9)	73.2 (17.3)	240.6 (41.6)	5.7 (10.9)	30.5	13.6
MK24	4	8	3.14E-02	1.052	0.986	0.962	1.067	1.025	1.093	-0.45	144.9 (13.7)	9.5 (10.5)	252.1 (17.7)	60.6 (11.6)	49.9 (18.2)	27.6 (6.0)	15.7	11.05
MK25	5	15	3.56E-02	1.03	0.996	0.973	1.034	1.024	1.059	-0.175	301.3 (11.6)	20.6 (6.1)	108.2 (15.1)	68.9 (8.7)	209.7 (13.6)	4.4 (6.6)	13.35	7.4
MK26	5	18	4.20E-02	1.019	0.998	0.983	1.021	1.015	1.036	-0.161	301.5 (8.5)	9.1 (8.0)	90.7 (16.2)	79.5 (8.4)	210.6 (16.3)	5.3 (7.9)	12.35	8.2
MK27	5	12	3.80E-02	1.025	1	0.976	1.025	1.024	1.05	-0.017	308.1 (17.6)	12.5 (9.8)	85.8 (22.2)	73.3 (10.0)	215.6 (21.3)	10.9 (13.9)	19.9	9.9
MK28	6	13	3.08E-02	1.007	1.003	0.99	1.004	1.014	1.018	0.505	143.2 (39.4)	21.9 (11.2)	263.0 (39.7)	51.0 (16.3)	39.6 (17.8)	30.5 (11.6)	39.55	13.75
MK29	6	12	3.67E-02	1.016	1.001	0.983	1.015	1.018	1.033	0.109	128.7 (19.1)	19.3 (13.5)	236.6 (22.4)	41.4 (14.9)	20.1 (20.7)	42.3 (10.6)	20.75	14.2
MK30	6	10	3.05E-02	1.016	1.002	0.982	1.015	1.02	1.035	0.143	112.8 (13.7)	18.7 (6.7)	220.6 (16.7)	42.0 (6.0)	5.0 (11.6)	42.1 (6.9)	15.2	6.35

Table 3.1 Table containing AMS data for all 31 sites. The dike number refers to the numbered dike segments in Figure 2.1. N refers to the number of specimens. K_{mean} is in SI units. D and I refer to the declination and inclination, respectively. E_1-E_2 D and I are determined by the arithmetic mean of the error for the D and I of K_1 and K_2. An '*' next to a site name indicates an anomalous AMS fabric and therefore they were not used in the final flow interpretations.

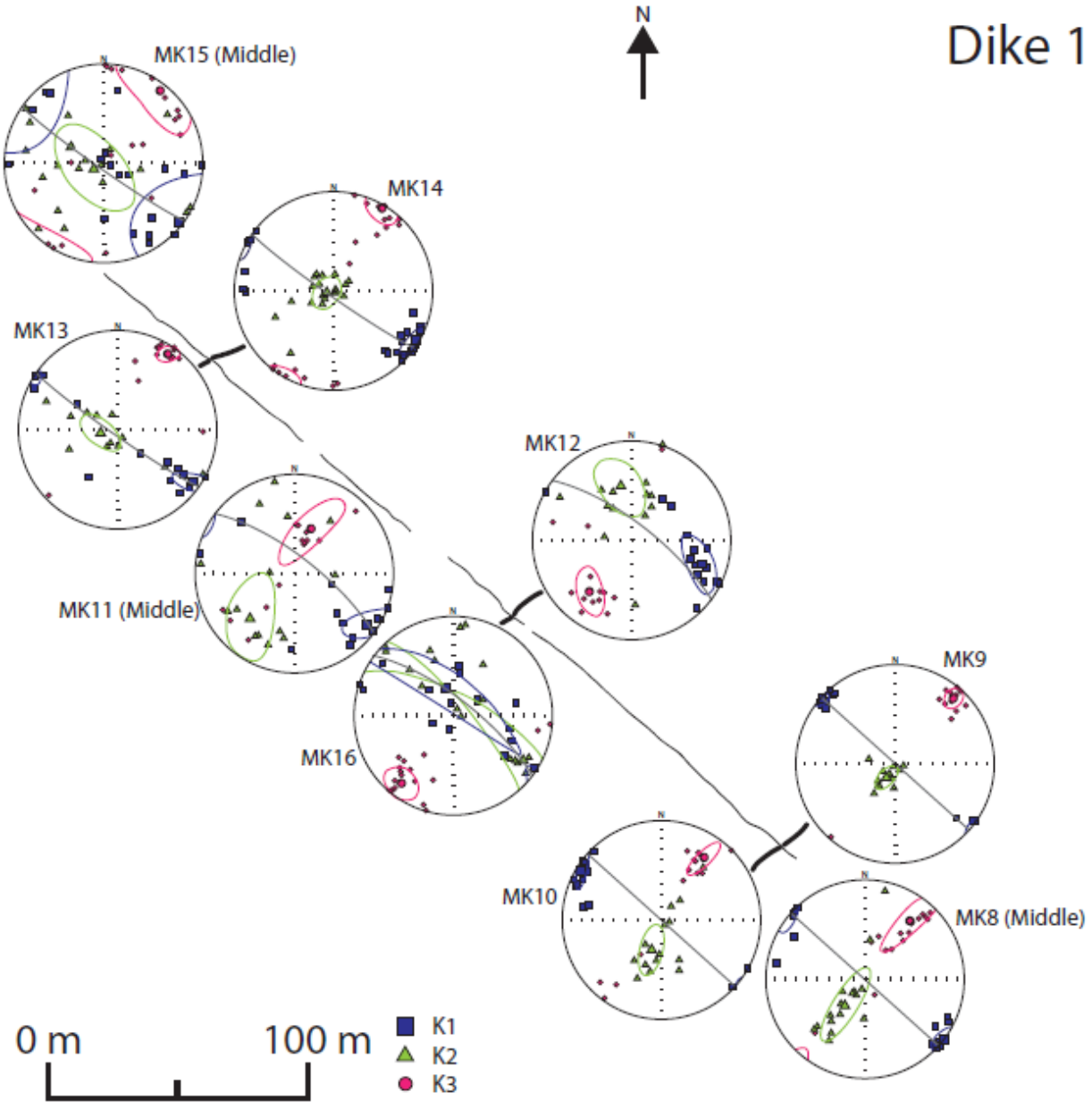

Figure 3.2 Map of sites located on dike 1 and their associated AMS plots. Middle sites are labelled with 'middle' in parentheses next to them and the margin sites are lined up relative to the dike according to whether they are from the north or south margin. MK15 shows a wide scatter of axes indicative of an anomalous fabric. On all the AMS plots the gray line denotes the dike plane. MK11 shows a dominantly intermediate fabric with K_1 and K_3 parallel to the dike plane and K_2 perpendicular. The remaining sites show normal fabrics with K_1 and K_2 parallel to the dike plane and K_3 perpendicular.

MK11, 12, and 16 are located in the middle portion of dike 1 (Figure 2.1). MK12 and MK16 are the northern and southern margins of the dike, respectively, and are distinguished from the middle by fewer (< 1%) vesicles that become slightly more abundant toward the boundary with the middle of the dike. The size of the vesicles ranges from one mm to three mm on average. Site MK11 is the middle of the dike and contains a higher density of vesicles (5-7%) that are two to three mm in size on average. It also has fewer (<1%) clinopyroxene phenocrysts than the dike margins. Sites MK11 and MK12 have stronger mean bulk susceptibilities than MK16 (Table 3.1). The dike margins also both have slightly stronger foliation than lineation, making the AMS ellipsoids oblate in shape. MK11 has a slightly stronger lineation (L) than foliation (F) and negative shape factor (T), making the AMS ellipsoid prolate (Table 3.1 and Figure 3.1). MK11 has a dominantly intermediate fabric with only a few specimens showing a reversal of K_2 and K_3 axis positions. MK12 exhibits a dominantly normal fabric with only two specimens showing an intermediate fabric. MK16 also has a dominantly normal fabric with only two specimens showing a reversal of K_2 and K_3 axis positions. The amount of scatter of the axes for all specimens at MK16 is much greater than MK12 (Figure 3.2).

MK8-10 are located on the southeastern end of dike 1 (Figure 2.1). Sites MK9 and MK10 are the northern and southern dike margins respectively, distinguished from the middle site by an abundance of elongate vesicles (~7%) and <1% clinopyroxene phenocrysts. Site MK8 is the center of the dike and has fewer vesicles (3-5%) and more clinopyroxene phenocrysts (~3%). The vesicles are also more round in shape than those in the margins. MK9 and MK10 show much lower mean bulk susceptibilities than the middle site, MK8 (Table 3.1). All three sites have L > F and negative T, making all of the AMS ellipsoids prolate (Table 3.1 and Figure 3.1). MK8

and MK10 both have dominantly normal fabrics with only a few specimens showing a reversal of K_2 and K_3 axis positions (Figure 3.2).

3.1.2 Dikes 2 and 3

MK5-7 are located on the northwestern end of dike 2, near where the dike segment thins and tapers to an end (Figure 2.1). MK5 and MK7 are the northern and southern dike margins respectively and are defined by a high concentration (7-10%) of small (1-2 mm) vesicles near the edges of the dike and have few (<1%) clinopyroxene phenocrysts. MK6 is the middle of the dike and is distinguished from the margins by a high concentration (7-10%) of larger vesicles (2-5 mm on average) with more (2-3%) clinopyroxene phenocrysts as well as rare phlogopite phenocrysts. MK5 and MK7 show distinctly lower mean bulk susceptibilities than the middle site (Table 3.1). Both MK5 and MK7 have F > L and positive T, indicating oblate AMS ellipsoids whereas MK6 has L > F and a negative T, indicating that it has a prolate AMS ellipsoid (Table 3.1 and Figure 3.1). MK5 shows a normal fabric. MK7 shows a dominantly normal fabric with a few specimens showing reversals of K_1 and K_3 axes. MK6 shows an anomalous fabric with a wide spread of K_2 and K_3 axes indicative of a mix of normal and intermediate fabrics (Figure 3.3).

MK1 and MK2 are sites located on the northwest end of Dike 3 (Figure 2.1). MK1 consists of cores taken from the northern margin of the dike and is distinguished from the middle by small (1-2 mm) vesicles and smaller (4-5 mm) clinopyroxene phenocrysts. MK2 is the middle of the dike, which is defined by more abundant (7-10%), larger (3-4 mm) vesicles at the contact with MK1 and grades into fewer, smaller vesicles toward the center of the dike. No site was drilled on the south side of the dike due to poor outcrop quality for drilling that margin. In the middle, there are also larger clinopyroxene phenocrysts, ranging from 0.5 cm to 1 cm in size.

MK1 has a distinctly lower mean bulk susceptibility than MK2 (Table 3.1). Both sites have L > F and negative T, indicating that they have prolate AMS ellipsoids (Table 3.1 and Figure 3.1). MK1 shows a dominantly normal fabric with some specimens showing a reversal of K_2 and K_3 axes. MK2 shows an anomalous fabric with a nearly even mix of normal and intermediate fabrics and a large amount of scatter of all three AMS axes (Figure 3.3).

MK3, MK4, and MK17 are located at the southeast end of dike 3 (Figure 2.1). Sites MK4 and MK17 are the northern and southern dike margins, respectively, and are distinguished by more vesicles (7-10%) and fewer (1-2%) clinopyroxene phenocrysts. The middle site, MK3, has fewer vesicles (3-5%) and more abundant (2-3%) clinopyroxene phenocrysts. MK4 and MK17 have similar mean bulk susceptibilities, whereas the mean bulk susceptibility for the inner site is much higher (Table 3.1). MK4 and MK17 both have F > L and positive T, indicating oblate AMS ellipsoids, whereas MK3 has a stronger lineation than foliation with a negative T, indicating that it has a prolate ellipsoid (Table 3.1 and Figure 3.1). MK3 shows a dominantly normal fabric with the positions of the K_2 and K_3 axes flipped for two specimens. MK4 also shows a dominantly normal fabric with the position of the K_2 and K_3 axes flipped for one specimen. MK17 shows a normal fabric with the clusters of K_1 axes being imbricated relative to the dike plane on either side of the dike plane (Figure 3.3).

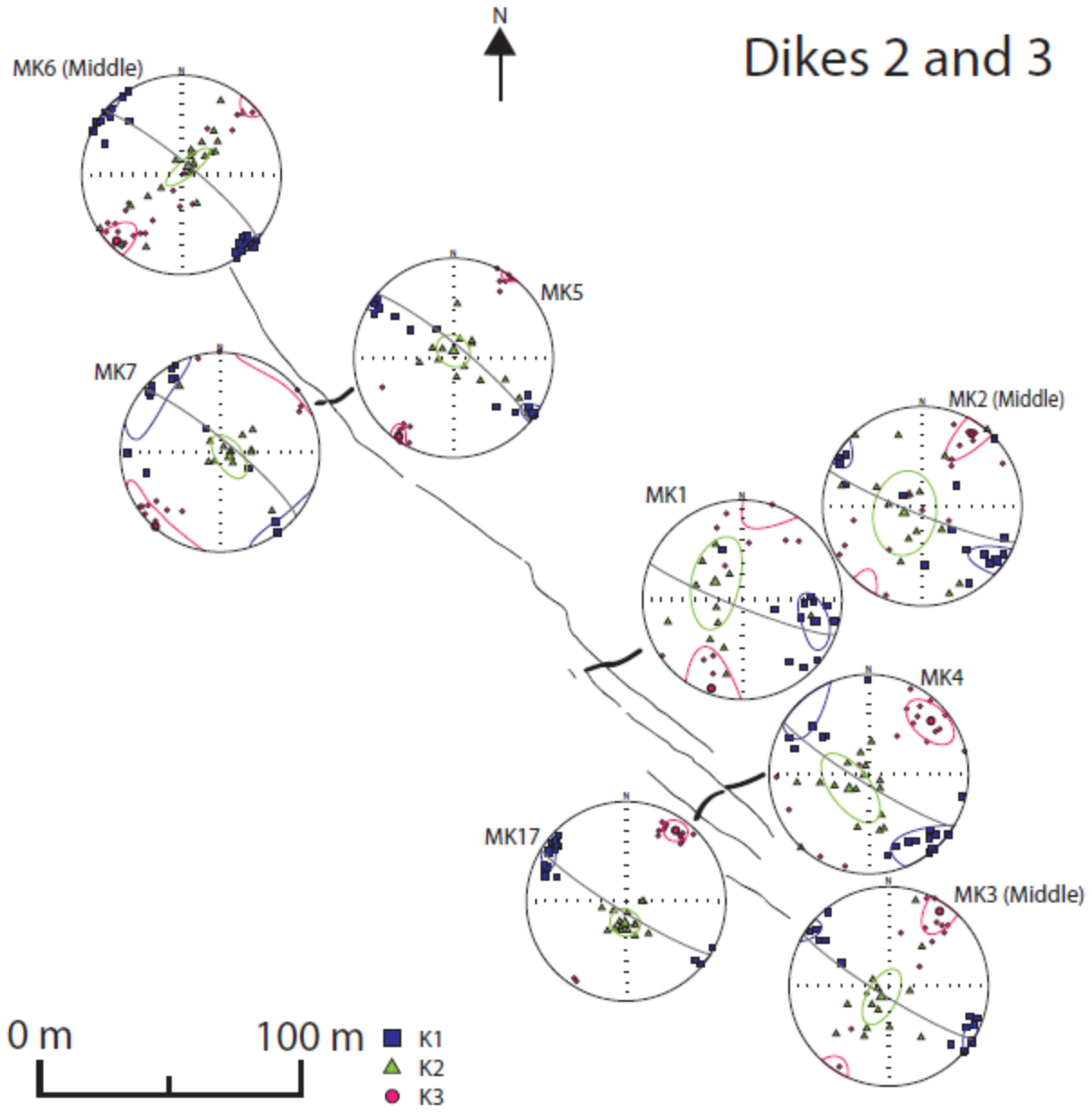

Figure 3.3 Map of sites located on dikes 2 and 3, and their associated AMS plots. Middle sites are labelled with 'middle' in parentheses next to them and the margin sites are lined up relative to the dike according to whether they are from the north or south margin. On all AMS plots the gray line denotes the dike plane. MK2 shows an anomalous fabric with a mix of normal (K_1 and K_2 parallel to the dike plane) and intermediate (K_1 and K_3 parallel to the dike plane) fabrics. The remaining sites all show normal fabrics with K_1 and K_2 parallel to the dike plane and K_3 perpendicular.

3.1.3 Dike 4

Sites MK20-24 are located on the northwest section of dike 4, which is located just east of massif 1 (Figure 2.1). This location is adjacent to an offset in the dike and the dike plane has a shallower dip (80°) than sections to the north and south of it. The outer most margin sites, MK20 and MK24, are defined by small (1 mm), elongate vesicles and few (<1%) clinopyroxene phenocrysts. The second, inner set of margin sites, MK21 and MK23, are characterized by slightly larger (3 mm) vesicles. The middle site, MK22, is defined by very fine (<1 mm), mostly round vesicles and more (2-3%) clinopyroxene phenocrysts. MK20 and MK21 are the northern margins of the dike, and MK23 and MK24 are the southern margins. The outermost dike margin sites have distinctly lower mean bulk susceptibilities, whereas the inner dike margin sites and middle site have higher mean susceptibilities (Table 3.1). MK20 and MK24 also have a distinctly stronger average degree of anisotropy than the other three sites when compared to the inner sites (Table 3.1). All of the sites have L > F as well as negative T, indicating that all five sites have prolate AMS ellipsoids (Table 3.1 and Figure 3.1).

MK20 shows a dominantly normal fabric with one specimen showing an inversion of the K_1 and K_3 axis positions. The majority of the K_1 axes are near parallel to the plane of the dike. MK21 has a dominantly normal fabric with the position of the K_2 and K_3 axes flipped for some specimens. MK22 shows a dominantly normal fabric with two specimens showing a flip of the K_2 and K_3 axes. The main cluster of K_1 axes lines up approximately parallel to the dike plane. MK23 shows a dominantly normal fabric. MK24 has a normal fabric with the K_1 axes aligning approximately parallel with the dike plane (Figure 3.4).

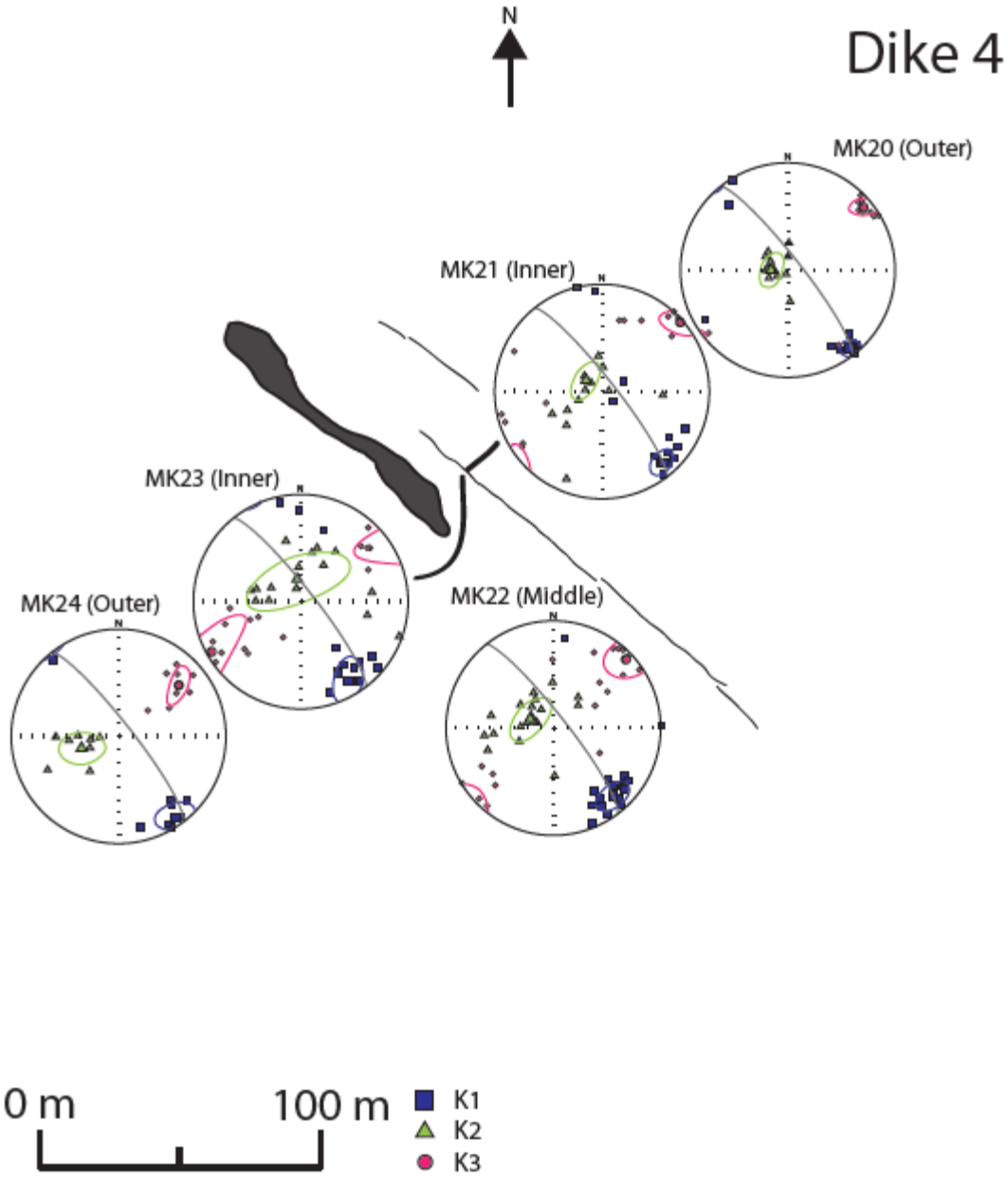

Figure 3.4 Map of sites located on dike 4, and their associated AMS plots. Middle sites are labelled with 'middle' in parentheses next to them and the margin sites are lined up relative to the dike according to whether they are from the north or south margin. On all plots, the gray line denotes the dike plane. All sites show normal fabrics with K_1 and K_2 generally parallel and K_3 perpendicular to the dike plane.

3.1.4 Dikes 5 and 6

MK18, MK19, and MK19a are located in the middle section of dike 5 (Figure 2.1). To the northwest, the dike continues to intersect with massif 2. Directly adjacent to this drilling location, there is a wedge of red, clayey sediment trapped in the middle of the dike, as well as a small bud just 2-3 meters to the northwest in line with the dike. This bud has a rounded characteristic that is distinctly wider than the intersecting dike. MK18 is the middle of the dike and is marked by fewer (1-2%), rounder vesicles and larger (5-6 mm on average) clinopyroxene phenocrysts. MK19 and MK19a are the northern and southern margins of the dike, respectively. Both sites are distinguished by a higher density (5%) of more elongate vesicles and generally smaller (2-3 mm on average) clinopyroxene phenocrysts. MK18 has a distinctly higher mean bulk susceptibility than MK19 and MK19a (Table 3.1). MK 18 and MK19 have L > F and a negative T, indicating that they both have a prolate AMS ellipsoid, whereas MK19a has a slightly stronger foliation than lineation, leading to a slightly oblate ellipsoid and a positive T (Table 3.1 and Figure 3.1). All three sites show normal fabrics (Figure 3.5).

Sites MK25-27 are located on the southeast end of dike 5 (Figure 2.1). MK25 and MK27 are the northern and southern dike margins, respectively. They are distinguished from the middle by smaller (1-2 mm) and less abundant (1-2%) vesicles along with few to no clinopyroxene phenocrysts. When phenocrysts are present, they are very small, only 2 mm at most. MK26 is the middle of the dike and is defined by larger (3-4 mm) vesicles. It also has more abundant (2-3%) clinopyroxene phenocrysts. MK25 and MK27 have similar mean bulk susceptibilities and they are both lower than the mean bulk susceptibility of the middle sites (Table 3.1). MK25 and MK26 both have L > F and negative T, indicating that they both have a prolate AMS ellipsoid. MK27 has a slightly stronger foliation than lineation and a positive T, indicating that it has an

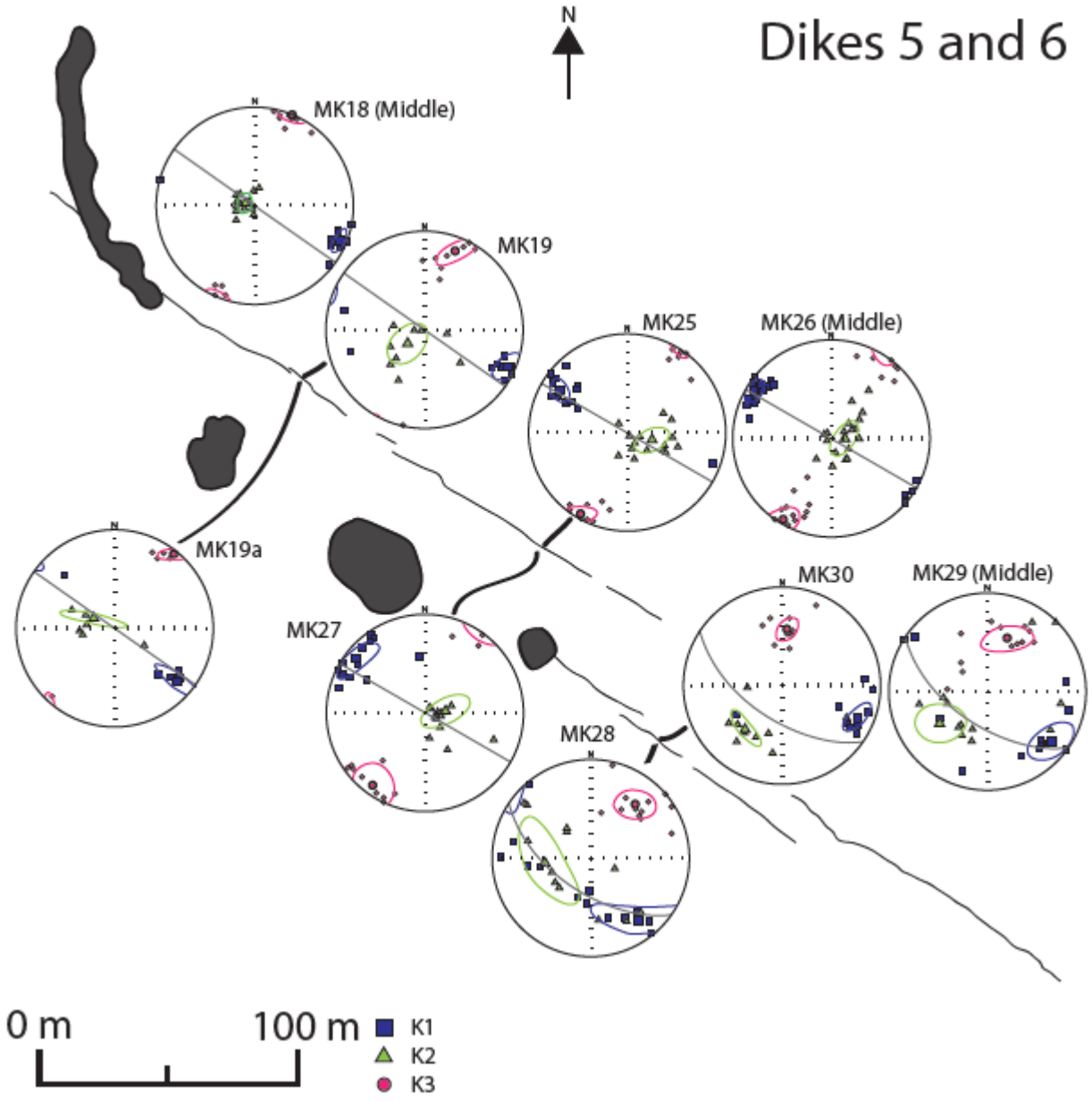

Figure 3.5 Map of sites located on dike 5 and 6, and their associated AMS plots. Middle sites are labelled with 'middle' in parentheses next to them and the margin sites are lined up relative to the dike according to whether they are from the north or south margin. On all AMS plots, the gray lines indicate the dike plane. All sites show normal fabrics with K_1 and K_2 parallel and K_3 perpendicular to the dike plane.

oblate AMS ellipsoid (Table 3.1 and Figure 3.1). MK25-27 all have normal flow fabrics (Figure 3.5).

MK28-30 are located on the northwest end of dike 6 (Figure 2.1). Sites MK28 and MK30 are the southern and northern margins of the dike, respectively, and are distinguished from the center of the dike by smaller (<1 mm) vesicles and generally smaller (1-2 mm) clinopyroxene phenocrysts. Site MK29 is the site in the center of the dike and is defined by larger (2-3 mm), less abundant (2%) vesicles with generally larger (3-5 mm) clinopyroxene phenocrysts. All three sites have similar mean bulk susceptibilities, but the middle site, MK29, has a slightly higher susceptibility than the margins. All three sites also have a slightly stronger F than L and positive T indicating that they all have oblate AMS ellipsoids (Table 3.1 and Figure 3.1). MK28 and MK30 show normal fabrics. MK28 has a wide spread of K_1 and K_2 axis orientations, generally aligning with the strike of the dike plane. MK29 shows a dominantly normal fabric, with two specimens having flipped K_2 and K_3 axis positions (Figure 3.5).

3.2 AARM Results

Anisotropy of Anhysteretic Remanent Magnetization (AARM) is a technique that is often used in AMS studies to understand the causes of anomalous or inverse fabrics, because it only measures the ferromagnetic anisotropy. In this case, it was used to analyze sites that show significant dispersion in their AMS axes and/or anomalous fabrics. Three sites were chosen (MK1, MK11, and MK16) based on these criteria and analyzed in order to possibly provide information on the source of the anomalous fabrics and dispersion of AMS axes. The results from these few sites can broadly be applied to other sites that show similar fabrics. Overall, MK1 showed a similar AARM fabric to the original AMS fabric whereas MK11 and MK16 showed

flips in the position of axes between the AARM and AMS plots that may be indicative of the presence of single domain (SD) magnetite grains.

The AARM plot for MK1 has a fabric similar to the original AMS plot and generally maintains the wide dispersion of the three magnetic axes. The K_1 axes for the specimens measured for AARM generally lie within the dike plane, with only two specimens showing a strong deviation from that trend. The K_2 and K_3 axes show the same broad scatter as the AMS plot (Figure 3.6). The similarities between the axes of the AARM and the AMS plots indicate that the AMS is not being influenced by the presence of SD grains. The AARM plots for MK11 and MK16 both deviate from their original AMS plots. For MK11, the AARM plot has a plane defined by the spread of the K_1 and K_3 axes that is perpendicular to the dike intrusion plane with the K_2 axes being perpendicular to the K_1 K_3 plane and parallel to the dike plane. When compared to the original AMS plot, the position of the K_1 axes has been flipped with those of the

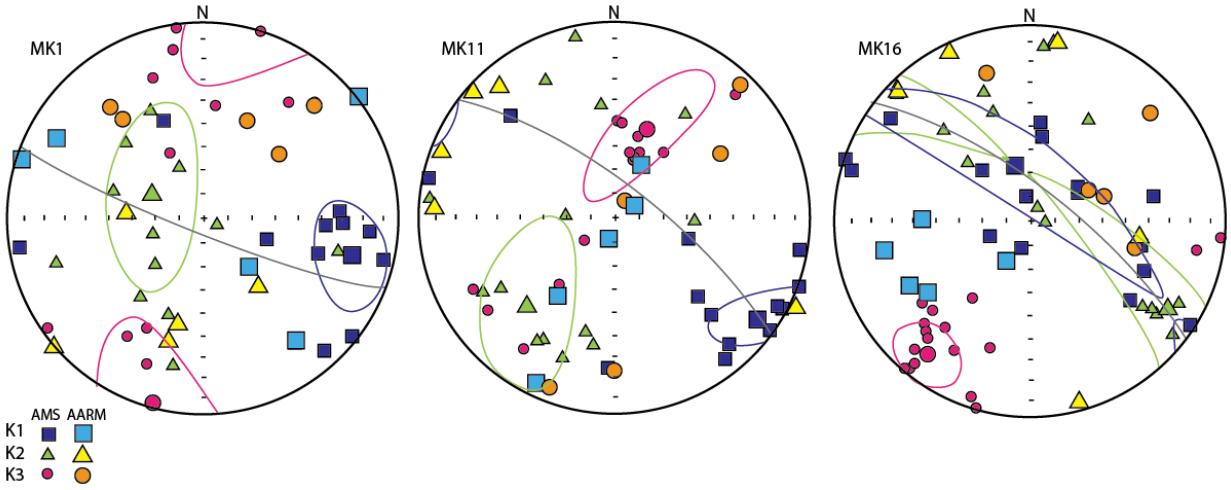

Figure 3.6 AARM and AMS plots superposed for MK1, MK11, and MK16 for comparison of fabrics from each.

K_2 axes for multiple specimens (Figure 3.6). Although the flip in axes is not the characteristic flip of K_1 and K_3 axes that indicates SD grains, it could be reflective of SD grains interacting with pseudo-single domain (PSD) grains. The AARM plot for MK16 shows the same amount of scatter of the three ellipsoid axes as the original AMS plot, but the positions of some of the axes have flipped. The K_2 axes are still generally parallel to the dike plane, but the K_1 and K_3 axes have flipped their locations for some of the specimens (Figure 3.6). The flip of K_1 and K_3 axes for some specimens may indicate the influence of SD grains on the AMS plot.

For MK1, the AARM results mirrored that of the AMS, making it unlikely that SD grains are causing the dispersion of the AMS axes. For sites MK11 and MK16, the AARM plots show some reversals in axis positions, indicating the possible presence of SD grains within these two sites. This information is helpful when looking at other sites that show anomalous fabrics or a great amount of dispersion in their AMS axes. Some of this behavior may be due to the presence of SD grains.

3.3 Curie Point and IRM Results

Curie point and Isothermal Remanent Magnetization (IRM) were analyzed for sites throughout the dike swarm in order to further understand the properties of the magnetic minerals within the dikes. Curie points were measured for one to two sites from each dike and allow for determination of the magnetic mineralogy. The IRM was analyzed for two specimens from each of three sites. The IRM curves allow for determination of the general magnetic mineralogy, i.e. magnetite vs. hematite, but can also be used to determine the domain type of the magnetite through the use of $B_{1/2}$ values, which are the field strength at which the specimen acquires half of its saturation magnetization. Both the magnetic mineralogy and grain domain type are valuable information when understanding the magnetic behavior represented in the AMS plots.

The Curie point analyses resulted in heating and cooling curves for all eleven specimens measured (MK1B, MK4J, MK6L, MK8N, MK14K, MK24B, MK26P, MK5N2, MK19K, MK22I, and MK28G). They all show one main, dominant peak, indicating the magnetic minerals are of one generally similar composition. The Curie points for the measured specimens range from 68.8-152°C (Table 3.2). Their range of temperatures is indicative of high-titanium titanomagnetite, which is most characteristic of MORBs (Keller and Schmidbauer 1999; Zitzelsberger and Schmidbauer 1999; Lanza and Meloni 2006). High-titanium titanomagnetite is unique and somewhat unexpected in this setting. This composition analysis has been corroborated by additional geochemical analysis done by Re et al. (in review), which found that the opaque minerals found in the JRC intrusions are titanomagnetite with high titanium content.

	Curie Point Temp (°C)
MK1B	113.4
MK4J	107.2
MK6L	75.2
MK8N	68.8
MK14K	152
MK24B	102.4
MK26P	72
MK5N2	106
MK19K	136
MK22I	85.8
MK28G	99.8

Table 3.2 Curie points for the 11 specimens measured. Specimens are spread throughout the sampled sites to get a good representation of the variations throughout the dike swarm. The temperature is the point of maximum susceptibility in the heating curve.

All six specimens analyzed for IRM show the specimen reaching saturation by 160-250 mT, and after that point, the magnetic moment (M) increases only very slightly or not at all for later measurements. The variability in the saturation of isothermal remanence (SIRM) values for each of the specimens is reflected in the differences in the shapes of the curves. The curves present three different shapes. The first one is a steep consistent increase to the SIRM, followed by little to no variation in the magnetization afterward. The second one is a curve with a slightly less steep increase, making it reach its SIRM at a higher field strength (Figure 3.7). The third type of curve shows a slight delay in the increase in magnetic moment for a couple steps, but then magnetizes quickly, resulting in a steep-sloped curve that reaches the SIRM quickly. The generally steep shape of the IRM curves and the low SIRM values are characteristic of the remanence-bearing minerals being magnetite. The calculated $B_{1/2}$ values range from 43.74 to 57.58 mT, indicating that the titanomagnetite grains are dominantly PSD magnetite grains edging on SD grains for the higher $B_{1/2}$ values (Table 3.3; Dunlop 1972; Heiniger 1979; Rolph 1997; Symons and Cioppa 2000).

Both the Curie point and IRM results indicate that the northwestern dike swarm contains high-titanium, dominantly PSD titanomagnetites as the main remanence-bearing grains. The corroboration of this analysis by Re et al. (In Review)'s geochemical analysis firmly defines the remanence-bearing minerals as high-titanium titanomagnetite. The magnetic analyses add additional compositional information as well as the domain of the magnetite grains which are important for accurate interpretations of AMS and AARM results and interpretation of the flow directions within the dikes.

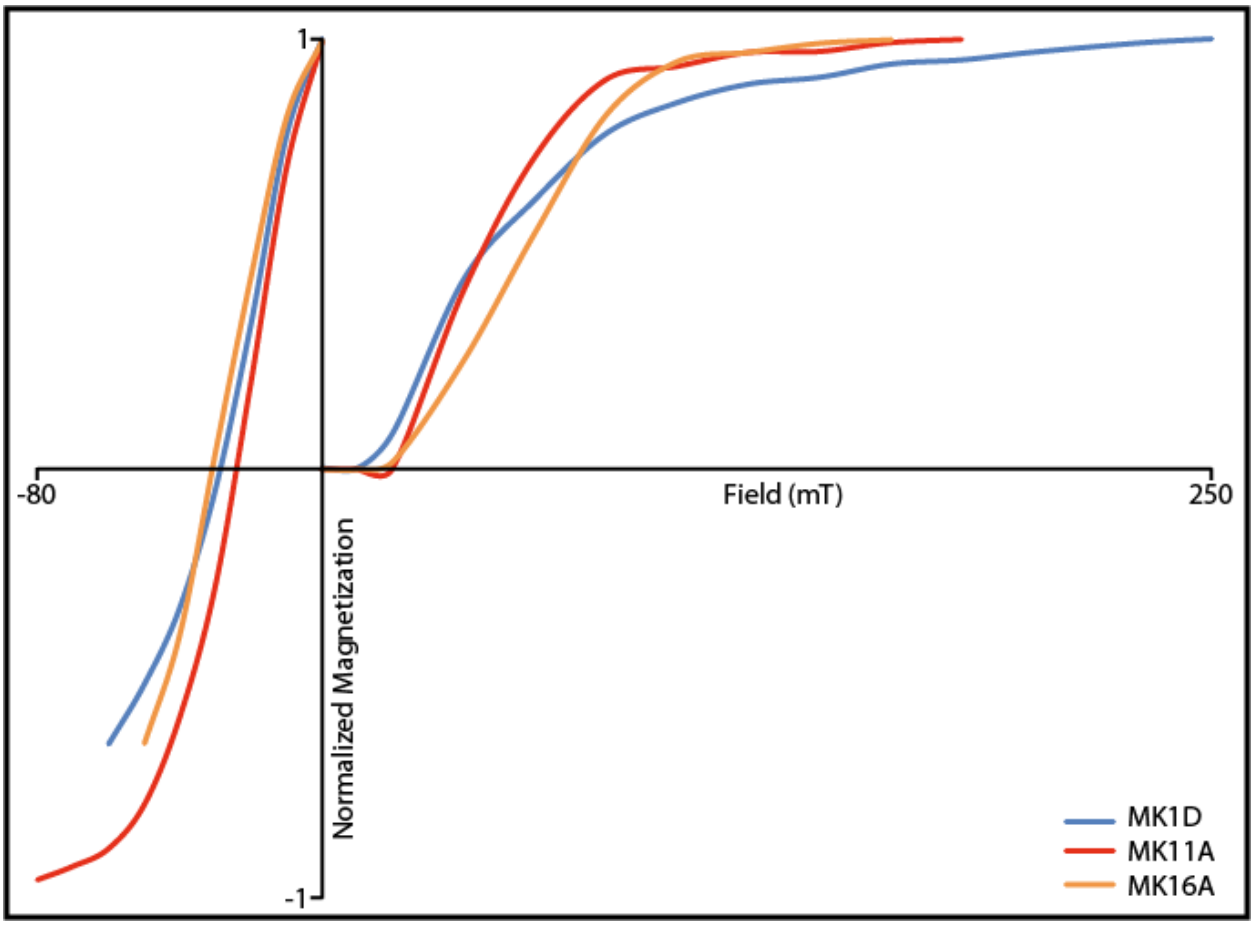

Figure 3.7 Plot of three example types of IRM curves for analyzed specimens. The field applied to the specimen in mT is plotted against the normalized magnetization for the specimen to produce the IRM and BIRM curves for all specimens. Some specimens took longer to reach saturation, resulting in a shallower curve shape (MK1D), whereas others were quicker to reach saturation, resulting in a steeper curve shape (MK11A). The third curve type is characterized by an initial delay in the change of the magnetization followed by a quick climb to saturation thereafter (MK16A). This results in a flat beginning of the curve followed by a relatively steep slope. The BIRM curves for all three specimens are shown as well on the negative x-axis, starting at 1 and decreasing toward -1.

Sample ID	SIRM (mT)	B1/2 (mT)
MK1D	250	57.58
MK1E	230	45.51
MK11A	180	44.7
MK11F	160	49.39
MK16A	160	55.33
MK16G1	160	43.74

Table 3.3 Table of Saturation Isothermal Remanent Magnetization (SIRM) and B1/2 values for all six specimens analyzed for IRM. Both are in mT.

3.4 ChRM Results

Characteristic Remanent Magnetization (ChRM) is a useful technique for determining whether a series of intrusions was emplaced within a close time frame, based on their magnetic pole positions. It was important to make sure all the studied dikes were emplaced at about the same time to verify the assumption that the dikes' fabrics all resulted from the same intrusion event. It is also important to determine whether any of the dikes had their magnetic characteristics or physical orientation altered by post-emplacement processes. The relative timing of the dikes is an important detail to understand when developing an understanding of the formation of the dike swarm as a whole.

At least six specimens from each location were measured. Some locations required more specimens to be measured due to specimens being thrown out because of the wide spread in their measurements. In the case of MK1-2, the entire location had to be disregarded due to the pole position resembling that of the modern-day pole position, indicating that section of the dike had been reset magnetically, possibly due to a lightning strike. The remaining locations all show generally similar pole locations and the suite mean generally reflects this trend with a declination

of 183.6°, an inclination of -40.5°, α_{95} of 19.3, and a κ of 41.8 (Table 3.4; Figure 3.8). The overall similarities in the pole positions indicate that the dikes were all intruded during a short time period when the magnetic pole was reversed which aligns with the magnetic pole position during the eruption of the Hopi Buttes Volcanic Field, around 7 Ma (Walker et al. 2012; Re et al. 2015). The general similarities also indicate that the dikes' physical orientation has not been altered by post-emplacement processes.

Sites in Location	Dike #-Loc#	n/N	D	I	α_{95}	κ
MK13-15	1-1	4/6	175.3	-43.7	8.7	112.1
MK11,12,16	1-2	4/5	194.1	-29.1	8.9	107.7
MK8-10	1-3	3/6	179	-47.7	13.7	84.5
MK5-7	2-1	6/8	173.7	-35.8	10.3	43.6
MK1-2**	3-1	3/6	4.8	-37.6	41.8	9.7
MK3,4,17	3-2	6/10	192.7	-41.8	15	21
MK20-24	4-1	6/7	171.1	-42.5	5.8	135.2
MK18-19	5-1	4/4	171.1	-44.6	7.1	168
MK25-27	5-2	5/5	176.1	-41.8	4.4	299.6
MK28-30	6-1	6/6	174.5	-48	5.5	149.5
	Suite Mean:	44/57	183.6	-40.5	19.3	41.8
**Thrown out in final suite mean calculation, see text for full discussion						

Table 3.4 Full table of ChRM results. n/N is the number of specimens used in the suite mean calculation out of the total specimens measured. D and I denote declination and inclination, respectively. The α_{95} is the error and the κ is the clustering parameter from the Fisher statistics.

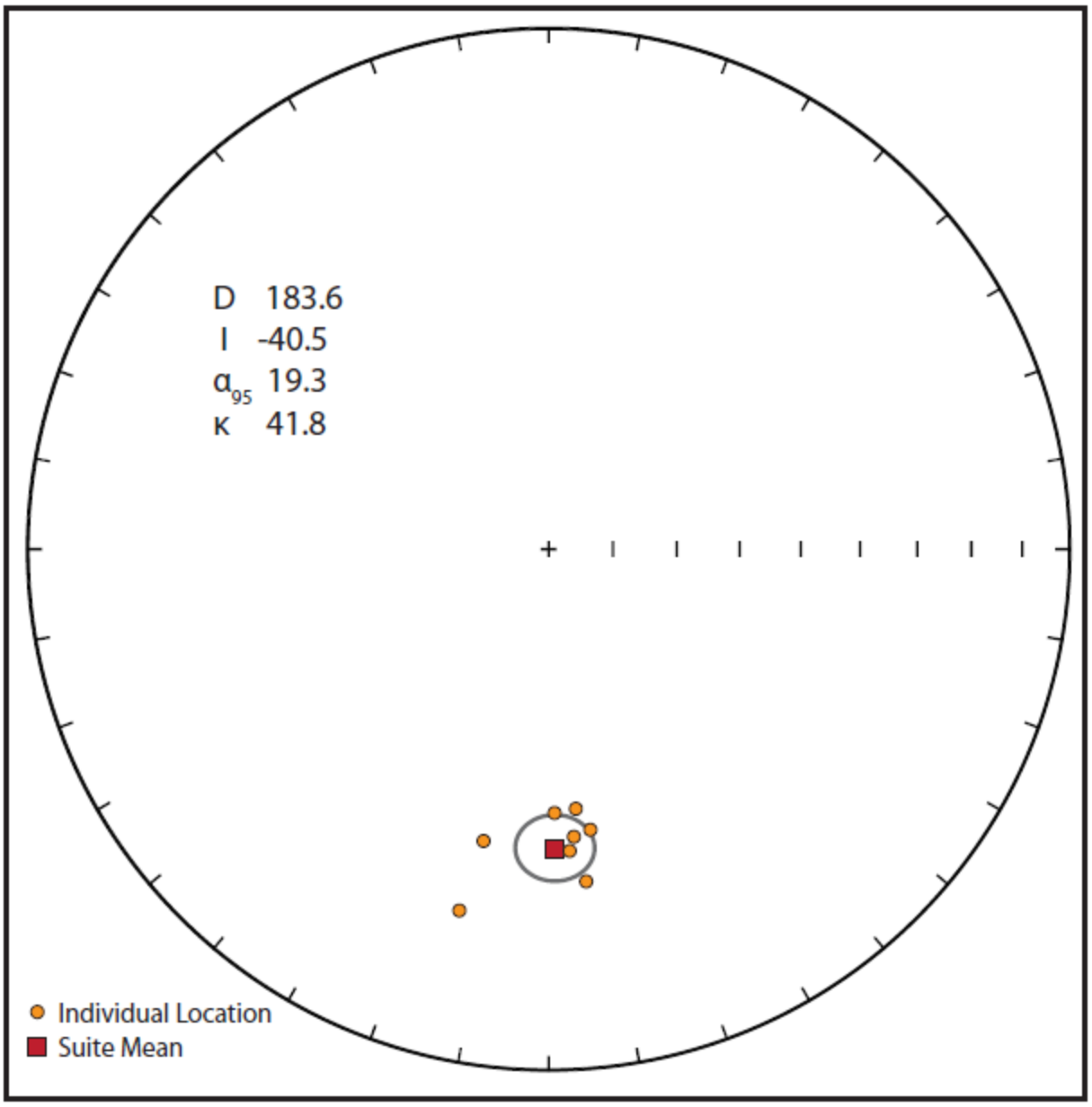

Figure 3.8 Equal-area plot showing the Fischer averages (green circles) for each location along the six dikes and the suite mean for the whole dike swarm (blue square). The gray ellipse represents the α_{95} confidence ellipse.

3.5 Magnetic Survey Results

Magnetic anomalies can provide information about how intrusive bodies continue at depth and laterally past their exposure at the surface. For the northwest dike swarm, transects were

concentrated in the northwest half of the swarm. The survey began just northwest of the current exposure of the dikes at the surface in order to understand if the dikes continued to the northwest in the subsurface. The survey then continued with transects approximately perpendicular to the strike of the dikes to gather information about the anomalies associated with the dikes. The size of the anomalies can provide valuable information about the relative depth (i.e. shallow or deep) of the intrusive bodies, which is critical information when interpreting the flow directions from the AMS and when trying to understand the dikes' emplacement during the formation of JRC.

The final magnetic survey map shows small anomalies along the dikes in the northwestern half of the dike swarm (Figure 3.9). An anomaly is also associated with the survey lines most to the northwest, showing evidence for the continuation of the dike in the subsurface past where the exposure ends. The dike in the subsurface is probably thin and does not continue to great depth because of the short wavelength of the anomaly (Marshall et al. 2015). The two transects used for the depth calculations are labelled on Figure 3.9. Line 1 produced an odd profile and was ultimately discarded. The approximate depth of the dikes based on the calculation from line 2 is 30 m. This depth confines the base of the dikes within the Chinle Formation.

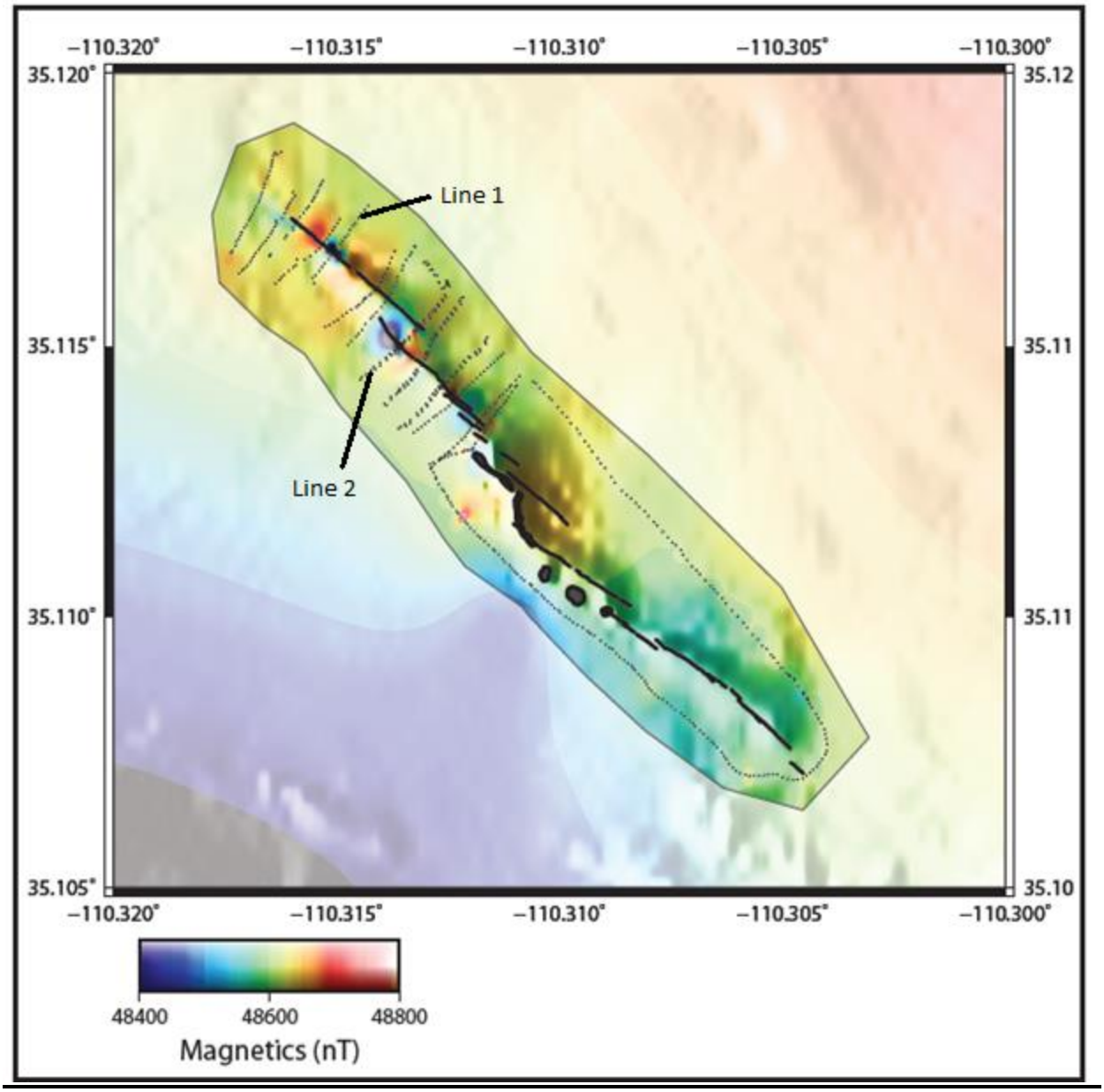

Figure 3.9 Georeferenced magnetic survey map with the survey transects overlaid. The topography and map of dikes and massifs are also overlaid to give a sense of the location of the anomalies along the exposed dikes. The area outside the survey area was grayed to help emphasize the magnetic anomalies along the dike. Line 1 and line 2 are the two profiles used in the depth calculations (see text for full discussion).

Chapter 4: Discussion

Twenty-seven of the 30 sites show normal AMS fabrics, with only three sites showing anomalous or intermediate fabrics. Paired margin sites generally show similar bulk magnetic properties, indicating a distinction between the margins and centers in magnetic properties as well as physical appearance. This information is supportive of each pair of margins having formed at the same time and from the same chilling event. The AARM results indicate the possible influence of single domain (SD) magnetite grains on anomalous AMS fabrics or fabrics that show a wide dispersion of AMS axes. The IRM results corroborate this, indicating that the domain type is pseudo-single domain (PSD) edging on SD. The IRM results also indicate that the main remanence-bearing minerals are magnetite. The Curie Point measurements provide further composition information, indicating that the remanence-bearing minerals are high-titanium titanomagnetite. ChRM results indicate that all the dikes in the northwest dike swarm formed around the same time. The magnetic survey results indicate that the dikes are confined to about 30 m below the exposed level. All of this information contributes to the understanding of the magnetic properties as well as the emplacement process of the northwest dike swarm. The details of these emplacement processes and the evolution of the northwest dike swarm are discussed in this section. Understanding the formation of the northwest dike swarm can aid in the understanding of the relation between the dikes and massifs exposed throughout the dike swarm as well as the role of shallow intrusions in monogenetic volcanic systems. Understanding the role of shallow magma storage in these systems is important for understanding how they change and evolve over time.

Perhaps the most important finding of this research is that the dikes in the northwest dike swarm of the Jagged Rocks Complex (JRC) record dominantly horizontal flow in a northwest

direction. This direction is generally away from the transgressive sill to the southeast, which is inferred to have formed below a cinder cone (Re et al. 2015; Muirhead et al. 2016). This is consistent with the hypothesis that the northwest dike swarm was injected as a diversion from a main conduit to the southeast. Its emplacement may have reduced pressure within the larger system, possibly resulting in a shift to phreatomagmatic activity. The northwest dike swarm contains both coherent dikes and massifs formed through explosive interaction of water and magma. Changes in the magma flux or magma water ratios within the northwest dike swarm itself possibly fueled phreatomagmatism at the level of exposure and above. The phreatomagmatic activity was likely fueled by the water-saturated sediments of the Chinle and Bidahochi Formations (White 1989; 1990).

The dikes in the northwest dike swarm in the Jagged Rocks Complex contain high-titanium titanomagnetite crystals that are pseudo-single domain (PSD) grains with some single domain (SD) grains. The presence of some SD grains is supported by the AARM measurements of anomalous fabrics, which show the possibility of some SD magnetite interference with the orientation of the AMS ellipsoid axes. The majority of sites show dominantly normal AMS fabrics, meaning that the K_1 and K_2 axes are generally parallel to the strike of the dike plane and the K_3 axes are roughly perpendicular. Only a few sites show anomalous fabrics that are characterized by a wide scatter of the AMS axes and a mix of fabrics.

Flow directions were determined for at least one set of margins along all dikes except for dike 1. Of the ten margin pairs and one unpaired margin that have dominantly normal flow fabrics (K_1 K_2 plane parallel to the dike plane, K_3 perpendicular to dike plane), five have imbricated AMS ellipsoid pairs that allowed for interpretation of discrete flow directions. Discrete flow directions are determined based on the imbrication of the mean K_1 axis (magnetic

lineation) relative to the dike plane for each margin site in a pair. This provides a general sense of the orientation of the ellipsoid relative to the dike walls, and ellipsoids with mirror-imbrication allow for flow direction interpretation. The azimuth and plunge of flow are then determined by averaging the inclination and declination of the mean K_1 axes of each margin. The one unpaired margin also shows imbrication of the AMS ellipsoid that allows for determination of the possible flow direction in that site, but the azimuth and plunge of the flow could not be calculated for that location given that there is only imbrication information for the one margin. All five pairs and the one unpaired margin indicate dominantly horizontal flow in a northwest direction. The remaining five margin pairs do not have mean AMS ellipsoids with mirror-imbrication that could be used for direction-of-flow interpretations, however, they show dominantly horizontal flow like that of the other margin pairs. The middle sites with dominantly normal fabrics also show dominantly horizontal flow, but flow directions cannot be determined due to the lack of paired margins. The middle sites with anomalous fabrics were not used in final flow interpretations due to the wide amount of scatter and mix of fabrics present in those sites.

The flow directions and behavior from the margin pairs in particular provide information about the direction of the initial injection of the dikes. Later movement of magma is recorded by the middle sites, which also allows for insights into the general flow behavior of the magma within the dikes after their initial formation. Together with the rock magnetic data, this provides an understanding of the history of the formation of the northwest dike swarm and gives insights into the role they may have played in maar-diatreme eruptions in JRC.

4.1 Determination of Dike Flow Directions

General flow behavior is determined through the mean K_1 axis (magnetic lineation) relative to the dike plane or the K_3 axis (magnetic foliation) relative to the pole to the plane. For

the K_1 method, the orientation of the K_1 axis is compared to the dike plane in order to understand the orientation of the AMS ellipsoid. The K_3 method involves comparing the orientation of the K_3 axis relative to the pole to the plane of the dike. The difference between the orientation between the K_3 axis and the pole allows for the determination of the orientation of the AMS ellipsoid relative to the dike plane. Based on the inclination of the mean K_1 axis for a site, the flow can be dominantly horizontal or dominantly vertical. For dominantly horizontal flow the inclination will be very shallow, whereas for vertically dominated flow, the inclination will be very steep. From these parameters, the general flow behavior of all sites with dominantly normal fabrics can be described. For determination of discrete flow directions, mirrored pairs of AMS ellipsoids are necessary to resolve the discrete flow direction, azimuth, and plunge. The flow direction is determined by the direction the mirrored pair of AMS ellipsoids point (Figure 4.1A). Mirror-imbrication is defined by the same sense of imbrication when reflected across a vertical plane between the two margins (Figure 4.1A). Margins that show parallel imbrication yield the opposite sense of flow direction when reflected across a vertical plane between the two margins (Figure 4.1B).

The magma-flow azimuth for a pair of sites is calculated from the average of the declination of the mean K_1 axis for each margin, and the plunge is determined from the average of the inclination of the mean K_1 axis for each margin (Figure 4.1A). Some margins only show slight imbrication (< 2°) relative to the dike plane, but are still used in the determination of discrete flow directions as long as they show more than 0.5° difference. Most sites display dominantly normal flow fabrics, allowing for interpretation of the general flow behavior recorded within them. Only three sites, MK15, MK11, and MK2, show anomalous or intermediate fabrics that do not allow for the determination of flow behavior. Of the sites that

show dominantly normal fabrics, half of the margin pairs show mirrored imbrication using the lineation (mean K_1 axis), allowing for the determination of the flow direction, azimuth, and plunge.

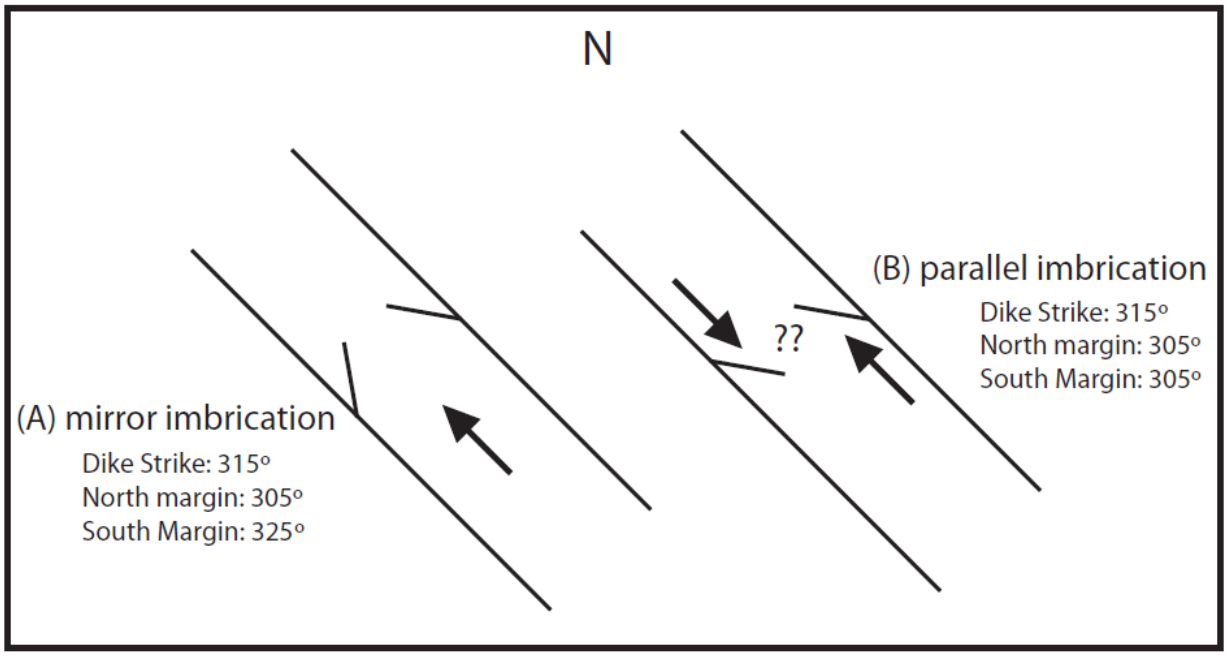

Figure 4.1 Example of mirror-imbrication and parallel imbrication of the K_1 axes in a theoretical dike, in plain view. The arrows indicate the directions of flow based off of the lines' (representing the magnetic lineation) imbrication against the dike walls. The mirror-imbrication results in one coherent flow direction whereas the parallel imbrication shows two opposing directions of flow, not allowing for determination of the exact flow direction.

4.1.1 K_1 vs K_3 Method for Determination of Imbrication

Imbrication of the AMS ellipsoids for a site can be determined through two main methods. One method relies on the mean K_1 axis position (or magnetic lineation) relative to the dike plane to determine the orientation of the ellipsoid. This method was first used by Knight and Walker (1988) in their pioneering work on flow determination in dikes using AMS, and has since been used in many other AMS studies of dikes (e.g. Rochette et al. 1992; Raposo and Ernesto

1995; Herrero-Bervera et al. 2001; Delcamp et al. 2014). More recently, the reliability of the magnetic lineation for determination of flow directions has been questioned, leading to the rise of the use of the mean K_3 axis (or magnetic foliation) relative to the pole to the dike plane for the determination of the orientation of the AMS ellipsoid. This method has been proven to sometimes provide interpretable mirror-imbricated pairs when the K_1 method does not (e.g. Geoffroy et al. 2002; Callot and Geoffroy 2004; Soriano et al. 2008; Delcamp et al. 2014). When looking at the imbrication of the AMS ellipsoids for the sites sampled, both methods were used in order to obtain the most possible margins with mirrored imbricated pairs for flow determination. Overall the K_1 method proved to provide the most mirrored imbricated pairs for the sites sampled in this study. The K_3 method for determination of imbrication often either yielded the same results as the K_1 method or resulted in parallel imbricated pairs. Therefore, when determining flow directions for the sampled sites, the K_1 method was used in the final determinations of flow direction, azimuth, and plunge.

For margin pairs MK13 and MK14, MK12 and MK16, MK20 and MK24, and MK25 and MK27, the K_1 and K_3 methods created imbrication pairs with mirror and parallel imbrication, respectively. The K_3 method in this instance did not provide a clearer understanding of the imbrication of the AMS ellipsoids relative to the dike plane. For the remainder of margin pairs, the K_1 and K_3 methods provided either both mirrored (MK 21 and MK23, MK28 and MK30, MK19 and MK19a) or both parallel (MK9 and MK10, MK5 and MK7, MK4 and MK17). For the one unpaired margin (MK1), the K_1 and K_3 methods provided the same sense of imbrication relative to the dike plane, but without the opposite margin the flow direction can only be determined from the one margin and an azimuth and plunge cannot be calculated.

4.1.2 Dike Flow Directions, Azimuth, and Plunge

Ten margin pairs and one single margin site are spread across all six studied dikes. Half (five) of the margin pairs show mirror-imbricated AMS ellipsoids, allowing for the determination of flow direction, azimuth, and plunge. All of the interpretable margin pairs indicate NW flow (Figure 4.2A; Figure 4.3; Table 4.1). The variability in the plunge shows a difference in the angle of the upward component of the movement of the magma. Its shallow orientation at all locations indicates that the horizontal flow component is dominant. The one single margin (MK1) does not allow for the determination of a flow azimuth and plunge. The imbrication of the mean K_1 axis relative to the dike plane indicates NW flow as well, although the flow direction cannot be definitively determined without the orientation of the AMS ellipsoid of the opposite margin (Figure 4.2B; Table 4.1).

The remaining margin pairs were uninterpretable for flow directions primarily due to the AMS ellipsoids showing parallel imbrication regardless of whether the magnetic lineation (mean K_1 axis) was used or the magnetic foliation (mean K_3 axis) (Figure 4.2; Table 4.1; Table 4.2). Two margin pairs (MK13 and MK14, and MK12 and MK16) were deemed uninterpretable for flow directions despite having mirrored imbrication. MK13 and MK14 were uninterpretable because the southern margin (MK13) showed very slight imbrication (0.2°) relative to the dike plane, making the AMS ellipsoid almost in line with the strike of the dike and any interpretations of flow direction unreliable (Figure 4.3; Figure 4.4; Table 4.2). MK12 and MK16 were uninterpretable because the southern margin (MK16) shows a wide scatter of K_1 and K_2 axes, possibly due to SD magnetite grain interference with the AMS. This created a large amount of error for the positions of these two axes (Figure 4.4, Table 4.2).

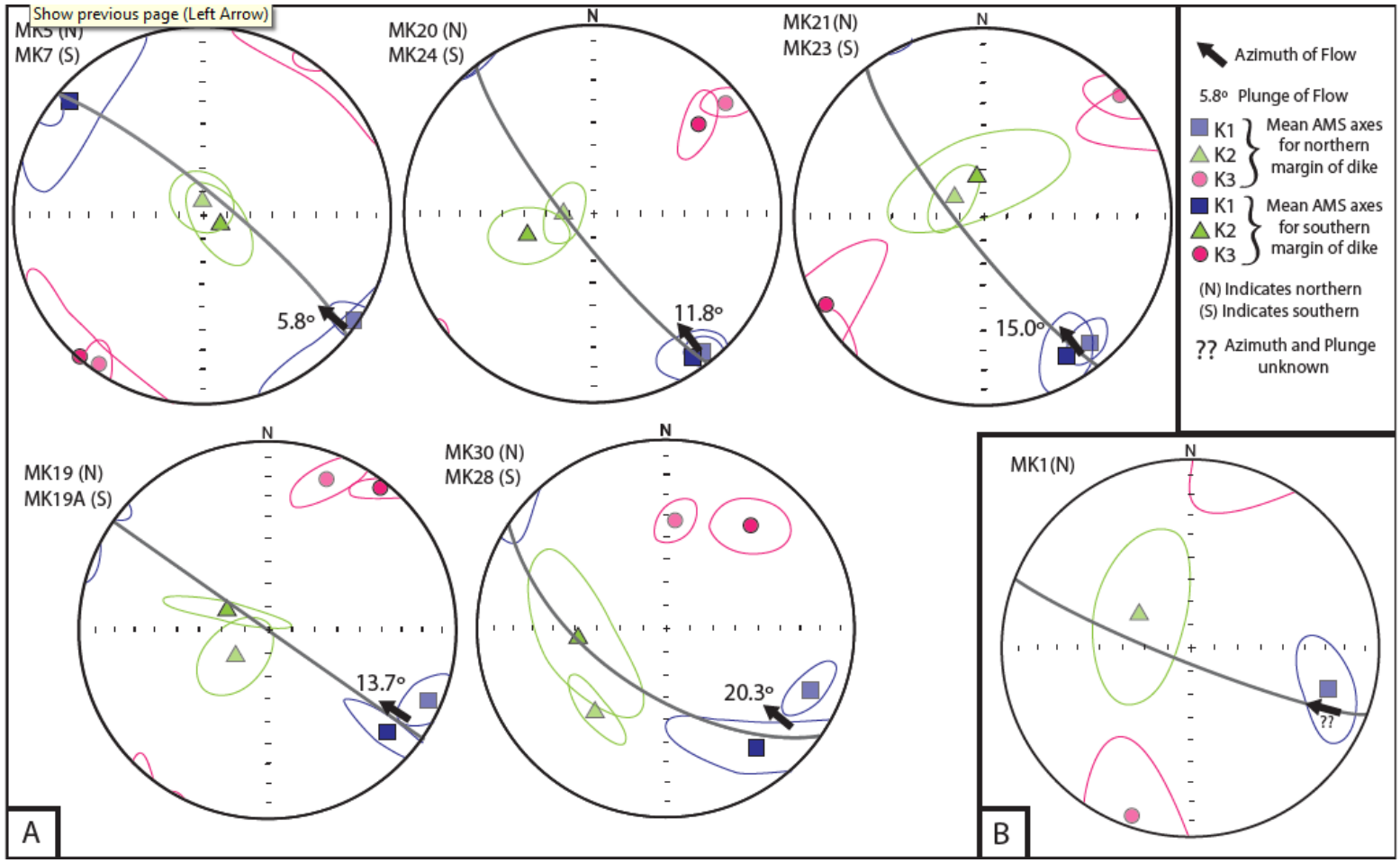

Figure 4.2 AMS plots for margins in which flow direction could be determined. A) Margin pairs where flow direction, azimuth, and plunge could be determined. The azimuth and direction of flow is represented by the black arrow and the angle next to it is the plunge of flow. B) AMS plot for the unpaired margin MK1 showing the interpreted direction of flow although the azimuth and plunge could not be determined.

Site	Dike Trend	Dike Plunge	Pole Trend	Pole Plunge	K1 D	K1 I	K2 D	K2 I	K3 D	K3 I
MK8	312	90	42	0	127.7	0.4	218.4	62.1	37.5	27.9
MK9	312	90	42	0	311.2	1.7	213.9	77.1	41.6	12.8
MK10	312	90	42	0	301.4	6.2	198.9	63.3	34.4	25.9
MK18	305	90	35	0	112.5	8.8	284.7	81.2	22.3	1.2
MK19	305	90	35	0	114	8.5	230.6	71.5	21.5	16.3
MK19A	305	90	35	0	130.2	18.9	293.3	70.3	38.4	5.3
MK13	305	85W	35	5	125.2	10.6	261.1	75.3	33.3	10
MK14	305	85W	35	5	120.8	3.8	251.4	84.2	30.5	4.4
MK15	305	85W	35	5	128.1	4.2	244.7	80.8	37.5	8.2
MK11	307	76E	217	14	125.5	12.8	225.2	36.5	19.5	50.6
MK12	307	76E	217	14	109	27.9	348.3	43.9	219.2	33.2
MK16	307	76E	217	14	345.2	66.1	122.4	18.1	217.5	15.2
MK1	291	83W	21	7	106.1	25.6	303.7	63.4	199.4	7
MK2	291	83W	21	7	126.4	9.1	249.4	73.7	34.2	13.5
MK5	310	80E	220	10	124.9	3.8	355.1	84	215.2	4.6
MK6	310	80E	220	10	134.5	1	38.1	81.3	224.7	8.6
MK7	310	80E	220	10	311.1	7.8	115.5	81.9	220.8	2.2
MK3	302	82W	32	8	124	0.4	216.4	79.8	33.9	10.2
MK4	302	82W	32	8	139.6	1.3	233.3	70.2	49.1	19.8
MK17	302	82W	32	8	302.4	8.5	183.9	72.6	34.7	15.1
MK20	322	80W	52	10	141.4	7.8	270.7	77.8	50.1	9.3
MK21	322	80W	52	10	139.7	14.1	303.8	75.4	48.7	3.9
MK22	322	80W	52	10	139.4	16.7	289.7	71	46.7	8.9
MK23	322	80W	52	10	149	15.8	349.9	73.2	240.6	5.7
MK24	322	80W	52	10	144.9	9.5	252.1	60.6	49.9	27.6
MK25	300	90	210	0	301.3	20.6	108.2	68.9	209.7	4.4
MK26	300	90	210	0	301.5	9.1	90.7	79.5	210.6	5.3
MK27	300	90	210	0	307.3	12.1	84.7	73.8	215	10.6
MK28	304	62W	34	28	143.2	21.9	263	51	39.6	30.5
MK29	304	62W	34	28	128.7	19.3	236.6	41.4	20.1	42.3
MK30	304	62W	34	28	112.8	18.7	220.6	42	5	42.1

Table 4.1 Table showing the declination and inclination for all three mean AMS axes for all sites measured. It also includes the dike trend and plunge as well as the pole trend and plunge for each site for comparison of the orientation of the mean K_1 and K_3 axes relative to the dike plane and pole respectively. D and I indicate declination and inclination, respectively.

Site Pair	Ellipsoid Shape(s)	Flow Azimuth/Plunge (K_1)	Flow direction
Dike 1			
MK 13 + 14	one of each	123/7.2	undeterminable
MK 12 + 16	both oblate	145.4/39.5	undeterminable
MK 9 + 10	both prolate	306.3/4.0	undeterminable
Dike 2			
MK 5 + 7	both oblate	128/5.8	NW
Dike 3			
MK 1	prolate	Undeterminable**	NW
MK 4 + 17	both oblate	131/4.9	Undeterminable
Dike 4			
MK 20 + 24	both prolate	142.3/11.8	NW*
MK 21 + 23	both prolate	144.4/15.0	NW
Dike 5			
MK 19 + 19a	one of each	122.1/13.7	NW
MK 25 + 27	both prolate	304.3/16.4	undeterminable
Dike 6			
MK 28 + 30	both oblate	128/20.3	NW

Table 4.2 Summary of flow directions for all dike margins. Azimuth and plunge were determined from the mean K_1 axes for dike margins with opposite imbrication. Margin pairs without opposite imbrication were labelled with undeterminable flow directions and no azimuth and plunge. The '**' indicates that only one dike margin was used and thus the azimuth and plunge of flow could not be determined.

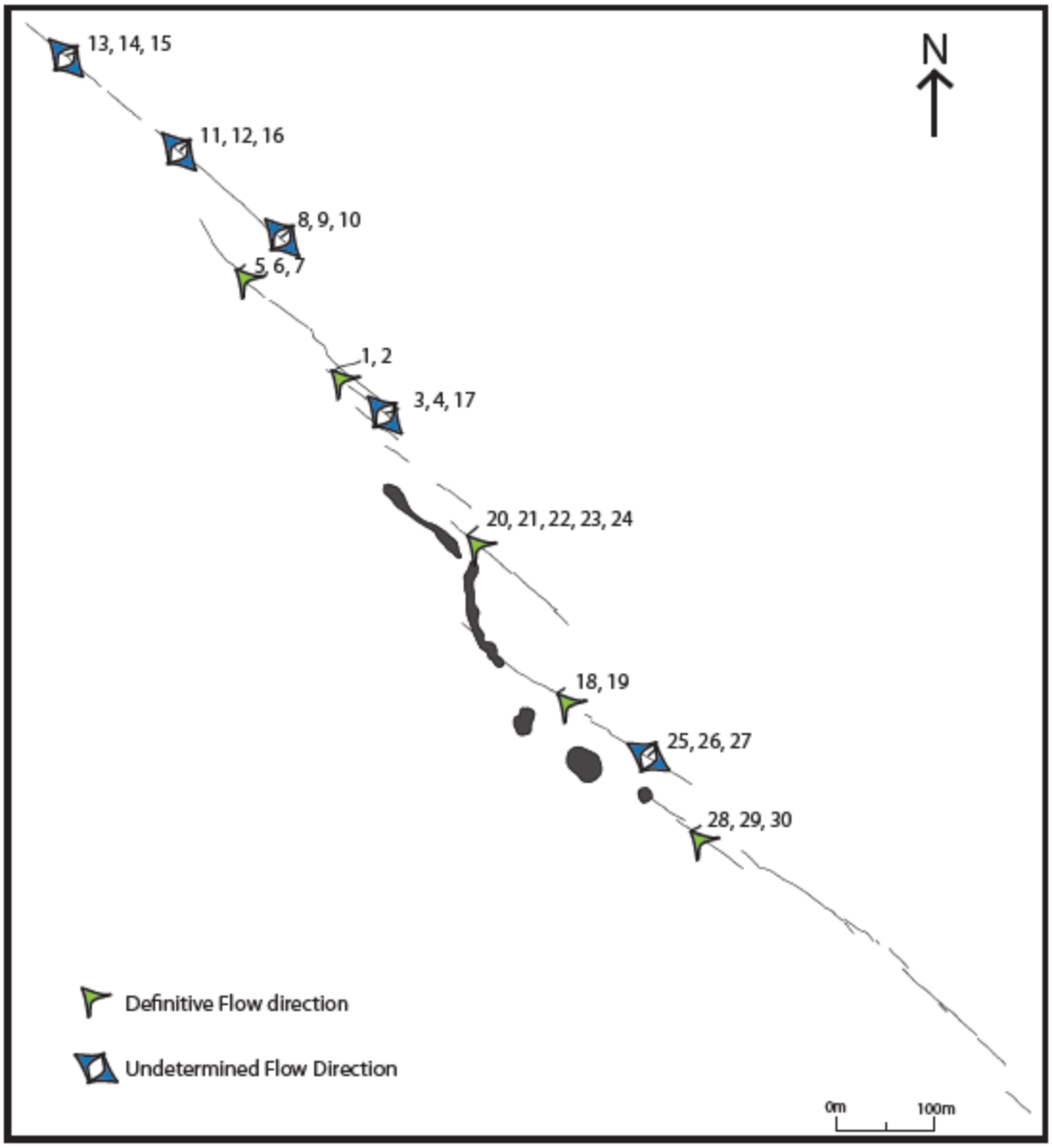

Figure 4.3 Map of northwest dike swarm showing determined flow directions. Single-headed arrows (green) indicate locations where the flow direction was determined. Double-headed arrows (blue) indicate locations where the flow direction could not confidently be determined although its near-horizontal trend could be inferred. The numbers indicate the sites associated with a location.

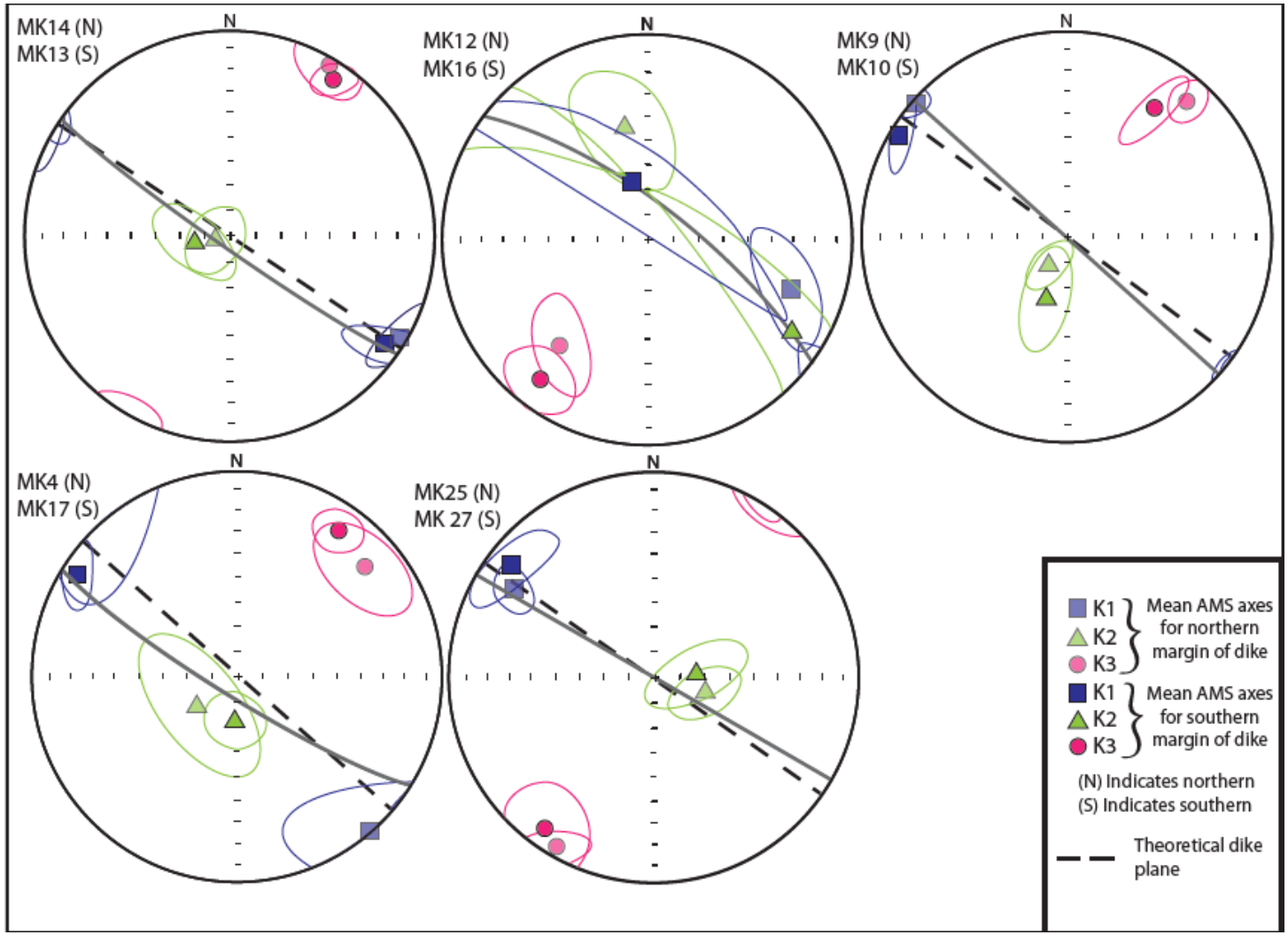

Figure 4.4 AMS plots for margin pairs that had undeterminable flow directions. In all cases, the K_1 axes show the same general sense of imbrication relative to the dike plane although the degree of imbrication can vary. The black dashed line indicates a theoretical dike plane that would yield mirror-imbricated pairs for four of the five margin pairs.

Flow trend can still be determined for these margins pairs based on their AMS. They all show dominantly horizontal flow similar to that of the paired margins that provided flow directions. Most pairs show a difference in the degree of imbrication relative to the dike plane, suggesting that, if the strike of the dike was slightly different, the margin pair would show mirror-imbricated AMS ellipsoids (Figure 4.4). This offset could possibly be due to very weak imbrication of the magnetic grains due to the low-viscosity of the magma, slow intrusive velocity of the magma, or slight undulations in dike flow, all of which could cause a wide spread of specimen K_1 axis orientations relative to the dike plane. Some of these margin pairs could also provide mirror-imbricated pairs, based on larger error ellipses for their mean K_1 axes. If the position of the mean K_1 axis was not in the exact center of the error ellipse, it would show the sense of imbrication necessary to create mirror-imbrication for flow direction determination (Figure 4.4). Through either the theoretical dike plane or adjustment of the K_1 axis position within the error ellipse a low-confidence flow direction can be determined. MK13 and MK14, MK4 and MK17, and MK25 and MK27 all would indicate NW flow as well. MK9 and MK10 would indicate SE flow. MK12 and MK16 would still be deemed undeterminable due to the large error ellipses on MK16. The error is so wide that the position of the mean K_1 axis could be anywhere along the dike plane, creating mirror or parallel imbrication depending on where the axis could be within the large error ellipse. Therefore, even a low-confidence flow direction cannot be determined for this pair of margins. Without further information or analyses, flow directions cannot be definitively determined for these margin pairs, so they are lower confidence and can only be used in a limited way when interpreting the emplacement of the northwest dikes swarm.

All of the middle sites with normal fabrics show horizontal flow generally in line with the strike of the dike and shallow plunges of the mean K_1 axes (Figure 4.5). The random sampling throughout the middle section does not allow for determination of flow directions, azimuths, and plunges. Even when individual specimens for a site are referenced to their position within the middle of the dike and relative to the dike plane on the AMS plot, there is no clear sign of imbricated pairs. The lack of imbricated pairs within the middle sites could have been a result of complex flow behavior, such as flow in both horizontal directions, within the dike during the cooling process. All of the middle sites show good clustering of the K_1 axes, except for MK29, which shows more variability in the position of K_1 axes and a larger error ellipse. MK6, MK22, MK26, and MK29 show a nearly even distribution of K_1 axes on either side of the dike plane, indicating a mix of imbrication behavior within these sections of the dikes. MK8 and MK18 have groupings of K_1 axes that are more dominantly oriented with declinations less than the strike of the dike plane, indicating a dominant imbrication among the specimens from those sites. This could be indicative of differences in the flow behavior of the dikes at these two sites. MK6 and MK8 also show a similar intermingling of K_2 and K_3 axes to MK11. The AARM for MK11 showed the possible influence of SD grains on the behavior of the AMS; MK8 and MK18 may also have some interference of SD grain behavior on their AMS.

The fabrics at the site scale were further defined through the use of E_1-E_2 calculations. These calculations are made post-analysis and can be used to understand the quality of the AMS fabrics on a site scale by averaging the errors in the declination and inclination for K_1 and K_2 in order to understand the quality of the lineation and foliation and whether it is coherent on the site scale. When the E_1-E_2 for the declination is plotted against the E_1-E_2 for the inclination, the majority of sites show a foliation and lineation (Figure 4.6). This general characteristic remains the same

whether the site is from a margin or middle of a dike. One outlier, MK16, shows only a foliation (Figure 4.6). The presence of only a foliation in MK16 is not completely unexpected given the wide spread of K_1 and K_2 axes in the AMS plot. Understanding the site-scale lineation and foliation present in the margins and middles is important when trying to understand the flow direction indicated by the magnetic lineation (K_1) or magnetic foliation (K_3). This shows a consistency of the fabrics from the specimen scale to the site scale.

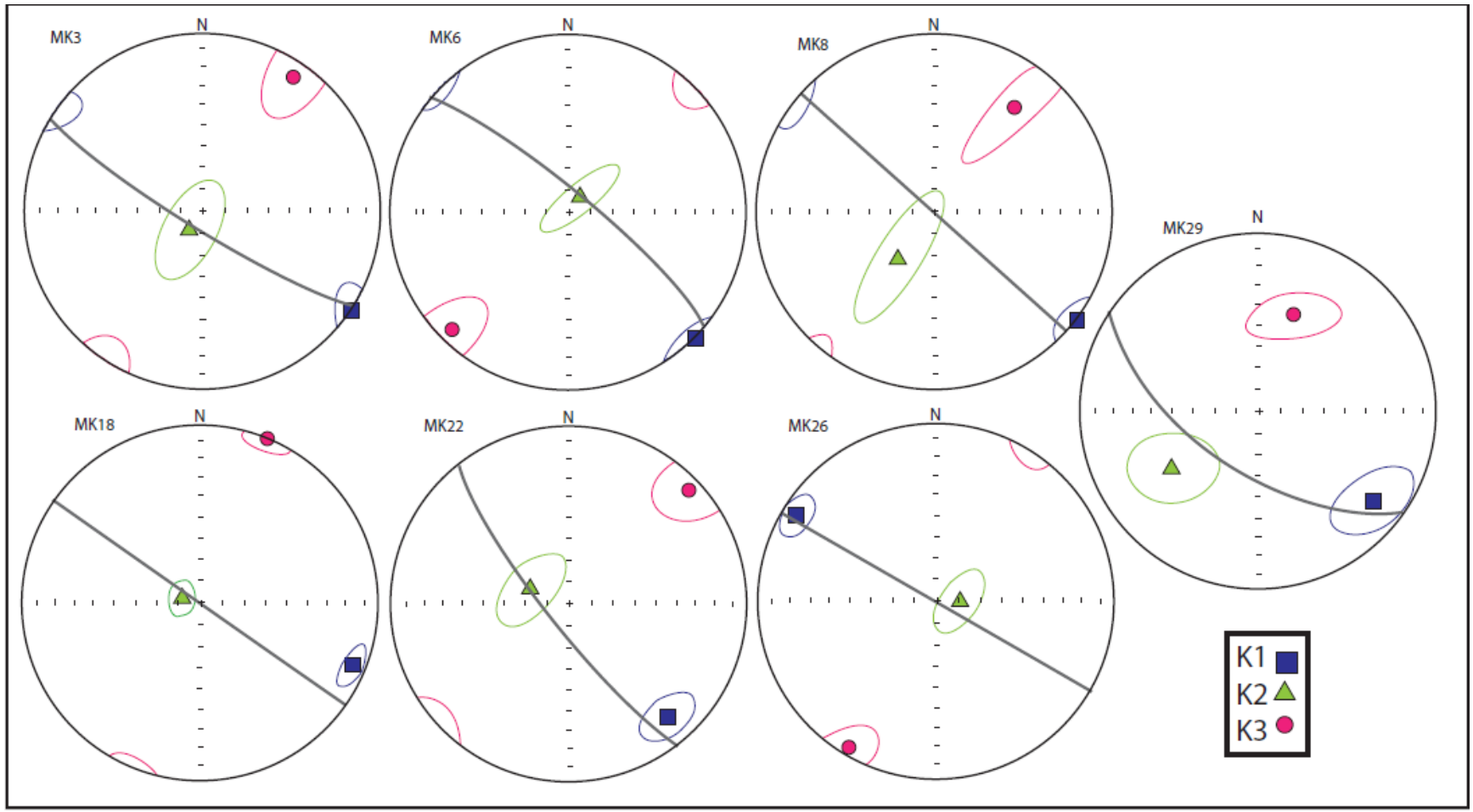

Figure 4.5 AMS ellipsoids for middle dike sites showing normal fabrics. The gray line indicates the dike plane.

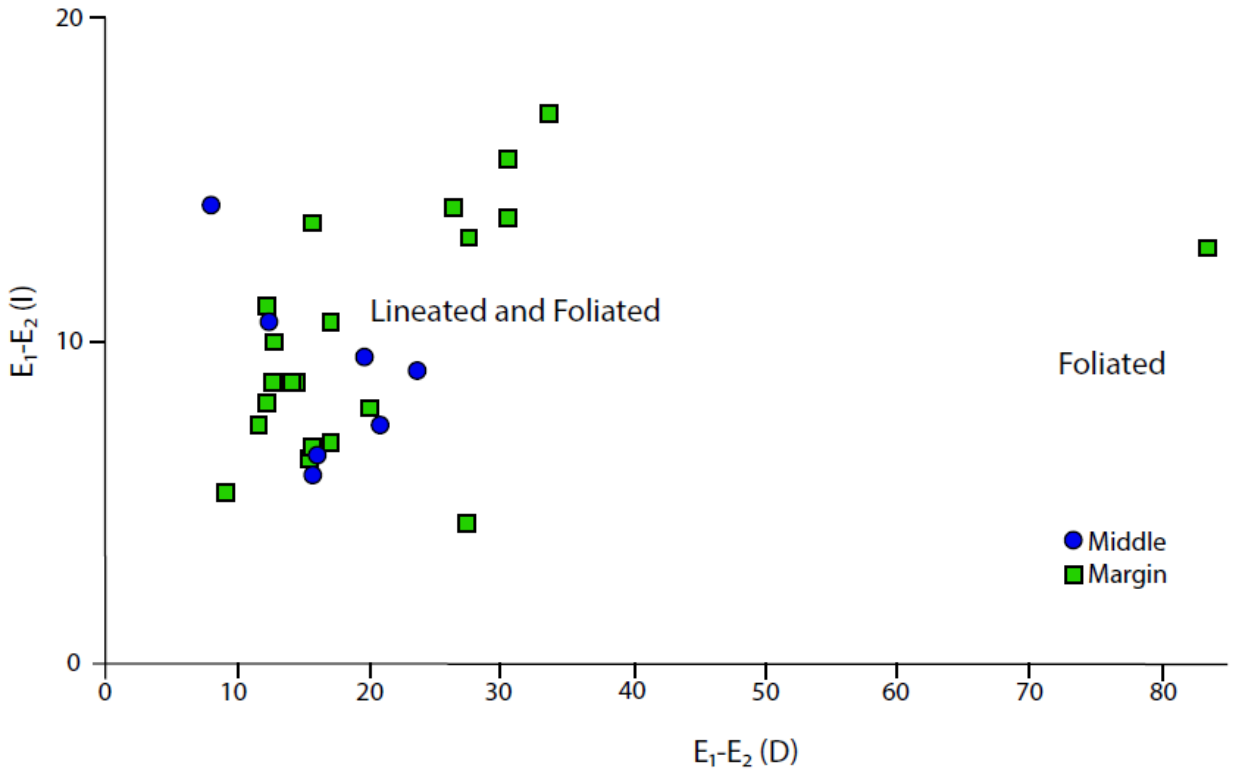

Figure 4.6 Plot of E_1-E_2 declination (D) versus inclination (I) comparing the site-scale fabrics of the middle sites versus the margin sites. The fabrics present in the dikes are similar at the site scale as indicated by most sites showing a lineation and foliation, regardless of whether they are middle or margin sites.

4.2 Implications for Injection of Northwest Dike Swarm

The dominantly horizontal flow behavior within all of the dikes indicates a lateral injection of the entire dike swarm. The magnetic survey data support this, showing that the intrusions do not continue below about 30 m beneath their current level of exposure. The northwest direction of flow is generally away from the transgressive sill that lies to the southeast, which formed in association with a volcanic conduit of some sort. This implies that the dikes were injected laterally away from the possible magma supply system. The magma supply system refers to the system of connected dikes that brought magma to the shallow subsurface from depth and fed eruptions and intrusions. The large mass of magma held within a vertical dike system in the

poorly consolidated Chinle Formation may have broken outward, pushing magma in lateral dikes. The three members of the Late Triassic Chinle Formation in this region primarily consist of unbedded or cross-stratified claystone, mudstone, siltstone, and sandstone deposits that were probably water-saturated at the time of eruption (See section 1.2 for further detail on regional stratigraphy; Reppening et al. 1969, Stewart et al. 1972a, White 1898, 1990). They would have made weak country rock around the intrusions. The diversion of the magma may have been a response to too much pressure in the shallow subsurface, limiting its vertical propagation, or it could simply have been a lateral breakout from the main magma supply system. Because the dike's propagation was limited vertically, the magma was then injected in the direction where the pressure gradient was greatest: horizontally. The injection of the dikes to the northwest may have played a critical role in changing the magma flux within the system and possibly triggered a shift from magmatic to phreatomagmatic eruptive behavior due to water ingress into the dike or a change in magma water ratios.

4.2.1 Implications of sub-horizontal flow for dike injection

Horizontal to sub-horizontal flow in dikes is a common behavior and has been observed in dikes of various ages (e.g. Raposo and Ernesto 1995; Callot et al. 2001; Herrero-Bervera et al. 2001; Callot and Geoffrey 2004; Poland et al. 2004; Eriksson et al. 2015). In some cases, the horizontal to sub-horizontal flow direction couples with consistent flow directions throughout a swarm or series of dikes to show lateral propagation of the dikes away from crustal reservoirs or volcanic centers, either in one direction or in a radial fashion (e.g. Callot et al. 2001; Callot and Geoffrey 2004; Poland et al. 2004; Eriksson et al. 2015). Callot et al. (2001) and Callot and Geoffrey (2004) used AMS to study dike swarms that formed in association with rifting in the east Greenland margin. Both studies found W-SW horizontal-dominated flow directions within

the studied dikes. They both conclude that the horizontal dominance of flow within the dikes indicates flow away from shallow magma reservoirs. The laterally injected dikes were also critical for feeding eruptions at the surface. Poland et al. (2004) studied a series of segmented dikes associated with the Summer Coon stratovolcano in southern Colorado. They also found dominantly horizontal flow within the studied series of dikes and flow directed generally away from the center of the volcano. Similarly to Callot et al. (2001) and Callot and Geoffrey (2004), they also concluded that the horizontal to sub-horizontal flow within the dikes recorded flow away from a shallow magma storage center beneath Summer Coon volcano. The lateral dike injection fed flank eruptions farther down the slope from the main volcanic conduit. Eriksson et al. (2015) analyzed the Álftafjörður dike swarm in Iceland. They found northerly directed, dominantly sub-horizontal flow. They also link the sub-horizontal flow directions to flow away from shallow magma chambers underneath the main volcanic conduit. They also concluded that the shallow lateral dikes fed fissure eruptions away from the main volcanic center.

AMS indicating dominantly horizontal to sub-horizontal flow within dikes is not uncommon behavior, but this flow behavior is typically linked to flow away from shallow magma chambers or shallow crustal reservoirs. Additionally, lateral injection of dikes has commonly been associated with feeding flank eruptions at the surface. The dikes studied by other workers are often part of more complex volcanic systems either being fed by a plume (i.e. Iceland) or in a system where shallow, crustal storage of magma is an expected feature (i.e. a stratovolcano). Porreca et al. (2016) studied a series of dikes in Spain that were part of a less complex system, more similar to JRC, and seems to be the only such study that focuses on AMS of dikes from a less complex volcanic system. Their AMS study found mostly vertical flow directions that they inferred to be indicative of vertical emplacement of the dikes. This differs

from the northwest dike swarm in JRC which shows dominantly horizontal flow indicative of horizontal emplacement. There is also no evidence for a shallow magma chamber in JRC, so emplacement away from a magma chamber is not applicable to the lateral propagation for the NW dike swarm. The dominantly horizontal flow in a northwestern direction does indicate flow away from the main magma supply system that was located to the southeast. The dikes in the northwest dike swarm acting as shallow crustal storage is unexpected given their emplacement in the shallow subsurface and likely connection to the main supply system for JRC.

The diversion of magma laterally in maar-diatreme systems has been reported elsewhere in the Hopi Buttes Volcanic Field. Lefebvre et al. (2012) studied a sequence of spatter dikes, diatremes, and maars at Castle Butte Trading Post volcanic complex. They found that the depositional units young to the northeast and that lateral movement of magma in the shallow subsurface played a critical role in the eruptive history of the spatter dikes. The spatter dikes record the lateral movement as well as the advance and retreat of magma that fueled the stops and starts in eruptive activity along multiple aligned vents. Cyclic withdrawal and ascent of magma fueled the northeastward propagation of the pyroclastic eruptions. The diversion of magma to the northeast in the form of a spatter dike caused eruptions to cease in the southwest Castle South maar before the eruptions ceased in the northeast Castle maar (Lefebvre et al. 2012). The spatter dikes present at Castle Butte Trading Post were important for the stops and starts of eruptions within the maars at the surface via the lateral diversion of magma to the northeast. Lateral diversion of magma in shallow structures plays a critical role in the evolution and connection of maar-diatreme conduits in the Hopi Buttes Volcanic Field. The lateral diversion of magma in the NW dike swarm in JRC may have played a similar role in the initiation and connection of maar-diatreme conduits.

4.2.2 Model for emplacement of NW dike swarm and SE intrusions in JRC

Re et al. (2015) proposed three possible models for the formation of the JRC intrusions based on the textural differences between the intrusions (i.e. the presence of phologopite phenocrysts in the NW dike swarm and larger clinopyroxene phenocrysts in the NW dike swarm than in the other intrusions):

1) The NW dikes and SE intrusions were fed by two non-communicating plumbing systems that experienced distinct stress conditions and were fed by two separate batches of magma.

2) The SE intrusions were emplaced first from a magma source at depth. A pause in magmatism allowed for the growth of crystals in the magma and a change in the shallow stress regime. A new batch of magma was then injected and emplaced into the NW dikes under the new stress conditions.

3) The magma was all derived from a single source, but different magma ascent processes occurred in the complex. Magma and crystals rose together and were emplaced to form the NW dikes, but the coarser crystals were filtered out from the magma before or during injection in the rest of the complex.

Based on the horizontal flow directions for the NW dike swarm and recent geochemistry data from Re et al. (in review) showing two distinct batches of magma formed the NW and SE intrusions, the first and third models are unlikely explanations for the relation between the different intrusions. If the first model were valid, the flow directions within the NW dike swarm should have showed flow dominated by vertical movement in at least some portions of the dikes, assuming that the supply system was located somewhere below the intrusions. Additionally, the

magnetic survey would have been expected to result in some broader magnetic anomalies if the dikes extended deep below their current level of exposure. Although this does not fully rule out the possibility of the intrusions being fed by separate plumbing systems, the horizontal flow directions and close spacing between the NW and SE intrusions indicate that it is unlikely that the NW dikes are fed by a completely separate feeder system. The third model is invalid due to the geochemical analysis done by Re et al. (in review) that showed that the intrusions in JRC were formed by two different batches of magma. The difference in phenocryst type and size in the NW versus the SE is due to differences in ascent rate and not a filtering process as suggested by the third model (Re et al. in review). This leaves the second model as the most probable explanation for the relation between the NW and SE intrusions. In this model, vertical flow is not necessary, thus allowing for the possibility of lateral injection for the formation of the NW dikes. It also fits the idea that the NW dikes were injected laterally away from a magma supply center.

4.2.3 Emplacement History of the Northwest Dike Swarm and Associated Massifs

If the second model most accurately represents the evolution of the system, it would indicate that the magma supply system formed in the SE portion of the complex first, possibly feeding eruptions of maar-diatremes and/or scoria cones at the surface. Both Re et al. (2016) and Muirhead et al. (2016) provide evidence for a volcanic edifice existing above the intrusions in the SE portion of JRC based on their understanding of the conditions necessary for the formation of a transgressive sill. Re et al. (2016) suggests that a volcanic load at the surface could alter the shallow subsurface stress regime below the volcano so that it becomes favorable for sill formation. They propose that these are the conditions under which the transgressive sill formed in the southeast portion of JRC, providing evidence for the possible existence of volcanic edifice at the surface above the intrusions in the SE. The second batch of magma entered the magma

supply system in JRC and rose vertically until it stalled at depth or reached the maximum overpressure level (MOL) in the shallow crust (Pinel and Jaupart 2004; Kervyn et al. 2009). The MOL is the level where the magma overpressure is largest due to the pressure inside the vertical magma column (Figure 4.7). This level was probably near the base of the Chinle Formation based on the depth calculations for the dikes. The magma was then either stored at this level or injected laterally (Figure 4.7; Pinel and Jaupart 2004). The batch of magma that formed the NW dikes was then injected horizontally away from the existing conduits and volcanic edifices because that is the direction in which the pressure gradient is the largest (Pinel and Jaupart 2004; Kervyn et al. 2009). The poorly lithified nature of the Chinle Formation may have aided this process. The direction of injection was most likely controlled by the local stress regime, given that most of the Chinle Formation lacks structures that would control the propagation laterally.

The injection of the NW dike swarm laterally may have been a response to increased pressure in the shallow crust due to the overburden created by volcanic deposits at the surface (e.g. a scoria cone). Lateral injection of dikes as a response to increased pressure in the shallow subsurface due to overlying volcanic edifices has been observed in models as well as in natural systems (e.g. Pinel and Jaupart 2004; Kervyn et al. 2009, Pinel et al. 2017) and it is a possible mechanism for the lateral injection of the NW dike swarm. Pinel et al. (2017) modelled dike propagation behavior when a surface load is present. They found that the dike orientation during propagation is governed by the magma excess pressure and the local external stress field. Magma excess pressure within the supply system could also be derived from the magma in the system above the ascending batch exerting pressure downward. The lateral injection could have also been a response to pressure within the overlying magma column. This may better explain why the dikes did not simply result in flank eruptions on the edges of existing conduits and instead

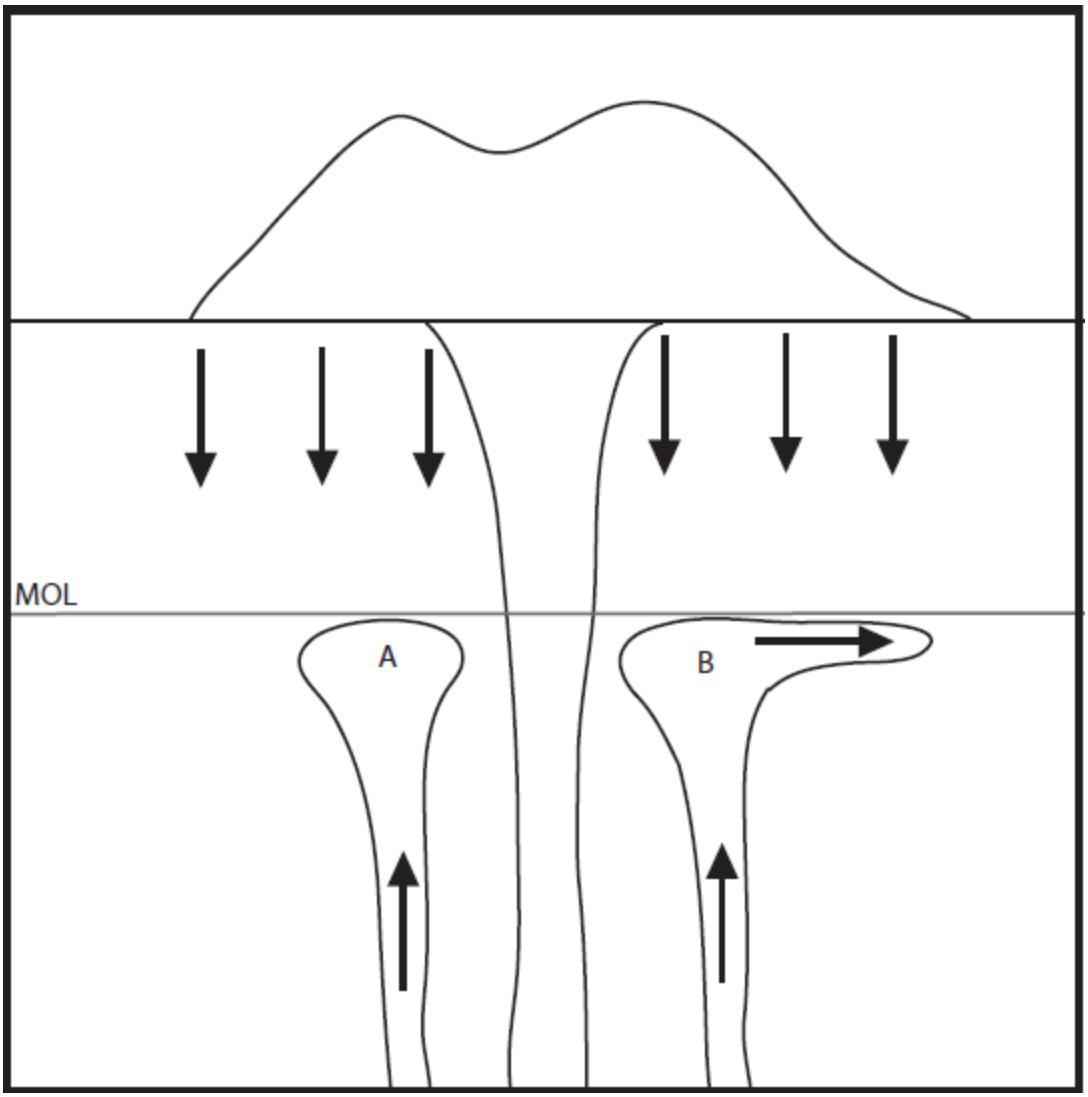

Figure 4.7 Schematic figure illustrating the maximum overpressure level (MOL) and its influence on a body of magma rising below a volcanic edifice. The magma can either be trapped at the MOL (A) or it can be injected laterally (B). The arrows below the volcanic edifice indicate the increased pressure within the shallow subsurface and the arrows within the rising magma bodies indicate the direction of flow within them.

the dikes propagated farther away from the existing volcanic edifices. Both of these mechanisms imply forceful intrusion due to the buildup of pressure within the magma supply system. It is also possible that the lateral injection of magma was simply a breakout from the main magma supply system and followed pre-existing weaknesses in the Chinle Formation. This would

suggest that the dikes' horizontal emplacement was controlled by the direction in which the pressure gradient was the greatest (i.e. in the direction that provided the least resistance).

Forceful intrusion due to high pressure within the magma supply system would result in an initially high injection velocity and thus also high magmatic flux. High flux would be a convenient explanation for the coherent intrusion of the dikes, given that some workers argue that high flux limits magma/water mixing necessary for phreatomagmatism (Valentine and White 2012, Valentine and Cortes 2013, Lefebvre et al. 2016). Pinel et al. (2017) found the dike propagation velocity is governed by the magma excess pressure and the local external stress field. If high velocity, forceful intrusion were the mechanism for the initial emplacement of the NW dike swarm, the magma would experience a high amount of shear in a narrow shear zone along he margins given the low viscosity of the magma (at least initially). This would account for the strong grouping of specimens' K_1 axes in some sites, but would not explain the weaker grouping of K_1 axis in some margin sites (e.g. MK21 in Figure 3.4). This results in variable imbrication of the mean K_1 axes between sites as well depending on how much variability they have in individual specimen K_1 axes. Therefore high-velocity, forceful intrusion due to overpressure in the magma supply system is not a fair assumption of the initial injection of the northwest dike swarm. It is possible that stalling of magma flow after initial injection could account for weaker imbrication and create the variability in K_1 axis orientations seen in most sites.

Lateral injection of the northwest dike swarm as the result of a breakout from the magma supply system due to weaknesses in the surrounding rock providing a magma pathway would probably result in a lower injection velocity. A lower injection velocity (especially with low viscosity magma) would result in less shear in a narrower zone of the margins and weaker

grouping of specimens' K_1 axes within a site. As the margins cooled, it is possible that the thickness of the shear zone increased, which could account for the variability in imbrication of K_1 axes seen in a single site. This explanation seems to more accurately reflect the variability in specimen K_1 axis orientations within site and is a more likely mechanism for the initial injection that formed the margins of the NW dike swarm. The lower injection velocity could have also limited the vertical propagation of the northwest dike swarm (Pinel and Jaupart 2004; Pinel et al. 2017), possibly confining it to the Chinle Formation. Most sites show weaker grouping of K_1 axes, but some sites show very strong grouping (e.g. MK13 in Figure 3.2). Therefore, a lower initial injection velocity is more likely, because it more accurately accounts for both strong and weak grouping of K_1 axes. In the instance of lower-velocity intrusion, the lack of magma/water interaction during the initial formation of the dikes may simply be due to magma/water ratios during initial intrusion.

Possible drain back after the initial formation of the dikes would allow for interaction with the wet sediments and possibly allow for water to infiltrate any existing conduits. This could possibly be the source of the buds and massifs present throughout the dike swarm (Figure 4.8; Re et al. 2016). Drain-back of magma within dikes causing a shift to phreatomagmatism has been interpreted in other systems and would have been possible in JRC (e.g. Houghton and Schmincke 1986; Geshi and Neri 2014). Some documented transitions between magmatic and phreatomagmatic eruptive styles within the same system appear to be related to magma or groundwater flux (Valentine and Cortes 2013). This can result in a transition from magmatic to phreatomagmatic, from phreatomagmatic to magmatic, or alternating between the two eruptive styles (Lorenz 1986; Houghton and Schminke 1986; White 1991; Houghton et al. 1999; Gutmann 2002; Valentine and Cortes 2013). Valentine and Cortes (2013) documented a

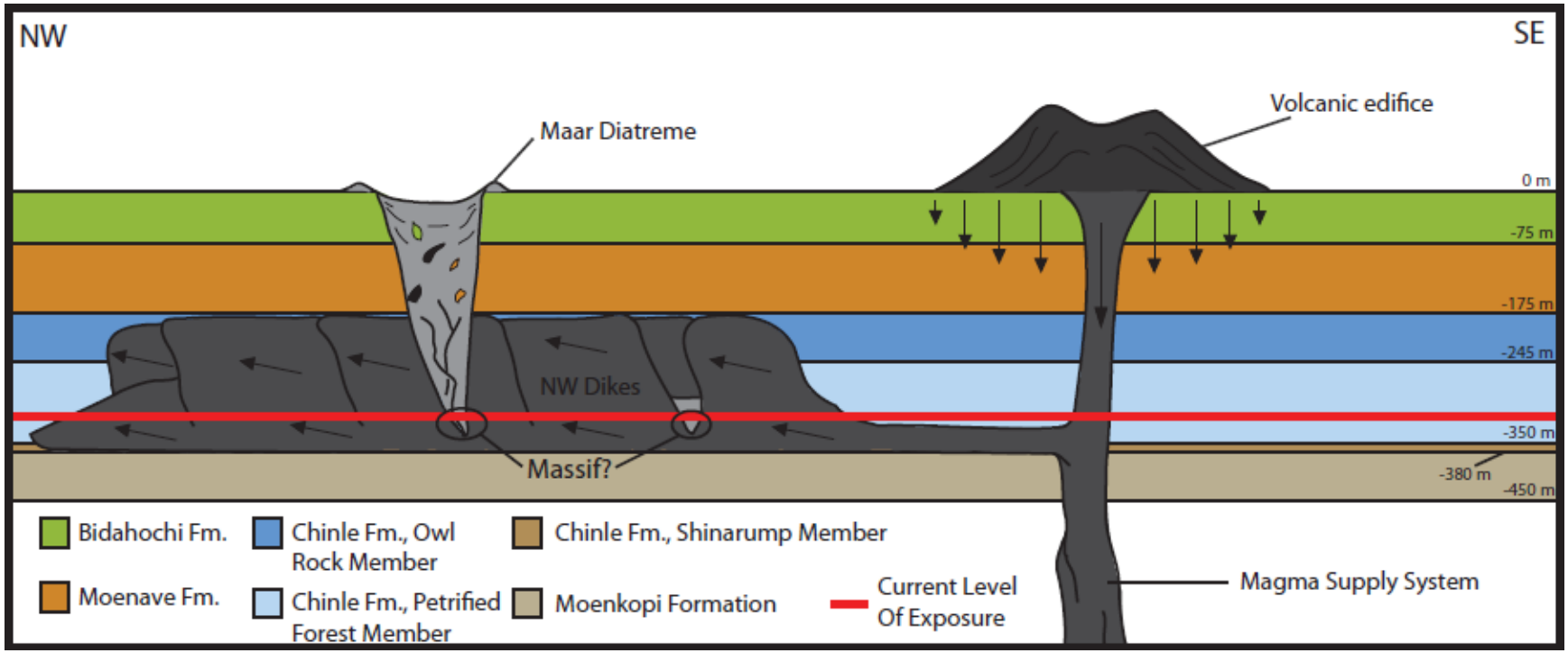

Figure 4.8 Simplified summary figure of the inferred lateral emplacement of the northwest dikes from the main magma supply system to the southeast. The arrows below the volcanic edifice indicate the downward pressure applied to the shallow subsurface while the arrow within the magma supply system below the volcanic edifice indicates downward pressure within the supply system. The arrows within the NW dikes indicate the general direction of flow recorded within them at the exposed level. The flow is assumed to be the same at the levels above the exposed area. The vertical extent both above and below the exposure level is based off of the magnetic survey data as well as the size of the dikes. The dikes may be confined to the Chinle Formation due to its weak lithologic characteristics. The areas circled and labelled as a massif indicate places where massifs may have formed either as part of a diatreme or as contained phreatomagmatic explosions below the surface. The scale on the right side of the figure indicates the depth and thickness of the strata in meters.

transition from a magmatic, cone-building eruption to a phreatomagmatic, maar-crater-forming eruption at Easy Chair volcano in the Lunar Crater Volcanic Field in central Nevada. They linked this transition to a change in magma flux within the system, allowing for magma/water mixing that resulted in phreatomagmatic activity later in the eruption. Gutmann (2002) documented magmatic to phreatomagmatic transitions within the Pinacate Volcanic Field in Mexico. He linked this change in behavior to a change in rates of magma rise. Higher magma flux during initial formation of the conduits overwhelmed the lower groundwater flux, creating magmatic activity initially. A change in magma flux and magma withdrawal allowed for the transition to phreatomagmatic activity in the conduits by creating the necessary water/melt mass ratios. He indicated that magma withdrawal in the conduits may have allowed for wet sediment or water to enter the conduit and initiate the explosive interactions between water and melt. Any of these mechanisms could be possibilities for the presence of coherent dikes alongside the massifs that formed through phreatomagmatic activity.

The presence of buds and massifs in the NW dike swarm indicates that magma/water ratios were within the preferred range at some point, resulting in phreatomagmatic activity at the level of the dikes and likely above as well. The phreatomagmatic activity could have been concentrated in conduits or in elongate fissures, allowing for the difference in the geometry of the massifs (i.e. sub-circular to elongate/tabular) (Re et al. 2016). Water/magma ratios are an important influence on the molten-fuel-coolant-interaction (MFCI)-driven fragmentation, which is the main eruptive mechanism in maar-diatreme systems (Zimanowski et al. 1991; Zimanowski et al. 1997; Hooten and Ort 2002; Sparks et al. 2006). The massifs are remnants of fissural conduits that may have fed surface eruptions similar to those observed at the Castle Butte in the Hopi Buttes Volcanic Field (Lefebvre et al. 2012; Re et al. 2016).

4.3 Problems with AMS Analyses on Dikes

For the dikes analyzed in this study, AMS analyses resulted in an unclear dataset when it came to reliable sets of imbricated AMS ellipsoids for flow direction interpretation. The mean AMS axes allowed for interpretation of flow directions for half of the margin pairs, but the other half of the dike margin pairs could not be interpreted for flow directions due to the K_1 axes showing parallel imbrication relative to the dike plane. While this still provides some meaningful information about flow within the dikes, it affected the robustness of the results. For example, all dike margin pairs along dike 1 did not provide flow directions despite there being three drilling locations spread along the length of the dike. This results in a data gap, which does not allow for any interpretations for distinct flow directions along the entire dike. The general behavior of the magma flow within the dike margins can still be described, but having a discrete flow direction, azimuth, and plunge for at least one of the locations along dike 1 would have been ideal.

AMS can be a very useful and quick technique for determining flow directions for dikes, but in some cases it provides more mixed results. The reliability of using the lineation (mean K_1 axis orientation relative to the dike plane) versus the foliation plane (mean K_3 axis orientation relative to the pole to the dike plane) for determination of flow directions has been discussed in several recent AMS studies of dikes (e.g. Callot et al. 2001; Geoffroy et al. 2002; Callot and Guichet 2003; Callot an Geoffroy 2004; Eriksson et al. 2015). In some cases, the magnetic lineation as defined by the mean K_1 axis does not line up with macroscopic flow indicators and/or phenocryst alignment in thin sections, showing a major discrepancy in flow directions determined from AMS and those determined through outcrop or thin section analysis (Geoffroy et al. 2002). This has called into question not only the reliability of the magnetic lineation method for determination of flow directions, but also the reliability of AMS results without a secondary

method for flow determination to corroborate them. Multiple studies have tried to understand the source of this discrepancy. Callot and Guichet (2003) suggested the possibility of several flow-related anisotropies derived from multiple superimposed rock textures. The use of different rock magnetic analyses besides AMS and AARM has shown that multiple magnetic fabrics of differing orientations can exist within a dike, possibly interfering with the AMS fabric that is assumed to represent only the flow-related fabric (Silva et al. 2014). Geoffroy et al. (2002) suggested that the variability in anisotropy could possibly be due to titanomagnetite being a late-crystallizing mineral phase and thus possibly post-dating the magma flow in the dike. In their study, they found a difference between the physical orientation of opaque minerals and plagioclase phenocrysts, possibly causing the difference between flow indicated by AMS and petrographic analysis. Either of these explanations could account for the discrepancies in flow direction present in some dikes.

The use of the magnetic foliation as another tool for determining the flow direction solely from AMS ellipsoid orientations arose as an alternative method to using the magnetic lineation and has proven to be more reliable in some cases (e.g. Eriksson et al. 2015; Soriano et al. 2008; Geoffroy et al. 2002). In my study, the use of the K_3 method and foliation plane orientation did not provide clearer imbrication results than the use of the magnetic lineation (K_1), indicating that while the use of the magnetic foliation plane can be more reliable than the use of the magnetic lineation, it does not always help in understanding the orientation of the AMS ellipsoid. Because neither method for determination of flow directions from AMS alone has proven to result in reliable interpretations of flow directions, some authors have encouraged the use of thin section analysis or macroscopic flow features in addition to AMS to ensure the reliability of the results (e.g. Callot et al. 2001). Determining whether a series of dikes is going to provide reliable AMS

results is impossible before specimen analysis. It would be ideal if it were common place to employ other techniques to reinforce the flow direction determinations from AMS plots from the beginning, especially when sampling an area or series of intrusions for the first time, thus ensuring the reliability of the interpretation.

Chapter 5: Conclusions

The dikes in the northwest dike swarm in the Jagged Rocks Complex contain mostly high-titanium titanomagnetite grains. They are dominantly pseudo-single domain grains with evidence for single domain grains influencing some of the AMS fabrics as supported by the isothermal remanent magnetization and the anisotropy of anhysteretic remanent magnetization results. Characteristic remanence magnetization analyses show that the dikes in the northwest dike swarm have similar magnetic pole declination and inclination, indicating that the dikes were roughly contemporaneous in their emplacement. The magnetic survey shows that the swarm continues in the subsurface to the northwest of where it is exposed, and that the dikes only continue about 30 m below their level of exposure. The depth calculation indicates that the dikes do not extend below the base of the Chinle Formation.

Half of the dike margin pairs sampled showed mirror-imbricated AMS ellipsoids, allowing for the determination of the flow direction in the dikes. The flow within the dikes is dominantly horizontal in a northwest direction. The northwest flow direction is away from the main magma supply system feeding eruptions and intrusions in the Jagged Rocks Complex. Lateral emplacement contradicts the expected formation of the northwest dike swarm as a separate, vertically emplaced system. It is unlikely that the dikes formed through forceful emplacement due to the buildup of pressure from magma rising from below, but instead they

may have formed through a breakout from the magma supply system that followed the direction of least resistance in the pre-existing stress regime. Their emplacement was also aided by the weakness of the poorly consolidated Chinle Formation. Their initial emplacement was probably at a low velocity, as recorded by the weak grouping of the K_1 axes in the AMS plots for most of the margin sites. Cooling of the margins possibly increased viscosity and the thickness of shear zones, resulting in the variability of K_1 axis positions within a single site. The dikes' emplacement was initially coherent and the dikes were confined to the Chinle Formation, never extending to the surface as dikes. The eruptions fed by the dikes involved phreatomagmatic activity at some point, the remnants of which are seen in the form of massifs exposed throughout the dike swarm (Figure 4.8). The transition from coherent intrusions to phreatomagmatic eruptions was most likely due to a change in magma/water ratios or water infiltration due to magma withdrawal.

The flow history preserved in the northwest dike swarm in the Jagged Rocks Complex provides critical information regarding the role of lateral diversion of magma in the eruptive activity in short-lived, monogenetic systems. Lateral dikes may be important as a means of shallow magma storage that could feed eruptions away from the main magma supply system. Shallow magma storage may be crucial for short-lived, monogenetic systems that lack the magma chambers of more complex and long-lived systems. Lateral magma storage in the form of dikes may play a more crucial role in monogenetic systems than previously thought. Understanding the source of changes in eruptive style and connection between conduits is critical for understanding and assessing the threats that are posed by monogenetic volcanic systems, because understanding the evolution of the eruptive history of monogenetic systems and the

variations in eruptive style can aid in the prediction and understanding of the continuation of eruptions throughout a field or complex.

References

Alva-Valdivia, L.M., Rosas-Elguera J., Bravo-Medina T., Urrutia-Fucugauchi J., Henry B., Caballero C., Rivas-Sanchez M.L., Goguitchaichvili A., López-Loera H. (2005) Paleomagnetic and magnetic fabric studies of the San Gaspar ignimbrite, western Mexico-constraints on emplacement mode and source vents. Journal of Volcanology and Geothermal Research 147 pp. 68-80

Billlingsley, G.H., Block D., Hiza-Redsteer M. (2013) Geologic map of the Winslow 30' x 60' Quadrangle, Coconino and Navajo Counties, northern Arizona. USGS Scientific Investigations, Map 3247.

Borradaile, G.J., Gauthier, D. (2001) AMS-detection of inverse fabrics without AARM, in ophiolite dikes. Geophysical Research Letters 28(18) pp. 3517-3520

Borradaile, G.J., Henry, B. (1997). Tectonic applications of magnetic susceptibility and its anisotropy. Earth-Science Reviews 42 pp. 49-93

Butler, R.F. (1992) Paleomagnetism: Magnetic domains to geologic terranes. Blackwell Scientific.

Callot, J.P., Geoffroy, L. (2004) Magma flow in the East Greenland dyke swarm inferred from study of anisotropy of magnetic susceptibility: magmatic growth of a volcanic margin. Geophysical Journal International 159 pp. 816-830

Callot, J.P., Geoffroy, L., Aubourg, C., Pozzi, J.P., Mege, D. (2001) Magma flow directions of shallow dykes from the East Greenland volcanic margin inferred from magnetic fabric studies. Tectonophysics 335 pp. 313-329

Callot, J.P., Guichet, X. (2003) Rock texture and magnetic lineation in dykes: a simple analytical model. Tectonophysics 366 pp.207-222

Callot, J.P., Gurevitch, E., Westphal, M., Pozzi, J.P. (2004) Flow patterns in the Siberian traps deduced from magneti fabric studies. Geophysics Journal Inernational 156 pp. 426-430

Cañon-Tapía, E. (2001) Factors affecting the relative importance of shape and distribution anisotropy in rocks: theory and experiments. Tectonophysics 340 pp.117-131

Delaney, P.T., Pollard, D.D. (1981) Deformation of host rocks and flow of magma during growth of minette dikes and breccia-bearing intrusions near Ship Rock, New Mexico. U.S. Geological Survey Professional Paper pp.1-61

Delcamp, A., Petronis, M.S., Troll, V.R. (2014) Discerning magmatic flow patterns in shallow-level basaltic dykes from the NE rift zone of Tenerife, Spain, using the anisotropy of magnetic susceptibility (AMS) technique. The use of palaeomagnetism and rock magnetism to understand volcanic processes. Geological Society, London, Special Publications 396 pp.87-106

Dunlop, D.J. (1972) Magnetic mineralogy of unheated and heated red sediments by coercivity spectrum analysis. Geophysical Journal International 27 pp.37-55

Eriksson, P.I., Riishuus, M.S., Elming, S.-Å. (2015) Magma flow and palaeo-stress deduced from magnetic fabric analysis of the Álftafjöður dyke swarm: implications for shallow

crustal magma transport in Icelandic volcanic systems. The use of palaeomagnetism and rock magnetism to understand volcanic processes, Geological Society, London, Special Publication 396 pp. 107-132

Geoffoy, L., Callot, J.P., Auborg, C., Moreira, M. (2002) Magnetic and plagioclase linear fabric discrepancy in dykes: a new way to define the flow vector using magnetic foliation. Terra Nova 14 pp.183-190

Geshi, N., Neri, M. (2014) Dynamic feeder dyke systems in basaltic volcanoes: the exceptional example of the 1809 Etna eruption (Italy). Frontiers in Earth Science 2 pp.1-11

Gutman, J.T. (2002) Strombolian and effusive activity as precursors to phreatomagmatism: eruptive sequence at maars of the Pinacate volcanic field, Sonora, Mexico. Journal of Volcanology and Geothermal Research 113 pp.345-356

Hack, J.T. (1942) Sedimentation and volcanism in the Hopi Buttes, Arizona. Bulletin of the Geologic Society of America 53 pp. 335-372

Heiniger, C. (1979) Palaeomagnetic and rockmagnetic properties of the Permian volcanics in the Western Southern Alps. Journal of Geophysics 46 pp. 397-411

Herrero-Bervera, E., Walker, G.P.L., Cañon-Tapia, E., Garcia, M.O. (2001) Magnetic fabric and inferred flow direction of dikes, conesheets and sill swarms, Isle of Skye, Scotland. Journal of Volcanology and Geothermal Research 106 pp. 195-210

Hillhouse, J.W., Wells, R.E. (1991) Magnetic fabric, flow directions, and source area of the lower Miocene Peach Springs Tuff in Arizona, California, and Nevada. Journal of Geophysical Research 96(B7) pp. 12,443-12,460

Hooten, J.A., Ort, M.H. (2002) Peperite as a record of early-stage phreatomagmatic fragmentation processes: an example from the Hopi Buttes volcanic field, Navajo Nation, Arizona, USA. Journal of Volcanology and Geothermal Research 114 pp. 95-106

Houghton, B.F., Schminke, H.-U. (1986) Mixed deposits of simultaneous strombolian and phreatomagmatic volcanism: Rothenberg volcano, East Eifel Volcanic Field. Journal of Volcanology and Geothermal Research 30 pp.117-130

Houghton, B.F., Wilson, C.J.N., Smith, I.E.M. (1999) Shallow-seated controls on styles of explosive basaltic volcanism: a case study from New Zealand. Journal of Volcanology and Geothermal Research 91 pp.97-120

Keller, R., Schmidbauer, E. (1999) Magnetic hysteresis properties and rotational hysteresis losses of synthetic stress-controlled titanomagnetite ($Fe_{2.4}Ti_{0.6}O_4$) particles-I. Magnetic hysteresis properties. Geophysical Journal International 138 pp. 319-333

Kervyn, M., Ernst, G.G.J., van Wyk de Vries, B., Mathieu, L., Jacobs, P. (2009) Volcano load control on dyke propagation and vent distribution: Insights from analogue modeling. Journal of Geophysical Research 114 pp. 1-26

Knight, M.D., Walker, G.P.L. (1988) Magma flow directions of the Koolau Dike Complex, Oahu, determined from magnetic fabric studies. Journal of Geophysical Research 93(B5) pp.4301-4319

Krása, D., Herrero-Bervera, E. (2005) Alteration induced changes of magnetic fabrics as exemplified by dykes of the Koolau volcanic range. Earth and Planetary Science Letters 240 pp. 445-453

Lanza, R., Meloni, A. (2006) The Earth's magnetism. Springer.

Lefebvre, N.S., White, J.D.L., Kjarsgaard, B.A. (2016) Arrested diatreme development: Standing Rocks East, Hopi Buttes, Navajo Nation, USA. Journal of Volcanology and Geothermal Research 310 pp.186-208

Lefebvre, N. S., White, J.D.L., Kjarsgaard, B.A. (2013) Unbedded diatreme deposits reveal maar-diatreme-forming eruptive processes: Standing Rocks West, Hopi Buttes, Navajo Nation, USA. Bulletin of Volcanology 75(739) pp. 1-17

Lefebvre, N. S., White, J.D.L., Kjarsgaard, B.A. (2012) Spatter-dike reveals subterranean magma diversions: Consequences for small multivent basaltic eruptions. Geology 40(5) pp. 423-426

Lorenz, V. (1986) On the growth of maars and diatremes and its relevance to the formation of tuff rings. Bulletin of Volcanology 48(5) pp. 265-274

Lurcock, P.C., Wilson, G.S. (2012) PuffinPlot: A versatile, user-friendly program for paleomagnetic analysis. Geochemistry, Geophysics, Geosystems 13(6) pp. 1-6

Marshall, A., Connor, C., Kruse, S., Malservisi, R., Richardson, J., Courtland, L., Connor, L., Wilson, J., and Karegar, M.A. (2015) Subsurface structure of a maar-diatreme and associated tuff ring from a high-resolution geophysical survey, Rattlesnake Crater, Arizona. Journal of Volcanology and Geothermal Research 304 pp.253-264

Muirhead, J.D., Van Eaton, A.R., Re, G., White, J.D.L., Ort, M.H. (2016) Monogenetic volcanoes fed by interconnected dikes and sills in the Hopi Buttes volcanic field, Navajo Nation, USA. Bulletin of Volcanology 78(11) pp. 1-16

Philpotts, A.R., Philpotts, E.P. (2007) Upward and downward flow in a camptonite dike as recorded by deformed vesicles and the anisotropy of magnetic susceptibility (AMS). Journal of Volcanology and Geothermal Research 161 pp. 81-94

Pinel, V., Carrara, A., Maccaferri, F., Rivalta, E., Corbi, F. (2017) A two-step model for dynamical dike propagation in two dimensions: Application to the July 2001 Etna eruption. Journal of Geophysical Research: Solid Earth pp.1107-1125

Pinel, V., Jaupart, C. (2004) Magma storage and horizontal dyke injection beneath a volcanic edifice. Earth and Planetary Science Letters 221 pp.245-262

Poland, M.P., Fink, J.H., Tauxe, L. (2004) Patterns of magma flow in segmented silicic dikes at Summer Coon volcano, Colorado: AMS and thin section analysis. Earth and Planetary Science Letters 219 pp. 155-169

Porreca, M., Cifelli, F., Soriano, C., Giordano, G., Mattei, M. (2015) Magma flow within dykes in submarine hyaloclastite environments: an AMS study of the Miocene Cabo de Gata volcanic units. Geological Society, London, Special Publication 396 pp. 133-157

Potter, D.K. (2004) A comparison of anisotropy of magnetic remanence methods-a user's guide for application to palaeomagnetism and magnetic fabric studies. Magnetic Fabric: Methods and Applications, Geological Society, London, Special Publication 238 pp. 21-35

Raposo, M.I.B., Ernesto, M. (1995) Anisotropy of magnetic susceptibility in the Ponta Grossa dyke swarm (Brazil) and its relationship with magma flow direction. Physics of the Earth and Planetary Interiors 87 pp. 183-196

Re, G., Palin, J.M., White, J.D.L., Parolari, M. (In Review) Unravelling the magmatic system beneath a monogenetic volcano complex (Jagged Rocks Complex, Hopi Buttes, AZ) Contributions to Mineralogy and Petrology.

Re, G., White, J.D.L., Muirhead, J.D., Ort, M.H. (2016) Subterranean fragmentation of magma during conduit initiation and evolution in the shallow plumbing system of the small-volume Jagged Rocks volcanoes (Hopi Buttes Volcanic Field, Arizona, USA) 78(55) pp. 1-20

Re, G., White, J.D.L., Ort, M.H. (2015) Dikes, sills, and stress-regime evolution during emplacement of the Jagged Rocks Complex, Hopi Buttes Volcanic Field, Navajo Nation, USA. Journal of Volcanology and Geothermal Research 295 pp. 65-79

Re, G., White, J.D.L., Ort, M.H. (2014) Overview of Jagged Rock, a frozen plumbing system exposed in Hopi Buttes, Navajo Nation, USA. Abstract with Program.

Reppening, C.A., Cooley, M.E., and Akers, J.P. (1969) Stratigraphy of the Chinle and Moenkopi Formations, Navajo and Hopi Indian Reservations Arizona, New Mexico, and Utah. Geological Survey Professional Paper 521-B pp.1-30

Reppening, C.A., Irwin, J.H.(1954) Bidahochi Formation of Arizona and New Mexico. AAPG Bulletin. 38(8) pp. 1821-1826

Rochette, P., Jackson, M., Aubourg, C. (1992) Rock magnetism and the interpretation of anisotropy of magnetic susceptibility. Review of Geophysics 30(3) pp.209-226

Rolph, T.C. (1997) An investigation of the magnetic variation within two recent lava flows. Geophysical Journal International 130 pp. 125-136

Shafiqullah, M., Damon, P.E. (1986) Hopi Buttes volcanism-Geochronology and geologic evolution. Arizona Geologic Society Digest 16 pp.499-500

Shoemaker, E.M., Roach, C.H., Byers, F.M. Jr. (1957) Diatremes on the Navajo and Hopi Reservations, Arizona. Trace Elements Investigation Report TEI-0700 pp. 141-151

Shoemaker, E. M., Roach, C.H., Byers, F.M. Jr. (1962) Diatremes and uranium deposits in the Hopi Buttes, Arizona. Petrologic studies: A volume to honor A. F. Buddington pp. 327-355.

Silva, P.F., Marques, F.O., Machek, M., Henry, B., Hirt, A.M., Roxerová, Z., Madureira, P., Vratislav, S. (2014) Evidence for non-coaxiality of ferromagnetic and paramagnetic fabrics, developed during magma flow and cooling in a thick mafic dyke. Tectonophysics 629 pp.155-164

Soriano, C., Beamund, E., Garcés, M., Ort, M. H. (2016) “Anomalous” magnetic fabrics of dikes in the stable single domain/superparamagnetic threshold. Geophysical Journal International. 204 pp.1040-1059

Soriano, C., Beamud, E., Garcés, M. (2008) Magma flow in dikes from rift zones of the basaltic shield of Tenerife, Canary Islands: Implications for the emplacement of buoyant magma. Journal of Volcanology and Geothermal Research 173 pp.55-68

Sparks, R.S.J., Baker, L., Brown, R.J., Field, M., Schumacher, J., Stripp, G., Walters, A. (2006) Dynamical constraints on kimberlite volcanism. Journal of Volcanology and Geothermal Research 155 pp.18-48

Stewart, J.H., Poole, F.G., and Wilson, R.F. (1972a) Stratigraphy and origin of the Chinle Formatoin and related Upper Triassic strata in the Colorado Plateau Region. Geological Survey Professional Paper 690 pp. 1-336

Stewart, J.H., Poole, F.G., and Wilson, R.F. (1972b) Stratigraphy and origin of the Triassic Moenkopi Formation and related strata in the Colorado Plateau Region. Geological Survey Professional Paper 691 pp. 1-195

Symons, D.T.A., Cioppa, M.T. (2000) Crossover plots: a useful method for plotting SIRM data in paleomagnetism. Geophysical Research Letters 27(12) pp. 1779-1782

Valentine, G.A., Cortés, J.A. (2013) Time and space variations in magmatic and phreatomagmatic eruptive processes at Easy Chair (Lunar Crater Volcanic Field, Nevada, USA). Bullentin of Volcanology 752 pp.1-13

Valentine, G.A., White, J.D.L. (2012) Revised conceptual model for maar-diatremes: Subsurface processes, energetics, and eruptive products. Geology 40(12) pp. 1111-1114

Walker, J.D., Geissman, J.W., Bowring, S.A., and Babcock, L.E., compilers (2012) Geologic Time Scale v. 4.0: Geological Society of America, doi: 10.1130/2012.CTS004R3C. ©2012 The Geological Society of America

White, J.D.L. (1991) Maar-diatreme phreatomagmatism at Hopi Buttes, Navajo Nation (Arizona), USA. Bulletin of Volcanology 53(4) pp. 239-258

White, J.D.L. (1990) Depositional architecture of a maar-pitted playa: sedimentation in the Hopi Buttes volcanic field, northeastern Arizona, USA. Sedimentary Geology 67 pp. 55-84

White, J.D.L. (1989) Basic elements of maar-crater deposits in the Hopi Buttes Volcanic Field, northeastern Arizona, USA. Journal of Geology 97(1) pp. 117-125

White, J.D.L., Fisher, R.V. (1989) Maar volcanism at Hopi Buttes, Arizona: Hydrovolcanic eruptions rooted in unconsolidated strata. Continental Magmatism Abstracts 131 pp. 292

White, J.D.L., Ross, P.S. (2011) Maar-diatreme volcanoes: A review. Journal of Volcanology and Geothermal Research 201 pp. 1-29

Williams, H. (1936) Pliocene volcanoes of the Navajo-Hopi country. Bulletin of the Geologic Society of America 47 pp. 111-172

Zimanowski, B., Büttner, R., Lorenz, V. (1997) Premixing of magma and water in MFCI experiments. Bulletin of Volcanology 58 pp.491-495

Zimanowski, B., Frölich, G., Lorenz, V. (1991) Quantitative experiments on phreatomagmatic explosions. Journal of Volcanology and Geothermal Research 48 pp.341-358

Zitzelsberger A., Schmidbauer, E. (1999) Temperature dependence of magnetic hysteresis properties, and thermoremanent and anhysteretic remanent magnetization of stress-controlled synthetic 1-125 μm titanomagnetite ($Fe_{2.4}Ti_{0.6}O_4$) particles. Geophysical Journal International 136 pp. 505-518